This is to certify that the
dissertation entitled

THE APPLICATION OF BORON-DOPED DIAMOND THIN-
FILM ELECTRODES FOR WATER TREATMENT AND
WATER QUALITY MONITORING

presented by

YANG SONG

has been accepted towards fulfillment
of the requirements for the

Ph.D   degree in   Chemistry - Environmental
Toxicology

_____
Major Professor's Signature

_____
Date

MSU is an Affirmative Action/Equal Opportunity Institution

PLACE IN RETURN BOX to remove this checkout from your record.
TO AVOID FINES return on or before date due.
MAY BE RECALLED with earlier due date if requested.

DATE DUE	DATE DUE	DATE DUE

THE APPLICATION OF BORON-DOPED DIAMOND THIN-FILM ELECTRODES FOR WATER TREATMENT AND WATER QUALITY MONITORING

By

Yang Song

A DISSERTATION

Submitted to
Michigan State University
in partial fulfillment of the requirements
for the degree of

DOCTOR OF PHILOSOPHY

**Department of Chemistry
and Center for Integrative Toxicology**

2006

ABSTRACT

THE APPLICATION OF BORON-DOPED DIAMOND THIN-FILM ELECTRODES FOR WATER TREATMENT AND WATER QUALITY MONITORING

By

Yang Song

In this Dissertation, the application of boron-doped diamond electrodes for water treatment (degradation of an organic compound (atrazine)) and water quality monitoring (detection of inorganic ions (arsenic)) is described.

In one project, boron-doped diamond thin-film coated on Ti (diamond/Ti) was used for the anodic degradation of atrazine. The specific aim was to learn how efficiently atrazine can be electro-oxidized at diamond to produce CO_2. The diamond/Ti anode was first evaluated during anodic polarization in 0.1 M H_2SO_4 and was found to exhibit a stable electrochemical response over time, good activity for the two redox systems, $Ru(NH_3)_6^{3+/2+}$ and $Fe(CN)_6^{3-/4-}$, and excellent morphological and microstructural stability. The electrooxidative degradation of atrazine was investigated by bulk electrolysis at constant current density (11 or 22 mA/cm^2). The intermediate degradation products were detected by HPLC-UV/Vis. The three common degradation products for atrazine, hydroxyatrazine deethylatrazine and deisopropylatrazine, were not detected during the electrolysis. However, radioisotope labeling studies proved that 81% of the ^{14}C-labeled atrazine was oxidized to $^{14}CO_2$ during a 2-h electrolysis period confirming that diamond is a suitable anode for complete mineralization.

In a second project, a Au-coated boron-doped diamond thin-film electrode

was used to detect total inorganic arsenic in water supplies using differential pulse anodic stripping voltammetry (DPASV). The specific aim of the work was to learn how the diamond support influences (i) the formation of Au metal phases and, in term, the formation of the Au-As complex during the deposition step and (ii) the resistance of the nearby Au particles toward adsorption of contaminants in solution (i.e., fouling). In the method, As is codeposited (preconcentrated) with Au on the diamond surface and detected oxidatively by DPASV. Au deposition was found to be uniform over the surface with a nominal particle size of 23 ± 5 nm under the potentiostatic conditions employed. The electrode provided a sensitive, reproducible and stable response for total inorganic arsenic detection and exhibited better performance than did Au-coated glassy carbon or Au foil electrodes. Sharp and symmetric stripping peaks were generally observed for the Au-coated diamond electrode. As(V) was chemically reduced to As(III) by Na_2SO_3 before analysis. Limits of detection (LOD) were 0.005 ppb (S/N = 3) for As(III) and 0.08 ppb (S/N = 3) for As(V) in standard solutions. An As(III) concentration of 0.6 ppb was found in local river water with a stable electrode response. Interferences, such as metal ions (e.g., Cu(II)) and organic matter (e.g., humic acid), that commonly cause decreased electrode response sensitivity for arsenic detection in real samples, were minimized through the use of solid phase extraction in the sample preparation. The method provided accurate and reproducible results for total inorganic arsenic detection in two contaminated water samples. The detected total inorganic arsenic concentration differed from the specified concentrations by less than 4%.

ACKNOWLEDGEMENTS

TABLE OF CONTENTS

viii

LIST OF TABLES

List of Figures

CHAPTER 1

INTRODUCTION

Ground water is one of the most important natural resources of the world. For example, in the United States, ground water accounts for about 40 percent of the water used for public utility and 97 percent of the drinking water for the rural population who do not have access to public water-supply systems.[1] However, water pollution has been a serious problem all over the world. It is suggested to be the leading cause of death and disease worldwide.[2] More than 14,000 people die daily due to water pollution.[3] Water pollution has also expedited the depletion of ground water. Reduction of ground water supplies are expected in many areas of the world in the coming century as the population increases.[2] Thus, technologies to economically, reproducibly and quickly remediate and monitor ground water contamination are of great need.

Electrochemical methods, being one of these technologies, have garnered increasing attention because of their versatility in application, low energy requirement, environmental compatibility (electrons as the main reagent), portability and cost effectiveness. The electrode material plays an important role in the application of the technology. The microstructure and morphological stability of the electrode and its electrochemical properties will affect the efficiency and outcome of the electrochemical method.

Electrically conducting diamond thin films provide scientists and engineers with an entirely new type of electrode material that meets the requirements for a wide range of electrochemical applications. Boron-doped diamond (BDD) is a

new sp^3 carbon material that possesses attractive properties compared with sp^2 carbon (e.g., glassy carbon) and metal electrodes (e.g., Hg). Its beneficial electrochemical properties include: (i) low and stable background current, (ii) wide working potential window, (iii) good activity for many redox analytes without conventional electrode pretreatment, (iv) stable surface microstructure and morphology over a wide potential range and (v) weak adsorption of polar molecules (i.e., fouling resistance).[4-7] The last two properties are key for long-term treatment and monitoring of real water samples.

The research in this Dissertation consists of two major parts: (1) application of a boron-doped diamond electrode on Ti substrate (diamond/Ti) for water treatment to study the physical and electrochemical properties of the electrode before and after electrolysis using atrazine as a sample pollutant and (2) developing a sensitive, stable and reproducible method for on-site inorganic arsenic monitoring using a Au-coated boron-doped diamond electrode.

1.1 Importance of Water Treatment

1.1.1 Methods of Water Treatment

With the increase in public knowledge about the consequences of environmental pollution and the development of modern industry, the demand for better water quality has also increased. The U.S. Environmental Protection Agency (USEPA) has set more strict regulations to control the effluent of industrial wastewater. Thus, the role of wastewater treatment has become more and more important to meet these strict regulations. Interest in the development

of advanced remediation and water purification technologies for the treatment of hazardous chemical wastes has grown enormously in the past 50 years. The methods used for highly contaminated wastewater treatment can be divided into three major categories: physical methods, biodegradation and chemical processes.[8] Currently, a typical treatment plant will use a combination of the three treatment methods. Physical methods are usually applied first to remove suspended, undissolved pollutants by sedimentation, flocculation, filtration or adsorption. Then biological and chemical methods are used to further remove the remaining pollutants. Biological treatment techniques are well established and relatively cheap. However, biodegradation depends on a variety of factors such as the concentration of pollutants, their chemical structure and biodegradability of the contaminants. The process is slow and not ubiquitous.[9, 10] Chemical processes are very important to efficiently remove persistent organic pollutants. Oxidation is the most commonly used chemical process and it produces degradation products that are non-toxic or easily bio-degradable intermediates.[8]

A special class of chemical oxidation techniques defined as advanced oxidation processes (AOP) was developed to oxidize pollutants that are difficult to deal with. The AOP methods are fairly new technologies developed since 1975 and are characterized by the capability to generate highly reactive free radicals, such as hydroxyl radicals (OH•) by means of energy or catalyst.[10] For example, hydrogen peroxide can generate hydroxyl radicals when irradiated with UV light (< 254 nm). These hydroxyl radicals are important for degradation of the pollutants because they are able to add to a double bond, abstract hydrogen or

transfer an electron from a halogenated compound as shown in the reactions:[10]

- Addition to double bond $OH\bullet + X_2C=CX_2 \rightarrow X_2C(OH)CX_2\bullet$

- Hydrogen abstraction $OH\bullet + RH \rightarrow H_2O + R\bullet$

- Electron transfer $OH\bullet + RX \rightarrow OH^- + XR^+\bullet$
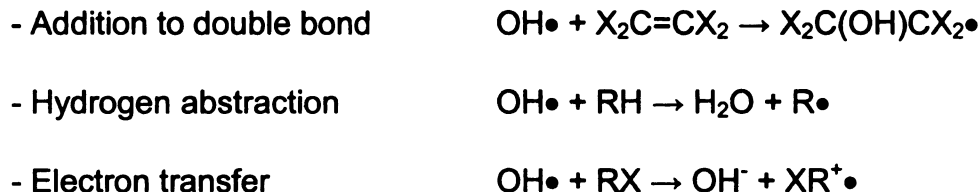
where R represents a typical hydrocarbon and X represents a halogenated group. The oxidation products could be intermediates (e.g., HCO_3^-, Cl^- and NO_3^-),[10] however, complete mineralization or ultimate degradation of the organics is ideal because the final products are CO_2 and H_2O.

Processes of the AOP methods that are capable of generating the free radicals include photochemical processes, ozonation processes and in situ generation of free hydroxyl radicals (Fenton or electrochemical methods).[8] The oxidants and methods used in the different processes and the generated free radicals are listed in Table 1.1.[10, 11] Many of the methods use a combination of the different processes shown in Table 1.1. The photochemical processes utilize artificial light source or natural sunlight to generate hydroxyl radicals. For example, when hydrogen peroxide is added, the reaction is:

$$H_2O_2 + h\nu \rightarrow 2\ OH\bullet$$

To effectively generate hydroxyl radicals, the photons have to be absorbed by the chemical partners (O_3 or H_2O_2).[11] Therefore, the intensity and wavelength of the light source has to be carefully selected and the processes are generally slow and leading to incomplete degradation.[8] Ozonation processes utilize dissolved ozone to attack C=C double bonds. The products of this reaction are compounds containing carbonyl groups (aldehydes and ketones) and hydrogen peroxide as

4

well as a group of free radicals as shown in Table 1.1. When used in combination with H_2O_2, the reaction is:[11]

$$2\ O_3 + H_2O_2 \rightarrow 3\ O_2 + 2\ OH\bullet$$
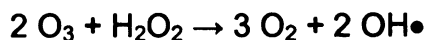
Table 1.1   Chemical processes generating free radicals.

	Oxidants and Methods	Generated Free Radicals
Photochemical Processes	UV	OH•
	TiO_2/UV	OH•
	O_3/UV	OH•
	H_2O_2/UV	OH•, HO_2•
	$O_3/UV/H_2O_2$	OH•, O_2^-•, HO_2•, O_3^-•, HO_3•
Ozonation Processes	O_3	OH•, O_2^-•, HO_2•, O_3^-•, HO_3•
	O_3/H_2O_2	OH•, O_2^-•, HO_2•, O_3^-•, HO_3•
In Situ Generation of Free Radicals	H_2O_2/Fe^{2+}	OH•
	$H_2O_2/Fe^{2+}/UV$	OH•

Although the ozonation processes are very efficient at producing hydroxyl radicals, they usually require in situ generation of ozone and are relatively expensive.[8] The Fenton reaction involves the reaction of H_2O_2 with Fe^{2+} to generate hydroxyl radicals. Under acidic conditions, the reaction is:

$$H_2O_2 + Fe^{2+} \rightarrow Fe^{3+} + OH\bullet + OH^-$$

This method is efficient and capable of completely degrading organic compounds

to CO_2. However, a potential environmental hazardous Fe^{2+} has to be added to the water.

Electrochemical processes are good alternatives due to their versatility, environmental compatibility and cost effectiveness. The electrochemical oxidation of organic pollutants in water occurs at high anodic potentials with concomitant generation of oxygen (O_2 evolution). The nature of the electrode material is an important factor affecting the selectivity and efficiency of the process. An anode material that possesses a wide working potential window, long service-life in harsh chemical environments and resistance to surface fouling and passivation are desired for good remediation efficiency.

Comninellis et al. proposed a model to comprehensively interpret the anodic oxidation of organics in acid medium on different electrode materials. They divided the electrodes into two limiting cases: active and nonactive anodes (Figure 1.1).[12] M represents the reaction sites on electrode surface and R represents the organic pollutants. Hydroxyl radicals are produced by the dissociation of water. The first step of reaction is the interaction of the hydroxyl radicals with the electrode surface (Figure 1.1, reaction a).[12]

$$H^+ + e^-$$
$$+$$
$$\text{Active anode} \qquad + R \longrightarrow M + RO$$
$$MO \begin{array}{c} e \end{array}$$
$$c \qquad\qquad d \longrightarrow M + \tfrac{1}{2} O_2$$

$$M \xrightarrow{\ OH\bullet\ } M(OH)\bullet \quad \begin{array}{c} O_2 \text{ evolution} \\ \xrightarrow{\ b\ } \end{array} M + \tfrac{1}{2} O_2 + H^+ + e^-$$

$$\xrightarrow[f]{\ +R\ } M + m\,CO_2 + n\,H_2O + H^+ + e^-$$
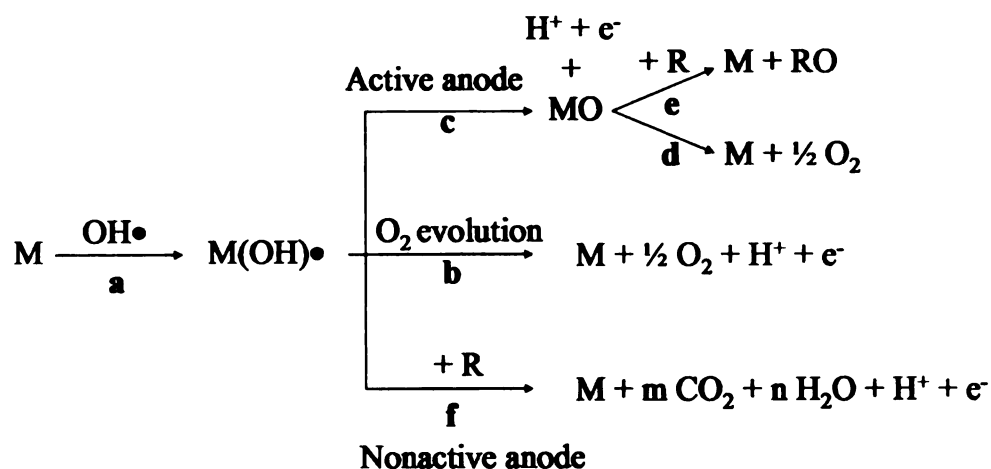
Nonactive anode

Figure 1.1 Scheme of the oxidation of organic compounds with simultaneous O_2 evolution: (a) interaction of the electrode surface with OH•, (b) O_2 evolution by electrochemical oxidation of OH•, (c) formation of the higher oxide on an active anode, (d) O_2 evolution by chemical decomposition of the higher oxide, (e) oxidation of the organics (R) via the higher oxide on an active anode and (f) complete oxidation of the organics via hydroxyl radicals on a nonactive anode.

An active anode is defined as one with a strong interaction with the hydroxyl radicals. Through the interaction, hydroxyl radicals transfer oxygen to the electrode surface and form a higher oxide MO (Figure 1.1, reaction c). The higher oxide MO can mediate the oxidation of organic pollutants R (Figure 1.1, reaction e) or dissociate back to M and O_2 (Figure 1.1, reaction d). The oxidation of organics mediated by the higher oxide MO tends to be much more selective than the oxidation reaction mediated by hydroxyl radicals on a nonactive anode. Nonactive anode has weak interaction with hydroxyl radicals. Instead of forming higher oxide on the electrode surface, hydroxyl radicals on an active anode

mediate the oxidation of organics and result in fully oxidized product, CO_2 (Figure 1,1, reaction f). In this case, the electrode serves as an inert substrate and a sink for the removal of electrons without participating in anodic reactions.

The hydroxyl radicals can also result in O_2 formation, which is a competitive process with the oxidation of organics (Figure 1.1, reaction b).[12] The nature of the electrode material determines the strength of its interaction with hydroxyl radicals, and thus affects the reactivity of O_2 evolution and the oxidation efficiency of organic pollutants. In general, nonactive anodes are desired because they have weak interaction with hydroxyl radicals, and thus have low activity toward the formation of O_2 and high efficiency for pollutant oxidation.[12]

1.1.2 Electrode Materials and Their Limitations

Electrochemical remediation treatments are often limited by the availability of a suitable anode material that is not active toward O_2 evolution and electrode oxidation. Properties such as a wide working potential window, long service-life in harsh chemical environments, and resistance to surface fouling and passivation are desired for anode material used for electrochemical treatment of wastewater. Several anode materials have been used in the past, such as Pt, glassy carbon, IrO_2/Ti, $SnO_2\text{-}Sb_2O_5/Ti$, PbO_2, and SnO_2.[13-16] These electrodes all have limitations in terms of their effectiveness for electrochemical remediation. Some, like glassy carbon, undergo rapid loss of activity due to surface fouling.[13] Toxic ions are liberated from others due to corrosion, such as Pb^{2+} from PbO_2.[14] The service-life of anodes that undergo corrosion at significant rates is another

8

limiting factor. For example, the service life of Ti/SnO_2-Sb_2O_5 is only about 12 h in 1 M H_2SO_4 due to surface oxidation and corrosion.[15]

1.1.3 Boron-Doped Diamond and Substrate Materials

A dimensionally stable anode is necessary for the electrochemical remediation of chemical waste, which can operate in chemically harsh environments with unchanging performance, resist fouling by matrix components and efficiently support anodic oxygen transfer reactions. Diamond electrodes appear to meet all of these requirements. Diamond electrodes have been successfully used for electrochemical oxidation of chemical compounds in aqueous media.[17-21] Iniesta et al. used a boron-doped diamond electrode to oxidize 3-methylpyridine (3-MP). They found that at low current density, 3-MP was oxidized to nicotinic acid, while at high current density it was directly converted to CO_2.[17] Canizares et al. used a diamond electrode to oxidize carboxylic acid wastes in water by galvanostatic electrolysis. 10 mM of formic acid, oxalic acid and maleic acid was fully or partially oxidized to CO_2 within 210 min. No intermediates were found.[18] Codognoto et al. studied the selective oxidation of pentachlorophenol (PCP) on diamond electrode, they found that under fairly mild conditions (lower applied potential), a dimerization process leads to the formation of an insoluable species; at more positive potentials, PCP was initially converted to hydroxyl-quinone and finally to CO_2 and water.[19] Real wastewater containing organic pollutants has also been studied by Panizza on a p-Si substrate diamond electrode.[21] All their work showed that diamond

electrodes can effectively degrade the organics in water without losing reactivity.

Electrically conducting (< 0.05 $\Omega \cdot cm$) boron-doped diamond thin films can be deposited on different substrate materials using chemical vapor deposition (CVD). Currently, the most popular substrate used for diamond growth is Si due to the simplicity of growth. However, boron-doped diamond electrodes grown on a Si substrate (diamond/Si) have some limitations for wastewater treatment applications due to their mechanical weakness and low electrical conductivity.[22] To overcome these limitations, diamond films grown on metal substrates can be used. Despite the good performance of Nb, Ta, and W as substrates for diamond growth, the high cost of these metals is a disadvantage for large-scale industrial application. Ti is much cheaper and is a technologically-important metal that possesses good electrical conductivity and high mechanical strength.[23] It is much more attractive than the others listed above for wastewater treatment applications. Diamond/Ti has been used as an electrochemical electrode for the remediation of chemical contaminants in water. For example, Chen and coworkers applied a diamond/Ti anode for the oxidation of carboxylic acids, phenol, orange II, and reactive red HE-3B.[23] Fryda and coworkers deposited large area diamond films on different substrate materials, including Ti, and used them for the oxidation of alcohols, organic acids and halogenated aromatic molecules.[24] They found that the organic molecules could be oxidized to CO_2 without major amounts of other detectable by-products even at very low concentrations (<3 ppm). Even with these reported results, there remains a need to comprehensively evaluate the electrochemical properties and remediation

performance of diamond films coated on Ti substrates.

1.1.4 The Herbicide – Atrazine

In this work, atrazine was the organic pollutant used due to its resistance to oxidation. Atrazine [2-chloro-4-(ethylamino)-6-(isopropyl-amino)-s-triazine] is a compound of particular interest due to its wide use as a herbicide.[25, 26] It is a chlorinated triazine compound that is difficult to oxidatively degrade using conventional electrode materials.[27] Atrazine undergoes slow hydrolysis, has low vapor pressure (3×10^{-7} mm Hg at 20^0C), is moderately soluble in water (30 ppm) and shows moderate adsorption to organic matter and clay. These properties make atrazine relatively persistent in soils and aquatic systems.[28] From 1991 to 1995, thousands of sampled wells and springs across the U.S. were studied by the United States Geological Survey (USGS). Among the seven herbicides of interest (atrazine, cyanazine, simazine, alachlor, metolachlor, prometon and acetochlor), atrazine was the only one found to exceed the allowable concentration level in drinking water (3 ppb), as mandated by the USEPA. Studies have shown that atrazine is harmful to both animals and plants.

Several methods have been employed to treat atrazine-contaminated water including ozonation[29, 30] and photochemical degradation.[31, 32] There are only a couple of reports describing the electrochemical treatment of such contaminated water.[27, 33] Ventura and coworkers used the electrochemical generation of Fenton's reagent and a mercury electrode to degrade atrazine and observed efficient atrazine degradation with the formation of deisopropylatrazine,

deethylatrazine and deethyl-deisopropylatrazine. They claimed no trace of hydroxyatrazine could be found.[33] Saltmiras and Lemley also performed atrazine degradation by anodic Fenton treatment using iron electrodes as both a sacrificial anode and an inert cathode. They reported that 70% of the atrazine was degraded in 3 min with the formation of dechlorinated ammeline as the primary product after 10 min.[27] Electrodes that can completely degrade atrazine to CO_2 are needed as well as fundamental studies of the reaction kinetics and mechanisms.

The research on water treatment in this dissertation sought to answer several key questions:

(1)   What are the morphological and electrochemical properties of diamond/Ti?

(2)   What is the efficiency of diamond/Ti for electrochemical oxidation of atrazine and if the electrode is stable?

(3)   What are the oxidation reaction products?

(4)   What is the conversion efficiency of the final oxidation product CO_2?

1.2 Importance of Water Quality Monitoring

1.2.1 Metal Ion Contaminants and Arsenic

Water quality monitoring is very important to determine the level of contaminants in water. Trace elements, especially heavy metals, are one of the major groups of contaminants in ground water.[34] Heavy metals such as copper, lead, and mercury are discharged from mining, smelting and industrial

12

manufacturing and can cause long-term effects on the environment and human health due to their extremely toxic nature even at trace concentrations, and their non-biodegradability.[35] The effects of hazardous metal ions are caused by mimicking of the essential elements.[36] Effects such as birth defects, cancer, skin lesions, mental and physical retardation, learning disabilities and liver and kidney damage are linked to many metal contaminations.[35]

Among the trace element contamination, arsenic contamination has been one of the most common and harmful types.[37] Arsenic naturally occurs in the ground and can be introduced into water through the erosion of rocks, minerals and ores. Industrial effluents are another source of arsenic in the environment. Ground water arsenic contamination has been reported in many countries of the world, such as Argentina, Bangladesh, Cambodia, Chile, China, Ghana, Hungary, Mexico, Mongolia, Nepal, New Zealand, Philippines, Taiwan, United States and Vietnam.[38] Chronic exposure to As-contaminated water can cause several health problems including pigmentation changes, hyperkeratosis and various cancers (e.g., skin, lung, urinary bladder, and kidney).[39] Symptoms can begin with exposure to concentrations as low as 50 ppb.[37]

Arsenic has been put into the heavy metal category because of its semimetal electronic properties. However, being in group five in the periodic table, arsenic also has many nonmetallic properties that are similar to nitrogen and phosphorus. Due to its valence electron configuration shown in Figure 1.2, arsenic can have all oxidation states between - 3 and + 5.

$$4s \qquad 4p \qquad\qquad 4d$$

| ↑↓ | | ↑ | ↑ | ↑ | | | | | |
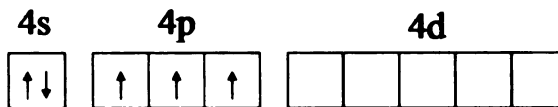
Figure 1.2 The valence electron configuration of arsenic in the ground state.

In ground water, the As(III) and As(V) inorganic forms are the most abundant forms and are much more toxic than the organic forms, with As(III) being the most toxic.[39, 40] The research in this dissertation is therefore focused on the detection of the toxic inorganic forms: As(III) and As(V) in water.

1.2.2 EPA Approved Methods for As Detection

In an effort to better protect society, the USEPA recently lowered the maximum contaminant level (MCL) for total arsenic in drinking water from 50 to 10 ppb.[41] This lowering creates a need for more sensitive, reliable and stable detection methods. The USEPA-recommended methods for arsenic analysis presently include inductively coupled plasma-mass spectrometry (ICP-MS) (Method 200.8), inductively coupled plasma-atomic emission spectrometry (ICP-AES) (Method 200.7) and graphite furnace atomic adsorption spectrometry (GFAAS) (Method 200.9). Each of these methods provide detection limits at or below the MCL (1.4, 8 and 0.5 ppb, respectively);[37] however, they are expensive in terms of the instrumentation cost, time consuming, labor intensive and the equipment is not easily deployed in the field. There is also a USEPA approved anodic stripping voltammetric method that makes use of a Au-coated glassy carbon electrode (Method 7063).[42]

1.2.3 Differential Pulse Anodic Stripping Voltammetry (DPASV)

Anodic stripping voltammetry (ASV) is generally used for metal ion analysis in water samples due to its high sensitivity and good resolution. ASV is capable of measuring four to six metal ions simultaneously at concentrations as low as the sub part-per-billion (ppb) level. The instrumentation is capable of being used on-site and is relatively low-cost.[43]

ASV measurements involve two steps: (1) deposition of a metal phase onto a solid electrode surface or into Hg (liquid) at cathodic potentials and (2) selective electrooxidation of predeposited metal on the electrode surface as shown in Figure 1.3.
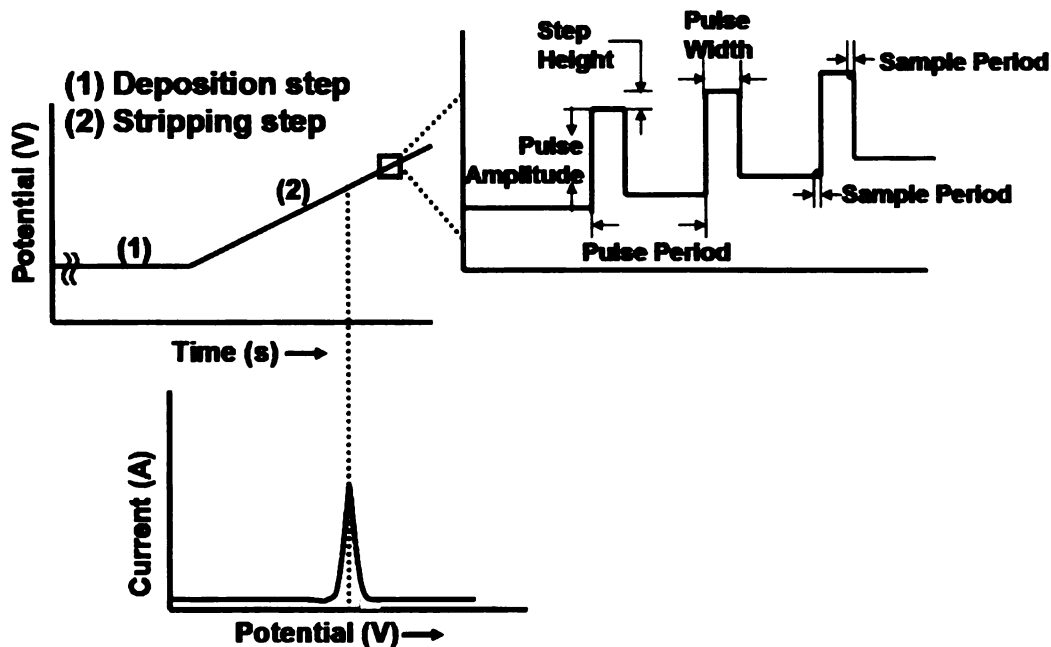
Figure 1.3 The differential pulse anodic stripping voltammetric (DPASV) potential waveform and resulting current response. (1) The deposition step involves a cathodic potential-step of certain magnitude and duration and (2) the

stripping step involves a potential scan in the positive direction to oxidize the predeposited metal phase formed in step (1). An enlarged view of the applied pulse program depicting the various parameters is also shown. The resulting voltammetric *i-E* curve is constructed by plotting the current difference of the two sampling points for each pulse as a function of the potential.

Due to the two-step measurement scheme, ASV offers a 2 to 3 order of magnitude lower limit of detection as compared with solution-phase voltammetric measurements.[43] In the deposition step, a controlled potential is applied for a definite time under reproducible hydrodynamic (mass-transport) conditions in the solution. The trace metal ions of interest are reduced and preconcentrated on the electrode surface at the controlled cathodic potential:

$$M^{n+} + n\ e^- \rightarrow M$$

The preconcentration greatly enhances the amount of metal at the electrode surface and it can be improved by increasing the deposition time or optimizing the deposition potential.[43] In the stripping step, pulses of equal amplitude are superimposed on a positive potential sweep and the predeposited metal is oxidized and stripped from the electrode surface:

$$M - n\ e^- \rightarrow M^{n+}$$
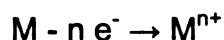
The pulses usually have a 10-100 mV pulse amplitude, a 5-100 ms pulse width and a 0.5-4 s pulse period. During each pulse period, the current is sampled twice: once right before the application of the pulse and once right before the termination of the pulse. The current difference between these two sampling

16

points is plotted against the scanned potential (Figure 1.3). Using this method, the charging current is subtracted from the total current and the signal to background ratio is greatly enhanced.[43] This is because when applying the pulse, the faradaic current and charging current both increase. However, the charging current ($i_c \sim e^{-t}$) decays much faster than mass transfer limited faradaic current ($i_f \sim t^{-1/2}$). At the sample point right before the termination of the pulse, the current is mostly faradaic current. At both sampling points, the charging current is essentially the same, so the current difference between these two sampling points is only attributed to faradaic current thus increasing the signal to background ratio and sensitivity of the method.[43] A further gain of the signal to background ratio is obtained because the stripped metal ions could redeposit onto the electrode surface during the waiting period between pulses, thus the same material can be repetitively stripped and deposited and contribute to the total current at potentials negative of the standard redox potential.[43]

The equation describing the differential pulse stripping peak current was derived by Lund and Onshus for hanging mercury drop electrode:[44]

$$\Delta i_p = kn^2 r \Delta E u^{1/2} t_d C_b$$

where k is the heterogeneous electron transfer rate constant, n is the number of the electrons transferred per equivalent, r is the radius of the mercury drop, ΔE is the pulse amplitude, u is the rotation speed of the stirrer, t_d is the deposition period and C_b is the concentration of metal ion in the sample solution. Even though it might not correctly describe the current response for a planar electrode, the equation shows the linear relationship between the stripping peak current and

the deposition time, pulse amplitude and metal ion concentration. These are important parameters to study when optimizing the stripping peak current.

1.2.4 Electrode Materials and Their Limitations for Arsenic Detection

For arsenic monitoring using DPASV method, an important factor that can strongly influence the detection is the electrode material. Arsenic detection has been accomplished using different electrodes: Hg,[39, 41, 45-48] Pt,[49-51] Au[40, 52-56] and Au-coated carbon electrodes (graphite[40, 54, 57, 58] and glassy carbon[59-61]). The limited solubility of As in Hg, as well as its toxicity make Hg less desirable for this application. Platinum electrodes are of limited use because of a narrow potential window and large background current.[53] It turns out that Au is the electrode of choice for measuring this analyte. This is because of the Au-As intermetallic compound that forms during the preconcentration step with the general formula Au_xAs_y, where x=1-3 and y=2-6.[62] In this form, all of the deposited As can be oxidatively removed at lower potentials than the Au, thus enabling its detection. Tikhomirova and Akhmedzhanova analyzed the Au-As intermetallic compound stability in HCl under different conditions using X-ray diffraction and found that the compounds decompose to arsenic oxides of the arsenolite type (As_2O_3) and fine-grained gold when exposed to oxidizing potentials.[62, 63] This facilitates the release of the As(III) during stripping step. Limits of detection (LOD) in the low ppb to sub-ppb range for As(III) are typical for Au and Au-coated carbon electrodes. Generally, Au particles supported on carbon materials provide lower

LODs and are more cost effective than solid Au electrodes due to the lower mass of metal needed. To cite a few examples in the literature, Kopanica et al. detected As(III) by ASV using a Au disc electrode and achieved an LOD of 0.15 ppb.[64] Feeney and Kounaves used a Au ultramicroelectrode array with 80 s deposition time and reported an LOD of 0.013 ppb and a sensitivity of 0.044 μA/ppb.[40] Dai et al. reported a low LOD of 0.0096 ppb for As(III) in 1 M HCl using linear sweep voltammetry with a Au-coated glassy carbon electrode,[59] and Simm et al. investigated the sonochemical detection of As with a Au electrode, obtaining an LOD of 0.28 ppb.[52] A general limitation with Au and Au-coated sp^2 carbon electrodes is the poor response precision and stability. Examples of this include the work by Davis et al. and Viltchinskaia et al. who reported passivation of the Au-coated graphite,[54, 60] Feeney and Kounaves who observed a 30% attenuation of the As stripping peak current with a Au ultramicroelectrode over 30 successive runs,[40] and Prakash et al. who reported a 20% variation in the results for 5 measurements using a Au disk rotating electrode.[56]

Diamond is a suitable alternate to Hg for ASV and has been successfully applied for the detection of several metal ions: Ag(I),[4, 65, 66] Cu(II),[4, 67] Pb(II),[4, 67-69] Cd(II),[4, 69, 70] Zn(II),[4] Mn(II),[71] Sn(II),[65] Hg(II)[72] and Au(III).[73] However, there are only a few reports of arsenic detection using diamond electrodes. Simm et al. detected As(III) using a Au plated BDD microelectrode array and reported an LOD of 2.85 ppb and a sensitivity of 17.6 μA/ppm.[74] Hignett et al. detected As(III) using linear sweep voltammetry by iodine-mediated oxidation of As(III) to As(V). They compared diamond with Au, Pt and glassy carbon and found that the LOD

to be lowest for BDD.[50] Salimi et al. modified a BDD electrode by electrodepositing hydrous iridium oxide, which enabled the oxidative detection of As(III) to As(V) at 0.5 V. They reported an LOD of 0.15 ppb and a sensitivity of 56 µA/ppm.[75]

The research on water monitoring in this Dissertation sought to answer several key questions:

(1)   What are the morphological and electrochemical properties of Au-coated diamond electrode and can it be used for As analysis in water?

(2)   What is the nature of Au deposition on diamond in terms of particle nucleation and growth, size and dispersion?

(3)   How do the figures of merit for a Au-coated diamond electrode compare with planar Au and Au-coated sp^2 carbon electrodes for arsenic monitoring?

(3)   How can common interferences (e.g. Cu(II) and humic material) in real water be minimized?

(4)   How do the electrode and method function for total inorganic As analysis in real samples?

1.3 Dissertation Outline

This dissertation describes studies using boron-doped diamond electrode for the application in both water treatment and water quality monitoring. Specifically, boron-doped diamond electrode grown on Ti substrate (diamond/Ti) was applied for atrazine remediation and Au-coated diamond electrode was applied for total inorganic arsenic monitoring in water supplies. In Chapter 2, the

experimental parameters of the work including materials, instrumentation and methods are presented. The water treatment studies are presented in Chapters 3 and 4. In Chapter 3, evaluation of the physical and electrochemical properties as well as the stability of diamond/Ti electrode is presented. Application of the electrode for the electrochemical remediation of atrazine is described in Chapter 4. The water monitoring studies are presented in Chapters 5 and 6. In Chapter 5, the Au-coated diamond electrode is evaluated in terms of the morphology, response stability and detection figures of merit for inorganic arsenic detection. Its performance for As detection is compared with planar Au electrode and Au-coated glassy carbon electrode. Chapter 6 presents the application of the established method for real water analysis with demonstrated mitigation of common interferences such as trace metal cations and humic material. The method is demonstrated for two different contaminated water samples provided by the U.S. Bureau of Reclamation. Finally, Chapter 7 provides a summary of the conclusions as well as future directions for this research.

1.4 References

(1) *U.S. Geological Survey* **1995**.

(2) Pink, D. H. *http://finance.yahoo.com/columnist/article/trenddesk/3748? p=1, Investing in Tomorrow's Liquid Gold*, Accessed July 23, 2006.

(3) West, L. *http://environment.about.com/od/environmentalevents/a/water dayqa.htm, World Water Day: A Billion People Worldwide Lack Safe Drinking Water*, Accessed July 23, 2006.

(4) Sonthalia, P.; McGaw, E.; Show, Y.; Swain, G. M. *Analytica Chimica Acta* **2004**, *522*, 35-44.

(5) Muna, G. W.; Tasheva, N.; Swain, G. M. *Environmental Science and Technology* **2004**, *38*, 3674-3682.

(6) Granger, M. C.; Witek, M.; Xu, J.; Wang, J.; Hupert, M.; Hanks, A.; Koppang, M. D.; Butler, J. E.; Lucazeau, G.; Mermoux, M.; Strojek, J. W.; Swain, G. M. *Analytical Chemistry* **2000**, *72*, 3793-3804.

(7) Strojek, J. W.; Granger, M. C.; Swain, G. M.; Dallas, T.; Holtz, M. W. *Analytical Chemistry* **1996**, *68*, 2031-2037.

(8) Merli, C.; Petrucci, E.; Pozzo, A. D.; Pernetti, M. In *Wastewater Treatment Technologies and Environment*; Kumar, A., Ed.; Daya Publishing House: Tri Nagar, 2004; Vol. 1, pp 48-62.

(9) Troster, I.; Fryda, M.; Herrmann, D.; Schafer, L.; Hanni, W.; Perret, A.; Blaschke, M.; Kraft, A.; Stadelmann, M. *Diamond and Related Materials* **2002**, *11*, 640-645.

(10) Tabrizi, G. B.; Mehrvar, M. *Journal of Environmental Science and Health* **2004**, *A39*, 3029-3081.

(11) Gulyas, H. *Water Science and Technology* **1997**, *36*, 9-16.

(12) Marselli, B.; Garcia-Gomez, J.; Michaud, P.-A.; Rodrigo, M. A.; Comninellis, C. *Journal of the Electrochemical Society* **2003**, *150*, D79-D83.

(13) Gattrell, M.; Kirk, D. W. *Canadian Journal of Chemical Engineering* **1990**, *68*, 997-1003.

(14) Tahar, N. B.; Savall, A. *Journal of the Electrochemical Society* **1998**, *145*, 3427-3434.

(15)   Correa-Lozano, B.; Comninellis, C.; Battisti, A. D. *Journal of Applied Electrochemistry* **1997**, *27*, 970-974.

(16)   Iniesta, J.; Michaud, P. A.; Panizza, M.; Cerisola, G.; Aldaz, A.; Comninellis, C. *Electrochimica Acta* **2001**, *46*, 3573-3578.

(17)   Iniesta, J.; Michaud, P. A.; Panizza, M.; Comninellis, C. *Electrochemistry Communications* **2001**, *3*, 346-351.

(18)   Canizares, P.; Garcia-Gomez, J.; Lobato, J.; Rodrigo, M. A. *Industrial and Engineering Chemistry Research* **2003**, *42*, 956-962.

(19)   Codognoto, L.; Machado, S. A. S.; Avaca, L. A. *Journal of Applied Electrochemistry* **2003**, *33*, 951-957.

(20)   Panizza, M.; Michaud, P. A.; Cerisola, G.; Comninellis, C. *Journal of Electroanalytical Chemistry* **2001**, *507*, 206-214.

(21)   Panizza, M.; Michaud, P. A.; Cerisola, G.; Comninellis, C. *Electrochemistry Communications* **2001**, *3*, 336-339.

(22)   Chen, X.; Chen, G. *Journal of the Electrochemical Society* **2004**, *151*, B214-B219.

(23)   Chen, X.; Chen, G.; Gao, F.; Yue, P. L. *Environmental Science and Technology* **2003**, *37*, 5021-5026.

(24)   Fryda, M.; Dietz, A.; Herrmann, D.; Hampel, A.; Schafer, L.; Klages, C.-P.; Perret, A.; Haenni, W.; Comninellis, C.; Gandini, D. *Proceedings - Electrochemical Society* **2000**, *99-32 (Diamond Materials)*, 473-483.

(25)   *National Agriculture Statistics Service* **1993**.

(26)   *Environmental Fact Sheet, Atrazine Label Amendment, January 23,* **1990**, U.S EPA Office of Pesticide Programs.

(27)   Saltmiras, D. A.; Lemley, A. T. *Water Research* **2002**, *36*, 5113-5119.

(28)   Erikson, L. E.; Lee, K. H. *Critical Reviews in Environmental Control* **1989**, *19*, 1-14.

(29)   Benitez, F. J.; Beltran-Heredia, J.; Gonzalez, T.; Acero, J. L. *Ozone: Science & Engineering* **1995**, *17*, 237-258.

(30) Beltran, F. J.; Garcia-Araya, J. F.; Alvarez, P. M.; Rivas, J. *Journal of Chemical Technology & Biotechnology* **1998**, *71*, 345-355.

(31) Bourgine, F. P.; Chapman, J. I.; Kerai, H.; Duval, J. L.; Green, J. G.; Hamilton, D. *Journal of the Chartered Institution of Water and Environmental Management* **1995**, *9*, 417-423.

(32) Hequet, V.; Gonzalez, C.; Le Cloirec, P. *Water Research* **2001**, *35*, 4253-4260.

(33) Ventura, A.; Jacquet, G.; Bermond, A.; Camel, V. *Water Research* **2002**, *36*, 3517-3522.

(34) Schwartz, F. W.; Zhang, H. *Fundamentals of Ground Water*; John Wiley & Sons, Inc.: New York, 2003.

(35) Singh, P.; Cameotra, S. S. *Biochemical and Biophysical Research Communications* **2004**, *319*, 291-297.

(36) Anon, E. *Principles of Biochemical Toxicology*, John Timbrell ed., 2000.

(37) World Health Organization, May 2001, pp Fact sheet N. 210.

(38) Dai, X.; Compton, R. G. *Electroanalysis* **2005**, *17*, 1325-1330.

(39) Li, H.; Smart, R. B. *Analytica Chimica Acta* **1996**, *325*, 25-32.

(40) Feeney, R.; Kounaves, S. P. *Analytical Chemistry* **2000**, *72*, 2222-2228.

(41) Ferreira, M. A.; Barros, A. A. *Analytica Chimica Acta* **2002**, *459*, 151-159.

(42) Pyle, S.; Miller, E. L. *USEPA* **1996**.

(43) Wang, J. *Stripping Analysis*; VCH publishers, Inc.: Deerfield Beach, 1985.

(44) Lund, W.; Onshus, D. *Analytica Chimica Acta* **1976**, *86*, 109-122.

(45) Sadana, R. S. *Analytical Chemistry* **1983**, *55*, 304-307.

(46) Holak, W. *Analytical Chemistry* **1980**, *52*, 2189-2192.

(47) Barra, C. M.; Correia dos Santos, M. M. *Electroanalysis* **2001**, *13*, 1098-1104.

(48) Adeloju, S. B.; Young, T. M.; Jagner, D.; Batley, G. E. *Analytica Chimica Acta* **1999**, *381*, 207-213.

(49)   Williams, D. G.; Johnson, D. C. *Analytical Chemistry* **1992**, *64*, 1785-1789.

(50)   Hignett, G.; Wadhawan, J. D.; Lawrence, N. S.; Hung, D. Q.; Prado, C.; Marken, F.; Compton, R. G. *Electroanalysis* **2004**, *16*, 897-903.

(51)   Wei, Z.; Somasundaran, P. *Journal of Applied Electrochemistry* **2004**, *34*, 241-244.

(52)   Simm, A. O.; Banks, C. E.; Compton, R. G. *Analytical Chemistry* **2004**, *76*, 5051-5055.

(53)   Forsberg, G.; O'Laughlin, J. M.; Megargle, R. G. *Analytical Chemistry* **1975**, *47*, 1586-1592.

(54)   Davis, P. H.; Dulude, G. R.; Griffin, R. M.; Matson, W. R.; Zink, E. W. *Analytical Chemistry* **1978**, *50*, 137-143.

(55)   Feeney, R.; Kounaves, S. P. *Talanta* **2002**, *58*, 23-31.

(56)   Prakash, R.; Srivastava, R. C.; Seth, P. K. *Electroanalysis* **2003**, *15*, 1410-1414.

(57)   Kamenev, A. I.; Orlov, S. E.; Lyakhov, A. B. *Jouranal of Applied Electrochemistry* **2001**, *56*, 850-854.

(58)   Simm, A. O.; Banks, G. E.; Wilkins, S. J.; Karousos, N. G.; Davis, J.; Compton, R. G. *Analytical and Bioanalytical Chemistry* **2005**, *381*, 979-985.

(59)   Dai, X.; Nekrassova, O.; Hyde, M. E.; Compton, R. G. *Analytical Chemistry* **2004**, *76*, 5924-5929.

(60)   Viltchinskaia, E. A.; Zeigman, L. L.; Garcia, D. M.; Santos, P. F. *Electroanalysis* **1997**, *9*, 633-640.

(61)   Munoz, E.; Palmero, S. *Electroanalysis* **2004**, *16*, 1528-1535.

(62)   Tikhomirova, V. I.; Akhmedzhanova, G. M.; Nekrasov, I. Y. *Experiment in Geosciences* **1994**, *3*, 1-9.

(63)   Akhmedzhanova, G. M.; Tikhomirova, V. I. *Experiment in Geosciences* **1995**, *4*, 26-28.

(64)   Kopanica, M.; Novotny, L. *Analytica Chimica Acta* **1998**, *368*, 211-218.

(65)   Chatterjee, A.; Wiltshire, R.; Holt, K., B.; Compton, R. G.; Foord, J. S.; Merken, F. *Diamond and Related Materials* **2002**, *11*, 646-650.

(66)   Saterlay, A. J.; Marken, F.; Foord, J. S.; Compton, R. G. *Talanta* **2000**, *53*, 403-415.

(67)   Prado, C.; Wilkins, S. J.; Marken, F.; Compton, R. G. *Electroanalysis* **2004**, *14*, 262-272.

(68)   Manivannan, A.; Tryk, D. A.; Fujishima, A. *Electochemical and Solid-State Letters* **1999**, *2*, 455-456.

(69)   Babyak, C.; Smart, R. B. *Electroanalysis* **2004**, *16*, 175-182.

(70)   Banks, C. E.; Hyde, M. E.; Tomcik, P.; Jacobs, R.; Compton, R. G. *Talanta* **2004**, *62*, 279-286.

(71)   Saterlay, A. J.; Foord, J. S.; Compton, R. G. *Analyst* **1999**, *124*, 1791-1796.

(72)   Manivannan, A.; Seehra, M. S.; Fujishima, A. *Fuel Processing Technology* **2004**, *85*, 513-519.

(73)   Hian, L. C.; Grehan, K. J.; Goeting, C. H.; Compton, R. G.; Foord, J. S.; Marken, F. *Electroanalysis* **2003**, *15*, 169-174.

(74)   Simm, A. O.; Banks, C. E.; Ward-Jones, S.; Davies, T. J.; Lawrence, N. S.; Jones, T. G. J.; Jiang, L.; Compton, R. G. *Analyst* **2005**, *130*, 1303-1311.

(75)   Salimi, A.; Hyde, M. E.; Banks, C. E.; Compton, R. G. *Analyst* **2004**, *129*, 9-14.

CHAPTER 2

EXPERIMENTAL METHODS

2.1 Diamond Thin Film Growth

Microcrystalline boron-doped diamond thin film was grown on a Ti or Si substrate using microwave plasma-assisted chemical vapor deposition (1.5 KW, 2.54 GHz, ASTeX Inc., Lowell, MA). A diagram of a typical reactor system is shown in Figure 2.1.
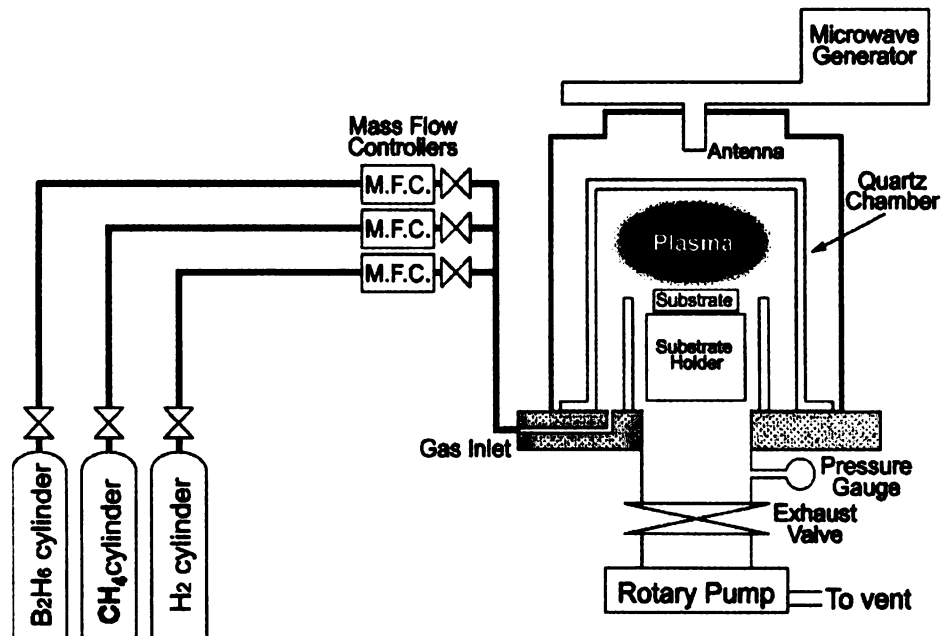
Figure 2.1 Diagram of a typical microwave CVD reactor set-up. (Copyright © 2003 From Electroanalytical Chemistry by Swain, G. M./Rubinstein, I.. Reproduced by permission of Routledge/Taylor & Francis Group, LLC)

Each component of the source gas mixture (CH_4, H_2 and B_2H_6) was introduced into the reaction chamber at a flow rate determined by a mass flow

controller. Microwave energy is generated and focused into the quartz chamber (1 L bell jar) to ignite the plasma. The plasma, which is in close proximity to the substrate, contains the reactive species important for growth. The chamber pressure is maintained by a throttle exhaust valve and rotary pump that is operated continuously during film growth.

Microcrystalline boron-doped diamond thin-film on Ti substrate (diamond/Ti) was grown on a polycrystalline Ti plate ($0.15 \times 2 \times 2$ cm^3, Sigma-Aldrich Chemical or Goodfellow Metals). The Ti substrate was first degreased sequentially with acetone, isopropanol and water, and then cleaned and roughened in a solution of 1% HF for 10 min. This was followed by ultrasonic cleaning for 3 min each in acetone, isopropanol and ultrapure water. The metal substrate was then dried in air before being mechanically polished on a felt pad for 5 min using 0.1 μm diamond powder (GE Superabrasives, Worthington, OH) slurried with ultrapure water. The polished substrate was then once again ultrasonically cleaned in acetone, isopropanol and ultrapure water for 3 min each to remove polishing debris. After cleaning, the substrate was examined under an Olympus BX60M optical microscope (Olympus America Inc.) to assess the surface morphology and cleanliness (removal of polishing debris). Finally, the substrate was placed in the CVD reactor for diamond growth (base pressure ~10 mtorr). The microwave power used for film growth was 500 W. The source gas mixture was 0.5% CH$_4$ in 99.5% H$_2$ (v/v) with 10 ppm B$_2$H$_6$ added for boron doping. Ultrahigh purity (99.999%) CH$_4$ (AGA Specialty Gas, Cleveland, OH) and H$_2$ (BOC Group, Inc., Murray Hill, NJ) were used as the source gases. The gas

mixture was supplied to the reaction chamber at a flow rate of 197 sccm for H_2, 1.00 sccm for CH_4, and 2.00 sccm for the 0.1% B_2H_6 (Matheson) in H_2 to achieve a 10 ppm boron gas phase concentration and a 200 sccm total flow rate. Diamond was deposited for 10 h. The growth temperature was estimated by optical pyrometry to be between 700 and 800 °C. After deposition, the CH_4 and B_2H_6 gas flows were stopped (plasma still ignited) and the films remained exposed to an H_2 plasma (atomic hydrogen) for 10 min under the deposition conditions. The samples were cooled in the H_2 plasma to a temperature less than 400 °C by slowly reducing the power and pressure over a 15 min period.

Microcrystalline boron-doped diamond thin-film on Si substrate (diamond/Si) was grown on a p-type Si (100) substrate ($\sim 10^{-3}$ Ω-cm, Virginia Semiconductor Inc., Fredricksburg, VA). The substrate ($0.1 \times 1 \times 1$ cm^3) was first cleaned sequentially with ultrapure water, methanol, and acetone, and then hand polished on a felt pad for 5 min with 0.1 μm diam. diamond powder (GE Superabrasives, Worthington, OH) mixed with ultrapure water. The substrate was then ultrasonically cleaned in acetone, isopropanol and ultrapure water (5 min each) to remove the polishing debris. The clean scratches and residual diamond particles serve as the initial nucleation sites for diamond growth. The growth conditions for diamond/Si were the same as those for diamond/Ti described above except that the microwave power used for diamond/Si growth was 1000 W. The resulting film properties (thickness, resistivity, carrier concentration and hole mobility) are listed in Table 2.1. The boron dopant concentration was determined from boron nuclear reaction analysis measurements of other films grown in an

29

identical manner. The film resistivity was measured with a tungsten four-point probe.

Table 2.1   Typical microcrystalline boron-doped diamond thin film properties[1,2].

Microcrystalline Diamond Electrode	
Film Thickness	5-7 μm
Resistivity	≤ 0.05 Ω-cm
Carrier Concentration	~ 1 × 10^{20} cm^{-3}
Carrier Mobility	1-10 cm^2/V-s

2.2 Material Characterization

The physical, chemical and electrochemical properties of the diamond/Ti electrode were probed by scanning electron microscopy, Raman spectroscopy, X-ray diffraction analysis, electrical measurements and electrochemical measurements.

2.2.1 Scanning Electron Microscopy (SEM)

The film morphology was probed by SEM using a S-4500 Hitachi electron microscope equipped with LaB$_6$ emitter at an accelerating voltage of 15 kV or a JSM-6300 F electron microscope (JEOL, Ltd., Tokyo, Japan) at an accelerating voltage of 10 kV. A 15 mm working distance was used for imaging the secondary and backscattered electrons. The electrodes were affixed to an aluminum specimen stub using double-sided carbon tape.

2.2.2 Raman Spectroscopy

The microstructure of diamond/Ti electrodes was evaluated by Raman spectroscopy. Spectra were obtained at room temperature using a Chromex RAMAN 2000 spectrograph (Chromex, Inc., Albuquerque, NM). The instrument consisted of a diode-pumped, frequency-doubled CW Nd:YAG laser (50 mW at 532 nm, COHERENT), a Chromex 500is spectrometer (f/4, 1200 grooves/mm holographic grating), and a thermoelectrically-cooled, 1024 × 256 element charge-coupled device (CCD) detector (ANDOR Tech., Ltd.). Spectra were collected with an incident power density of ca. 50 kW/cm^2 (10 mW at the sample and 5 μm diameter spot size) and a 10-s integration time. A white-light spectrum was collected under the same conditions and used as the background to which to reference the film spectra. The Raman instrument was calibrated by the spectrum of 4-acetamidophenol and the diamond scattering was calibrated using a high-pressure, high temperature (HPHT), single crystal diamond sample (first order phonon position = 1332 cm^{-1}).

2.2.3 X-Ray Diffraction Spectroscopy (XRD)

The crystallinity of diamond/Ti electrode was studied by XRD. Spectra were obtained by a Rigaku Rotaflex RTP300 RC diffractometer equipped with a rotating anode and a Cu Kα radiation source (1.540 Å) scanning 2θ from 30 to 90°.

2.2.4 Electrical Measurements

The electrical resistivity of diamond electrodes was measured using a tungsten tip, four-point probe connected to an analog multimeter (HP 3478A, Hewlett-Pachard, Palo Alto, CA), which was operated in a four-wire resistance measurement mode. The probe spacing was 0.1 cm. A constant current was applied between the outer two probes, the voltage drop between the inner two probes was measured. The measured resistance, R, from the I-V data was converted to a resistivity, ρ, according to the equation:

$$\rho \ (\Omega \cdot cm) = 4.532\,l\,R\ (\Omega)$$

where l is the film thickness (cm). Multiple measurements were usually made at different locations on film.

2.2.5 Electrochemical Characterization

Cyclic voltammetry was used to access the electrochemical properties of the diamond/Ti electrode. Two redox systems, $Fe(CN)_6^{3-/4-}$ and $Ru(NH_3)_6^{3+/2+}$, were used. Prior to a measurement, the diamond electrode was soaked in distilled isopropanol for at least 20 min and dried with N_2. The electrode was pressed against a Viton® o-ring (0.22 cm^2) and clamped to the bottom of the cell. Ohmic contact was made to the backside of the conducting Si substrate with a Cu plate. Before contact, the Si substrate surface was scratched, cleaned and coated with graphite or colloidal Ag paint. The copper plate was secured against the back of the electrode using a clamp to assure a good electrical connection to the electrode. The cell is shown in Figure 2.2. The cell was housed in a Faraday

cage for electrical shielding. All of the electrochemical measurements were performed using a CH instruments Model 650A electrochemical workstation (CH Instruments, Inc., Austin, TX) with a Ag/AgCl reference electrode (4 M NaCl, $E^{o'}$ = -45 mV vs. SCE) and a graphite rod counter electrode. All measurements were made in solutions purged with N_2 for at least 15 min and at room temperature (25 ± 1 °C).[2] The solution remained blanketed with N_2 at all times.
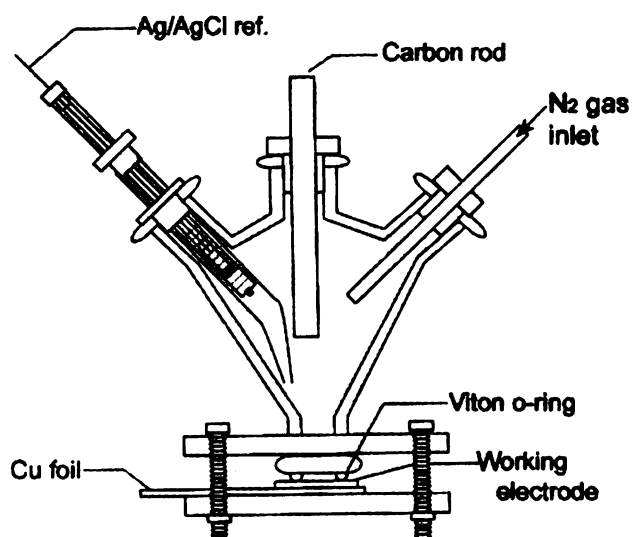
Figure 2.2 Design of the single compartment three-electrode electrochemical cell. (Reproduced with permission from *Anal. Chem.* **2000**, *72*, 3793-3804. Copyright 2000 American Chemical Society.)

2.3 Water Treatment

The degradation of atrazine was used to evaluate the effectiveness of the diamond/Ti electrode for oxidative decontamination. Oxidation reaction products were monitored by HPLC. The final degradation product, CO_2, was determined

by measuring the radioactivity of a ^{14}C-labeled atrazine solution.

2.3.1 Electrolysis of Atrazine

Atrazine (ATZ) electrolysis was performed in an H-cell using a diamond/Ti anode at constant current as shown in Figure 2.3. The glass cell consisted of two compartments separated by a porous glass frit, which allowed for ion transport but inhibited bulk solution mixing. The cell volume in the anolyte and catholyte compartments was ca. 6 mL each. A commercial Ag/AgCl (4 M KCl, Cypress Systems, Inc.) electrode was used as the reference and was positioned in the anolyte compartment. A diamond/Ti electrode was used as both the working and counter electrodes. The electrodes were pressed against a Viton® o-ring (i.d. 4.5 cm^2) at the opening of each compartment using a metal clamp. A constant current was applied by a Model 273 potentialstat/galvanostat (EG&G).
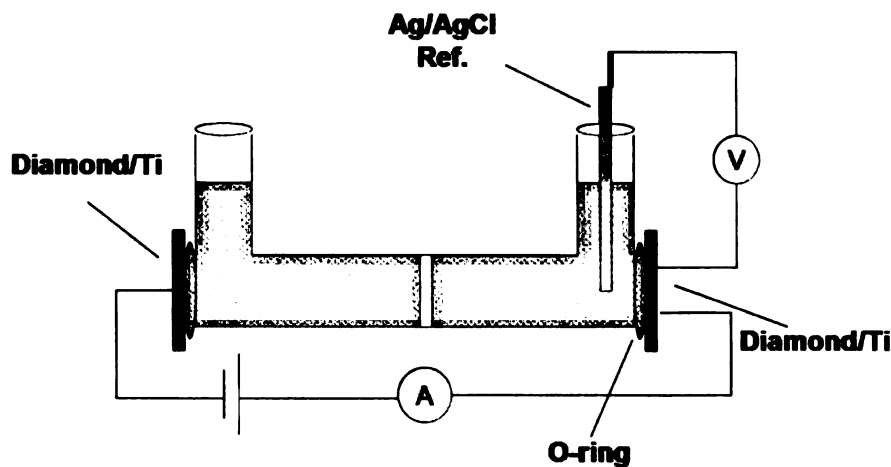
Figure 2.3   Design of the two-compartment H-cell for atrazine electrolysis.

Prior to electrolysis, the catholyte compartment was first filled with 6 mL of

0.1 M H_2SO_4 and then the anolyte compartment was filled with 6 mL of 0.1 M H_2SO_4 solution containing 5 ppm of ATZ. This is about the highest concentration that can be solubilized in the solution. The electrolysis was conducted for 120 min using a constant current of 50 or 100 mA. The concentrations of ATZ and its three major metabolites, hydroxyatrazine (HA), deethylatrazine (DEA) and deisopropylatrazine (DIA), were monitored by HPLC every 20 min during the electrolysis. After each electrolysis period, the solution in the anolyte compartment was quantitively removed and 1.0 mL of this solution was mixed with 1.0 mL of 0.05 M phosphate buffer (pH 3.5) in acetonitrile (60/40 v/v). 20 μL of the resulting solution was then injected into an HPLC system for separation and detection. A fresh ATZ solution was used for each electrolysis period. The experimental details of the HPLC system and analysis are given below.

2.3.2 Separation and Detection of Atrazine and Metabolites by HPLC-UV/Vis

A Shimadzu UV-2401 PC UV/Vis spectrophotometer was used to measure the optical absorption of ATZ, hydroxyatrazine (HA), deethylatrazine (DEA) and deisopropylatrazine (DIA). The maximum absorbance for all four was found to be around 216 nm so this wavelength was used for analysis. Reversed-phase HPLC with UV/Vis detection at 216 nm was performed using a home-made system consisting of a Milton Roy ConstaMetric III metering pump, an Adsorbosphere HS C_{18} column, (150 mm×4.6 mm, 5 μm particle size), a Shimadzu SPD-6AV UV-Vis spectrophotometric detector and an XYT strip chart

recorder. Separation was performed isocratically in a solution of 0.05 M phosphate buffer (pH 3.5) mixed with acetonitrile at a volumetric ratio of 60/40. This ratio was carefully selected to achieve the best separation of the compounds. The mobile phase flow rate was 1.0 mL/min.

2.3.3 Electrolysis of ^{14}C-Labeled Atrazine

To determine the oxidative conversion efficiency to CO_2, ^{14}C-ring-labeled ATZ was electrolyzed and the $^{14}CO_2$ produced was trapped in a 0.1 M KOH solution. For these experiments, all openings of the cell were sealed so as to eliminate gas escape. A syringe needle directed the gas generated from both compartments to a CO_2 trap (0.1 M KOH) through rubber tubing, as shown in Figure 2.4. The CO_2 trap was sealed with a balloon. 30 µL of ^{14}C-labled ATZ (stock solution in methanol, 2.2 g/L) was added to a solution containing 5 ppm ATZ and 0.1 M H_2SO_4. 6 mL of this mixed solution was then added to the anolyte compartment and 6 mL of 0.1 M H_2SO_4 was added to the catholyte compartment of the H-cell. Bulk electrolysis was conducted as described above. A constant current (50 or 100 mA) was delivered with a DC power supply (Model WP 711 A, VIZ MFG Co.). The conversion efficiency to CO_2 was monitored by dividing the radioactivity of the KOH trap solution by the total radioactivity of the ATZ solution before electrolysis. The radioactivity of the solution was determined in a ready-to-use high flash point safety-solve counting cocktail (Research Products International Corp.) using a 1500 Tri-Carb liquid scintillation Analyzer (LSA) (Packard Instrument Company).
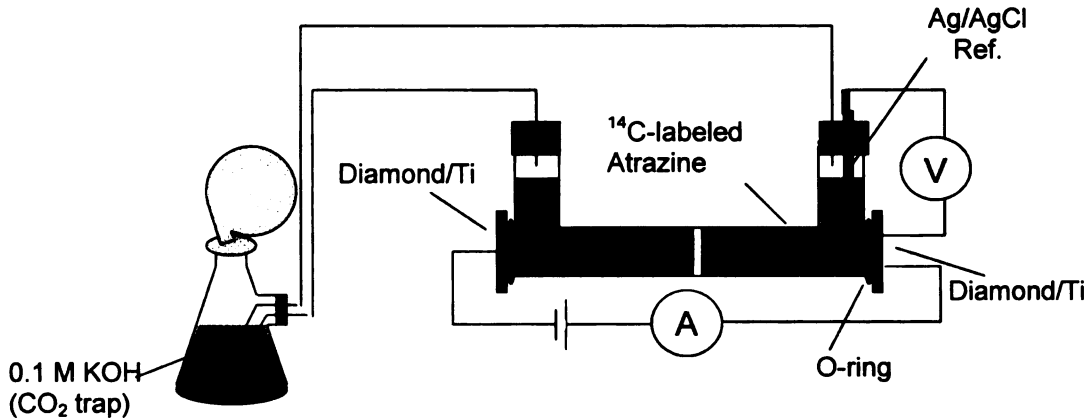
Figure 2.4 Design of the two-compartment H-cell for the ^{14}C-labeled atrazine analysis.

2.4 Water Quality Monitoring

2.4.1 Gold and Arsenic Electrodeposition

A Au-coated diamond/Si electrode was used to monitor the inorganic arsenic concentration in water supplies. The deposition of Au and As was performed by an amperometric method. Four electrodes, all grown in one batch, were used for these studies. One electrode was bare, another was coated with As for 90 s at -0.45 V from a solution containing 10 ppm As(III) in 1 M HCl, another was coated with Au for 90 s at -0.45 V from a solution containing 10 ppm Au(III) in 1 M HCl and another was coated with Au and As for 90 s at -0.45 V from a solution containing 10 ppm As(III) and 10 ppm Au(III) in 1 M HCl. After deposition, the electrodes were carefully rinsed with ultrapure water and dried with N$_2$. They were then attached to a specimen stub for SEM analysis using

double-sided carbon adhesive tape. A JSM-6300F scanning electron microscope (JEOL, Ltd., Tokyo, Japan) was used with an accelerating voltage of 10 kV to obtain the surface images of these electrodes. Particle size and density were determined using the AnalySIS imaging software (Software Imaging System Corp., Lakewood, CO). All particle analysis data are reported as a mean ± standard deviation.

2.4.2 Preparation of Au-Coated Diamond and Planar Au Electrode

Au-coated diamond electrode was used for arsenic detection. No pretreatment was applied to the diamond electrode prior to use other than a 15 min soak in distilled isopropanol. 100 ppb of $AuCl_3$ was added to the solution containing 1 M HCl and arsenic before detection. Au was co-deposited with As at a deposition potential of -0.45 V vs. Ag/AgCl for 120 s.

The performance of a planar Au electrode was compared with that of a Au-coated diamond electrode for arsenic analysis. The Au foil was supported on a 1×1 cm^2 piece of glass and polished under clean conditions using 0.05 μm diameter (deagglomerated) alumina powder slurried in ultrapure water for 15 min prior to use. The electrode was then rinsed and ultrasonically cleaned in ultrapure water and 0.1 M H_2SO_4 for 3 min each to remove polishing debris. The planar Au electrode was not repolished between measurements.

2.4.3 Differential Pulse Anodic Stripping Voltammetry (DPASV)

Differential pulse anodic stripping voltammetry (DPASV) method was used for arsenic analysis. The same electrochemical instrumental set-up was used as described above. The typical measurement with the Au-coated diamond or glassy carbon electrode consisted of 3 steps: (i) a 120 s deposition at -0.45 V (vs. Ag/AgCl) to preconcentrate the As, (ii) a differential pulse anodic scan (stripping step) from -0.45 to 0.5 V using a 4 mV step height, a 50 mV pulse amplitude, a 50 ms pulse width and a 200 ms cycle period and (iii) a constant potential of 0.6 V for 180 s after completion of the anodic sweep to fully oxidize all metal deposits prior to the next measurement. The typical analysis with the Au foil was the same except that the optimum deposition potential was -0.15 V. For codeposition on diamond and glassy carbon, a solution containing both As(III) and Au(III) was added to the cell. Standard addition was employed to determine the detection figures of merit and the As(III) concentration in the unknown solutions. All data are reported as mean ± standard deviation. All the DPASV *i-E* stripping voltammograms were background corrected.
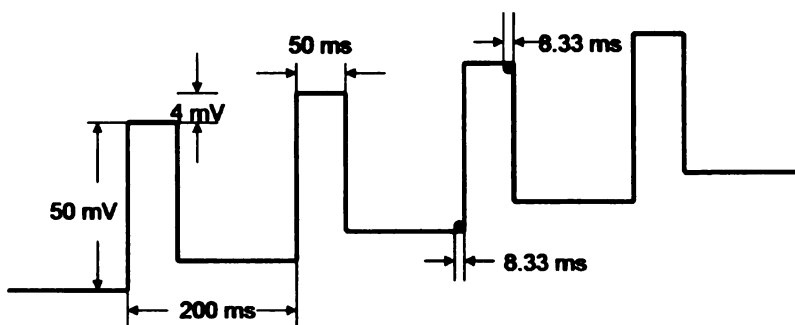
Figure 2.5   The differential pulse anodic stripping voltammetric potential

waveform and parameters.

2.4.4 Stability Test in River Water

The response reproducibility and stability of a Au-coated diamond and a planar Au electrode were evaluated in spiked river water samples. For real water analysis, samples were collected from the Red Cedar River (Lansing, MI, March 2005) using a 500 mL Nalgene bottle. Each bottle was rinsed with the river water three times before collecting a sample. It was then sealed, labeled and stored in a plastic bag until time for analysis. Prior to measurement, the river water was filtered by passage through a sterilized 0.22 μm PES (polyethersulfone), low protein binding membrane (Corning Incorporated Filter System). 250 mL of the filtrate was then acidified to pH 0 by adding 20.5 mL of 37% HCl. The reproducibility and long-term response stability of the Au-coated diamond was assessed using acidified Red Cedar River water (1 M HCl) spiked with 20 ppb As(III). Au-coated diamond and glassy carbon electrodes were compared under the same conditions. A run-to-run reproducibility test was performed over 10 consecutive measurements. Longer term stability studies were carried out by leaving the electrode exposed continuously to the As(III) solution for 10 h and periodically measuring the As stripping peak current (each hour). The relative standard deviation of peak current and peak charge was then calculated and reported.

2.4.5 Cation Exchange Method to Remove Interfering Metal Ions

A cation exchange method was developed for the removal of metal ions that interfere with arsenic detection. Water samples containing As(III) or As(V) and other metal ions were passed through the sorbent. This was performed using an Alltech vacuum manifold consisting of a glass chamber, a vacuum gauge and valve, manifold lid, and stopcocks. 1.0 g of a Chelex 100 cation exchange resin (50-100 dry mesh, Sigma) was packed into a 3 mL cartridge (Supelco). The cartridge was then conditioned by 10 bed volumes (~ 30 mL) of ultrapure water before use at a flow rate of ~ 5 mL/min. After conditioning, the solid phase was dried under vacuum for 5 min prior to introducing the analyte solution. The analyte solution (5 mL) was then added and immediately pulled through the cartridge by vacuum at a constant flow rate of ~ 5 mL/min. The solution passing through the solid phase contained the inorganic arsenic for analysis.

2.4.6 Detection of As(V)

The detection of As(V) consisted of two steps: (i) a chemical reduction from As(V) to As(III) and (ii) DPASV detection of reduced As(V). Na_2SO_3 was used as the reducing agent because it did not interfere with the electrochemical detection and had high conversion efficiency in reasonable reaction time. 4 mL of an As(V) solution in 1 M HCl was added to 0.01 g Na_2SO_3 (~ 20 mM) in a sealed plastic test tube. The solution was then heated in an oven (VWR Scientific, VWR 1410) at 50 °C for 30 min. Na_2SO_3 was used as the reducing agent, converting As(V) to As(III) by the following reactions:

$$Na_2SO_3 + 2\ HCl \rightarrow 2\ NaCl + H_2SO_3$$

41

$$H_3AsO_4 + H_2SO_3 \rightarrow H_3AsO_3 + H_2SO_4$$
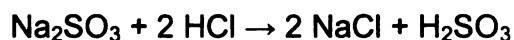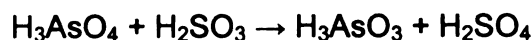
After cooling the solution to room temperature, ASV was performed as described above.

2.4.7 Inductively Coupled Plasma Mass Spectrometry (ICP-MS) and Graphite Furnace Atomic Absorption Spectroscopy (GFAAS)

The results obtained by DPASV method were compared with those obtained by ICP-MS and GFAAS. An inductively-coupled plasma mass spectrometer (Micromass Platform ICP-MS), fitted with a hexapole collision cell, was used for the measurements. A Meinhard concentric nebulizer was used for sample introduction. The As(III) concentration was determined from a response curve generated using a series of standard solutions of known As(III) concentration. Each standard was prepared from a 1000 ppm commercial stock solution of As(III) (Spex Certiprep, Metuchen, NJ) diluted with 2% HNO_3. For the analysis, 2 mL of the standard solution was transferred to a sample tube containing 2 mL of a 10 ppb In(III) internal standard. A measurement time of 1 min was used for each sample. The torch was thoroughly rinsed with 2% HNO_3 between measurements. The response curve for calibration was generated using peak intensities. For the GFAAS measurements, a Hitachi Z-9000 spectrophotometer with a graphite tube furnace attachment was used. The instrument possessed a diffraction grating monochromator, which was set to 195 nm for monitoring arsenic. Hitachi arsenic hollow cathode lamp was used with

emission wavelengths of 195 nm. The lamp current was set at 10 mA. The sheath gas flowing through the tube furnace was argon at 200 mL/min. A 20 μL sample volume was introduced into the furnace via an auto injector. The sample was dried and ashed using manufacturer-specified times and temperatures. The experimental parameters are summarized in Table 2.2. Calibration was accomplished by recording the responses for standard solutions containing known concentrations of arsenic.

Table 2.2   Detection conditions for arsenic analysis using GFAAS.

Lamp Current	10 mA
Wavelength	195 nm
Slit	1.2 nm
Carrier Gas	200 mL/min
Carrier Gas in Atomization	30 mL/min
Sample Volume	20 μL

2.4.8 Total Inorganic Arsenic Detection in Real Water Samples

Well water samples (Well 119 water and UV plant influent) from two contaminated sites were provided by the U.S. Bureau of Reclamation. The samples were received after being acidified with HNO_3 to a pH of ~2. The samples contained no visible sediment so filtration was not performed. The samples were first neutralized by adding solid NaOH to adjust the pH to > 4. Then, 4 mL of the solution was passed through the cation exchange cartridge, as

described above, to remove interfering metal ions. 2 mL of this solution passing through was collected and mixed with 2 mL of 2 M HCl. After adding 0.01 g Na_2SO_3, the solution was then mixed and heated at 50 °C for 30 min to convert the As(V) to As(III). Minimal volume change occurred during this period. After cooling to room temperature, the solution was ready for analysis by DPASV, as described above. Quantification of the total inorganic arsenic was accomplished by the standard addition method. The procedure used for analyzing the water samples is illustrated in step-wise fashion in Figure 2.6.

```
┌─────────────────────┐
│ Water sample        │
│ acidified with HNO₃ │
│ to pH = 2           │
└─────────────────────┘
          │
          ▼
┌─────────────────────┐
│ Adjusted to pH > 4.0│
│ by adding solid NaOH│
└─────────────────────┘
          │
          ▼
┌─────────────────────┐
│ Passed through a    │
│ cation exchange     │
│ resin               │
└─────────────────────┘
          │
          ▼
┌──────────────────────────────┐
│ Collected solution and       │
│ acidified with               │
│ 2 M HCl (1:1 v/v)            │
└──────────────────────────────┘
     As(III)            As(V)
     analysis           analysis
      /                      \
┌──────────────────┐   ┌──────────────────┐
│ Detected As(III) │◄──│ Reduced As(V) to │
│ by DPASV with a  │   │ As(III) by adding│
│ Au-coated        │   │ Na₂SO₃ and       │
│ diamond electrode│   │ heating at 50 °C │
│                  │   │ for 30 min       │
└──────────────────┘   └──────────────────┘
          \
           ▼
      ┌──────────────────┐
      │ Standard addition│
      │ used to determine│
      │ the arsenic      │
      │ concentration    │
      └──────────────────┘
```

Figure 2.6   Total inorganic arsenic detection in real water samples.

2.5 Reagents

All chemicals were analytical-grade quality, or better, and were used without additional purification. All solutions were prepared with 18 MΩ·cm ultrapure water (Barnstead E-pure).

For the water treatment experiments, the chemicals and suppliers were as follows: atrazine [2-chloro-4-ethylamino-6-isopropylamino-s-triazine] (97.2%, Crop Protection, Inc.); hydroxyatrazine [2-hydroxy-4-isopropylamino-6-ethylamino-s-triazine] (97%, Crop Protection, Inc.); deethylatrazine [2-amino-4-isopropylamino-6-chloro-s-triazine] (94%, Crop Protection, Inc.); deisopropylatrazine [amino-2-chloro-6-ethylamino-s-triazine] (96%, Crop Protection, Inc.); ^{14}C-ring-labeled atrazine (100 uci, Sigma); HPLC grade acetonitrile (EMD Chemicals Inc.); sulfuric acid (98%, Aldrich); phosphoric acid (Aldrich); potassium phosphate monobasic (Spectrum Chemical Mfg. Corp.) and isopropanol (Columbus Chemical Industry Inc.). All glassware was cleaned in a KOH-ethanol bath followed by thorough rinsing with ultrapure water.

For the water quality monitoring experiments, all glassware was acid washed sequentially in 1 M HCl (reagent grade) and 1 M HNO_3 (reagent grade), followed by rinsing thoroughly with purified water before use. The chemicals and materials used were arsenic trioxide (As_2O_3, Aldrich, 99.95%-100.0%), arsenic pentaoxide (As_2O_5, MV Laboratories, Inc., 99.999%), gold foil (Au, Aldrich, 0.1 mm thick, 99.99%), sodium hydroxide (NaOH, Spectrum Quality Products, Inc. Reagent A.C.S.), hydrochloric acid (HCl, Aldrich, 37%, 99.999% purity), gold (III)

chloride (AuCl$_3$, Aldrich, 99.99+%), cupric nitrate (Cu(NO$_3$)$_2$, 99.999%, Aldrich), lead nitrate (Pb(NO$_3$)$_2$, 99.999%, Aldrich), mercuric acetate (Hg(CH$_3$COO)$_2$, 99.999%, Aldrich), sodium sulfite (Na$_2$SO$_3$, Columbus Chemical Industries, Inc., ACS grade), nitric acid (HNO$_3$, EM Science, Reagent A.C.S.), Chelex 100 sodium form ion exchange resin (50-100 dry mesh, Sigma), 3 mL cartridge (Supelco), and humic acid, sodium form (Aldrich).

2.6 References

(1)   Swain, G. M. In *Electroanalytical Chemistry*; Rubinstein, I., Ed.; Marcel Dekker, Inc.: New York, 2003; Vol. 22, pp 181-277.

(2)   Granger, M. C.; Witek, M.; Xu, J.; Wang, J.; Hupert, M.; Hanks, A.; Koppang, M. D.; Butler, J. E.; Lucazeau, G.; Mermoux, M.; Strojek, J. W.; Swain, G. M. *Analytical Chemistry* **2000**, *72*, 3793-3804.

CHAPTER 3

ELECTROCHEMICAL AND PHYSICAL PROPERTIES OF DIAMOND/Ti

3.1 Introduction

Ti is an attractive substrate material for diamond growth due to its low cost, good electrical conductivity and high mechanical strength.[1] However, compared with Si, Ti has received less attention as a substrate material due to the difficulty of depositing a high quality, crack-free and well adhering diamond film on Ti. In this work, we opted to use Ti as a substrate for the growth of conductive diamond film and to employ this electrode for wastewater treatment. In order to optimally remediate organic contaminants with a boron-doped diamond electrode on a Ti substrate (diamond/Ti), it is necessary to first characterize the electrochemical, morphological and microstructural properties of the diamond/Ti electrodes.

There are two challenges to depositing a well adhering, conductive diamond overlayer on Ti or Ti alloy.[2, 3] One is the severe embrittlement of Ti that can occur from the diffusion of hydrogen and carbon into the lattice to form hydrides and carbides during the early stages of deposition. The hydrides can erode the diamond surface and inhibit diamond growth.[4] Carbide formation competes with diamond nucleation and forms a layer on Ti preferentially to diamond nucleation. Although this carbide layer ensures good conductivity between the diamond and Ti, it can result in poor adhesion of the diamond layer.[5] The other challenge is the residual stress, primarily compressive in nature, that

develops from the difference in thermal expansion coefficients, as the coefficient for Ti (8.50×10^{-6} C^{-1}) is about 10 times larger than the coefficient for diamond (0.84×10^{-6} C^{-1}). Additionally, the thermal expansion coefficient of the TiC interfacial layer (7.42×10^{-6} C^{-1}) is significantly larger than the coefficient for diamond.[5] The compressive stress that is introduced into the diamond is detrimental to good film adhesion and leads to the formation of microcracks and even debonding if severe enough. The presence of any microcracks is critical for diamond electrochemical electrodes because the electrolyte solution can permeate them and reach the underlying metal substrate. Contact with solution combined with anodic electrode potentials can cause corrosion of the Ti through the formation of soluble Ti^{+2} and Ti^{+4} species and this leads to the debonding of the diamond overlayer.[1, 6]

Several factors are known to affect the adhesion of diamond to Ti during hot filament CVD growth, such as substrate temperature, filament temperature, filament substrate distance, the deposition temperature,[6] substrate surface roughness[7, 8] and boron concentration.[5] The substrate temperature determines the thickness of TiC layer. A high substrate temperature will cause the formation of a thick TiC layer and poor diamond film adhesion, while a low substrate temperature can cause the formation of sp^2 carbon and poor diamond quality and durability. An optimum substrate temperature was found to be about 850 °C.[6] High filament temperature, short filament-substrate distance and long deposition time tend to cause film debonding.[6] To prevent this effect, polishing the substrate before growth to increase the surface roughness can improve the adhesion

strength and decrease the internal stress within the film.[7, 8] Boron can positively influence diamond deposition on Ti as it was found to increase the diamond adhesion with Ti, facilitate diamond nucleation and inhibit the formation of a TiC layer by forming borides or carbo-borides in the interlayer.[5] Judicious choice of the growth temperature and control of the substrate morphology and chemistry through appropriate pretreatment are, therefore, of paramount importance.

An ideal anode for wastewater treatment should exhibit (i) a large overpotential for oxygen evolution, (ii) high electron-transfer rates for general redox reactions and (iii) morphological and microstructural stability as discussed in Chapter 1. Up to now, few studies have been performed comparing the diamond/Ti electrode properties before and after an electrolysis event.

It has been reported that diamond/Ti electrodes have a large working potential window of 2.5 to 4.7 V in acidic, neutral or alkaline solution.[5, 6, 9-11] However, in terms of the electrochemical activity, the reported cyclic voltammetric response for $Fe(CN)_6^{3-/4-}$, a common redox test system, is quasireversible to have ΔE_p values between 96 and 188 mV.[6, 12] The heterogeneous electron-transfer rate constant, k°_{app}, was calculated to be (1.0 ~1.5) × 10^{-3} cm/s,[11, 12] lower than a typical k°_{app} value for this system at high quality diamond (0.050 cm/s).[13] Moreover, a 3-4 fold decrease in response sensitivity was reported for diamond/Ti after 1 month of use[14] and a passivation layer was found after 10 cycles in 1 M H_2SO_4.[11] The passivation was probably caused by poor film adhesion, microcrack formation and debonding, and the subsequent formation of TiO_2 because of solution reaching the Ti substrate (i.e.,

the passivation layer).

In this Chapter, the physicochemical and electrochemical properties of the diamond/Ti electrode are compared before and after exposure to an anodic current of 22 mA/cm^2 for 50 h in 0.1 M H_2SO_4. Cyclic voltammetry was used to study the electrochemical activity of the electrode using two different redox systems, $Fe(CN)_6^{3-/4-}$ and $Ru(NH_3)_6^{3+/2+}$. The electrode morphology and microstructure were characterized by scanning electron microscopy (SEM), Raman spectroscopy and X-ray diffraction spectroscopy (XRD).

3.2 Results and Discussion

3.2.1 Electrochemical Properties of Diamond/Ti

Background cyclic voltammetric *i-E* curves can be very informative about the boron-doped diamond film quality. The technique provides information about the presence of nondiamond sp^2 carbon impurity at the surface, the electrode working potential window and the electrical conductivity. Figure 3.1 shows background cyclic voltammetric *i-E* curves for diamond/Ti and diamond/Si electrodes (same geometric area in each case) in 0.1 M H_2SO_4 at the scan rate of 100 mV/s. The curves for both electrodes are flat and featureless with a wide potential window and low background current. The flat and featureless curve shape is typical of high quality, hydrogen-terminated boron-doped diamond as the electrode is devoid of redox-active impurities, reactive sp^2 carbon and redox-active carbon-oxygen functional groups (e.g., quinone/hydroquinone) that will result in faradaic current and cause an increase of the background current.[15] For

wastewater treatment, a large overpotential for oxygen evolution is a useful property for an anode in terms of enabling high current efficiency during pollutant oxidation.
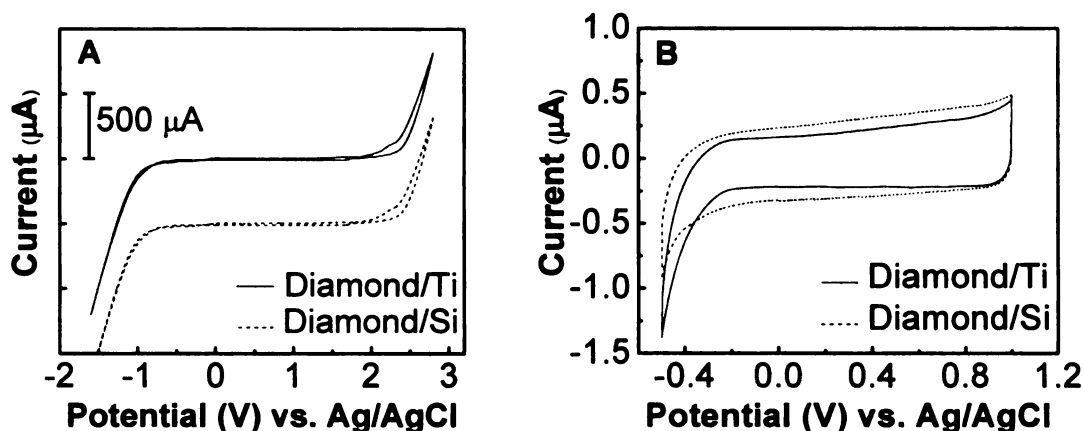
Figure 3.1 Background cyclic voltammetric *i-E* curves for diamond/Ti and diamond/Si electrodes in 0.1 M H_2SO_4 over a (A) wide and (B) narrow potential range. Scan rate = 100 mV/s. Geometric area = 0.2 cm^2.

Figure 3.1A shows that the working potential window for both electrodes is about 3.2 V. The onset of hydrogen evolution for diamond/Ti occurs slightly more positive of that for diamond/Si while the onset of oxygen evolution for both electrodes is greater than 2 V vs. Ag/AgCl. The potential window seen for this diamond/Ti electrode is comparable to what has been reported for diamond/Ti (2.5 to 4.7 V)[5, 6, 9-11] and is characteristic of good quality diamond. From Figure 3.1B, it is clear that the background current for both electrodes is low and featureless. The anodic current at 0.5 V was 0.25 µA for diamond/Ti and 0.34 µA for diamond/Si. In contrast, sp^2-bonded carbon and metal electrodes usually

52

have about 5-10 times higher background current. The low background current for diamond is due to a reduced pseudocapacitance because of the absence of redox-active and/or ionizable surface carbon-oxygen functional groups and a reduced capacitance due to a slightly lower internal charge carrier concentration.[15] The lower background current leads to improved signal to background ratio in electroanalytical measurements.

The diamond/Ti electrode response for two different redox systems, $Fe(CN)_6^{3-/4-}$ and $Ru(NH_3)_6^{3+/2+}$, was studied by cyclic voltammetry method. Redox reactions of $Fe(CN)_6^{3-/4-}$ and $Ru(NH_3)_6^{3+/2+}$ are redox systems that represent two major categories of heterogeneous electron-transfer reactions: inner-sphere (or surface sensitive) and outer-sphere (or relatively surface insensitive) reactions. Inner sphere redox reactions involve specific interaction with the electrode and heterogeneous electron-transfer rate constants are sensitive to surface cleanness and surface termination. $Fe(CN)_6^{3-/4-}$ proceeds through a more inner-sphere electron-transfer pathway. At diamond electrodes, the peak separation, ΔE_p, for $Fe(CN)_6^{3-/4-}$ is particularly sensitive to the surface chemistry.[16] The lowest ΔE_p is generally observed for the hydrogen-terminated surface, introducing surface oxygen can block the reactive surface sites, slow the electrode reaction kinetics and cause an increase in ΔE_p.[16] The apparent heterogeneous electron-transfer rate, k^o_{app}, for $Fe(CN)_6^{3-/4-}$ at a high quality diamond/Si is typically 0.01-0.1 cm/s.[16-21] Outer-sphere reactions do not involve interaction with the electrode and proceed by simple mass transport of the electrolyte to the electrode-solution interface, with the electrode only serving as a

source or sink of the electrons. $Ru(NH_3)_6^{3+/2+}$ proceeds through an outer-sphere electron-transfer pathway. ΔE_p for this redox system at carbon electrodes (e.g., diamond, glassy carbon and HOPG) is most sensitive to the electronic properties of the electrode, that is, the density of electronic states (electrons and holes) near the standard redox potential. ΔE_p of $Ru(NH_3)_6^{3+/2+}$ is less sensitive to factors such as the surface microstructure, surface chemistry and surface cleaness.[16] The most important factor controlling the density of electronic states in polycrystalline diamond is probably the boron-doping level, but other factors such as non-diamond sp^2 carbon impurity, defects, and lattice hydrogen may also be influential.[16] The lowest ΔE_p is generally seen for the high electron density surface with high electron-transfer rate constant. The apparent heterogeneous electron-transfer rate constant, k^o_{app}, for $Ru(NH_3)_6^{3+/2+}$ at a high quality diamond/Si is typically 0.01-0.2 cm/s.[16-21]

The electrochemical responses for $Fe(CN)_6^{3-/4-}$ and $Ru(NH_3)_6^{3+/2+}$ were evaluated at five different diamond/Ti electrodes in order to test the electrode activity and response reproducibility. Representative cyclic voltammetric i-E curves for diamond/Ti in 1 mM $Fe(CN)_6^{3-/4-}$ and $Ru(NH_3)_6^{3+/2+}$ in 1 M KCl are shown in Figure 3.2. A summary of the data is presented in Table 3.1. The voltammetric responses for these five electrodes are reproducible and stable from film-to-film. All five electrodes exhibited active responses for $Fe(CN)_6^{3-/4-}$ and $Ru(NH_3)_6^{3+/2+}$ without any conventional pretreatment (e.g., polishing); something that is normally required for sp^2-bonded carbon and metal electrodes.

Current (µA) / **Potential (V) vs. Ag/AgCl**
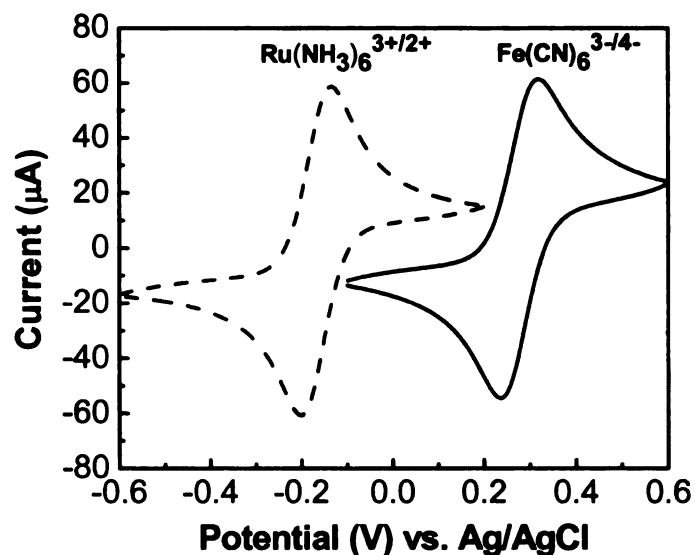
Ru(NH$_3$)$_6$$^{3+/2+}$ Fe(CN)$_6$$^{3-/4-}$

Figure 3.2 Cyclic voltammetric *i-E* curves for 1 mM Fe(CN)$_6$$^{3-/4-}$ and Ru(NH$_3$)$_6$$^{3+/2+}$ in 1 M KCl at a diamond/Ti electrode. Scan rate = 100 mV/s.

Table 3.1 Summary of cyclic voltammetric data for diamond/Ti electrodes at a scan rate of 100 mV/s.

Redox System	ΔE$_p$ (mV)	E$_{p/2}$ (mV)	i$_p$^{ox} (µA)	i$_p$^{ox}/i$_p$^{red}
Ru(NH$_3$)$_6$$^{3+/2+}$	76 ± 8	-188 ± 5	58 ± 5	1.0 ± 0.1
Fe(CN)$_6$$^{3-/4-}$	76 ± 5	251 ± 2	50 ± 16	1.0 ± 0.1

ΔE$_p$ for Fe(CN)$_6$$^{3-/4-}$ is 76 ± 5 mV (RSD = 7%) at 100 mV/s. The value is comparable with others reported for a diamond thin film on Si (65-70 mV at 100 mV/s)[20] and is smaller than values reported for diamond on Ti by other researchers (96-188 mV at scan rate of 20-200 mV/).[6, 11, 12, 14] The results for Fe(CN)$_6$$^{3-/4-}$ indicate that the diamond/Ti has a clean hydrogen-terminated

surface. ΔE_p for $Ru(NH_3)_6^{3+/2+}$ is 76 ± 8 mV (RSD = 11%) at 100 mV/s. This is comparable to values reported by Granger et al. for diamond thin films on Si (74 mV).[16, 22] The results for $Ru(NH_3)_6^{3+/2+}$ demonstrate that the diamond/Ti electrode possesses a density of electronic states sufficiently high to support rapid electrode reaction kinetics. ΔE_p values for both redox systems increased with increasing scan rate, which is consistent with quasireversible reaction kinetics. i_p^{ox} varied linearly with the scan rate$^{1/2}$ between 10 and 500 mV/s with a near zero y-axis intercept, as shown in Figure 3.3, indicating the current is limited by semi-infinite linear diffusion. The i_p^{ox}/i_p^{red} and Q_p^{ox}/Q_p^{red} ratios were near 1.0 as expected for reversible systems and the values were stable with cycling.
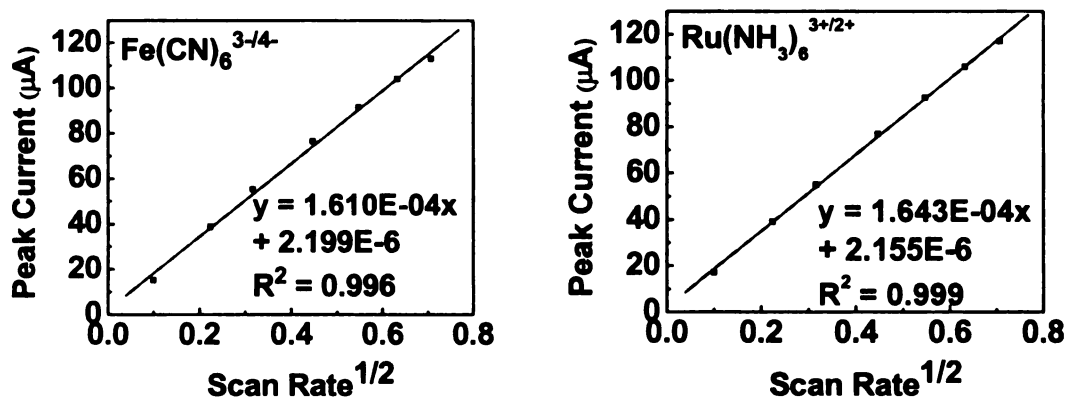
Figure 3.3   Plots of the anodic peak current versus the square root of scan rate for 1 mM $Fe(CN)_6^{3-/4-}$ and $Ru(NH_3)_6^{3+/2+}$ in 1 M KCl.

The electrode apparent heterogeneous electron-transfer rate constant, k^o_{app}, for $Fe(CN)_6^{3-/4-}$ and $Ru(NH_3)_6^{3+/2+}$ before and after a 50-h electrolysis at 22 mA/cm^2 in 0.1 M H_2SO_4 were compared and the results are listed in Table 3.2.

k^0_{app} was determined from cyclic voltammetric data (ΔE_p - v dependence) using a method developed by Nicholson.[17] According to the theory, ΔE_p for an electrochemical reaction is dependent upon the scan rate (v, V/s), transfer coefficient (α) and apparent heterogeneous electron-transfer rate constant (k^0_{app}, cm/s). He derived an equation for quasireversible reactions showing this relation:

$$\psi = \frac{\left(D_{ox}/D_{red}\right)^{\alpha/2}k^0_{app}}{\left(\pi D_{ox}fv\right)^{1/2}} \tag{3.1}$$

where D_{ox} and D_{red} (cm^2/s) are the diffusion coefficients of the oxidized and reduced forms of analyte, respectively, f is the Faraday constant divided by the ideal gas constant and temperature (F/RT) and Ψ is a dimensionless parameter. Nicholson derived an experimental relationship between Ψ and ΔE_p, so that k^0_{app} can be calculated from the above equation at different scan rates.[17]

Table 3.2 Cyclic voltammetric and the apparent heterogeneous electron transfer rate constant data for diamond/Ti electrodes for $Fe(CN)_6^{3-/4-}$ and $Ru(NH_3)_6^{3+/2+}$ in 1 M KCl before and after electrolysis in 0.1 M H_2SO_4 at 22 mA/cm^2.

	$Fe(CN)_6^{3-/4-}$		$Ru(NH_3)_6^{3+/2+}$	
	Before	**After**	**Before**	**After**
ΔE_p **(mV)**	83	99	71	75
Ψ	1.08	0.62	2.25	1.75
k^0_{app} **(cm/s)**	0.010	0.006	0.019	0.014

Before electrolysis, for both $Fe(CN)_6^{3-/4-}$ and $Ru(NH_3)_6^{3+/2+}$, the electrode

k°_{app} was near 0.01 cm/s. This value is consistent with others reported for diamond/Si (0.01-0.2 cm/s)[6, 11, 12, 14] and is higher than the values previously reported for diamond/Ti electrodes (1.94×10^{-4} to 1.5×10^{-3} cm/s).[7, 8, 11, 12, 14] The results indicate that prior to electrolysis, the diamond/Ti electrode surface is clean and hydrogen-terminated and possesses a sufficiently high density of electronic states to support rapid rates of electron-transfer. However, after a 50-h electrolysis at 22 mA/cm^2 in 0.1 M H_2SO_4, the k°_{app} value for $Fe(CN)_6^{3-/4-}$ decreased to 0.006 cm/s while k°_{app} for $Ru(NH_3)_6^{3+/2+}$ decreased only from 0.019 to 0.014 cm/s. Because the k°_{app} value for $Fe(CN)_6^{3-/4-}$ is very sensitive to the surface carbon-oxygen functional groups, the introduction of surface oxygen can inhibit this redox reaction presumably by blocking active sites. Surface oxygen typically causes an increase in ΔE_p, thus, a decrease of k°_{app} for this redox system.[16] During the electrolysis, hydroxyl radicals as well as oxygen are formed which leads to the incorporation of oxygen functional groups. The functional groups cause an increase in the $Fe(CN)_6^{3-/4-}$ ΔE_p and a decrease in the k°_{app}. Apparently, the density of electronic states on the surface does not change significantly because ΔE_p and k°_{app} for $Ru(NH_3)_6^{3+/2+}$ is fairly constant before and after electrolysis.

The cyclic voltammetry results indicate that the diamond/Ti electrode possesses the requisite surface structure, chemical composition and electronic properties to support relatively rapid electron transfer for these two redox systems. It is noteworthy that low ΔE_p values were observed even though the electrodes were exposed to the laboratory atmosphere for days to weeks prior to

use with no pretreatment applied for activation. The diamond electrode, due to the non-polar nature of the sp^3-bonded surface (absence of π electrons), is resistant to deactivation by contaminant adsorption and typically does not require pretreatment for activation.

3.2.2 Morphological and Microstructural Properties of Diamond/Ti

The morphological and microstructural stability of the diamond/Ti electrode during the 50-h electrolysis in 0.1 M H_2SO_4 (at 22 mA/cm^2) was evaluated. Characterization was performed with scanning electron microscopy (SEM), Raman spectroscopy and X-ray diffraction spectroscopy (XRD).

Figure 3.4A shows a typical SEM image of a diamond/Ti electrode prior to electrolysis. A well-faceted, polycrystalline diamond film completely covers the substrate with no sign of any cracks or pinholes. The film possesses a wide variety of crystallite sizes ranging from several micrometers down to several hundred nanometers. There is also considerable secondary nucleation observed as evidenced by the large number of smaller crystallites formed on the larger crystallites or in the grain boundaries between the larger crystallites. Clearly, the film grows via a more progressive nucleation mechanism across the metal surface. This probably is due to the spatial variability in the substrate morphology and chemistry as well as non-uniform seeding of diamond particles during the preparation of the electrode substrate for deposition. The diamond film has a rolling, undulating character to it, which tracks the topography of the underlying Ti

substrate. For comparison, an SEM image of a diamond/Ti electrode after 50 h of polarization at 22 mA/cm^2 in 0.1 M H_2SO_4 is shown in Figure 3.4B. The diamond film morphology was unaltered with no sign of cracks, pinholes or debonding. The observed dimensional stability is consistent with previous observations for diamond/Si electrodes.[19, 23-25] The SEM images confirm that the diamond/Ti electrode is morphologically stable during these electrolysis conditions.

Figure 3.4 SEM images of a diamond/Ti electrode (A) before and (B) after electrolysis in 0.1 M H_2SO_4 at 22 mA/cm^2 for 50 h.

Figure 3.5 shows the cross sectional SEM image of a diamond/Ti

electrode including three phases: diamond, a TiC layer and the Ti substrate. The thickness of the diamond film is about 10 μm which is typical for microcrystalline diamond films. The film is dense and homogeneous. The TiC layer is clearly observed between the diamond film and the Ti substrate. It is porous and rough with uneven thickness ranging from 5 to 20 μm. The TiC layer is formed by the diffusion of carbon atoms into the Ti substrate during the early stages of film growth. The formation of the TiC layer competes with diamond nucleation during the growth. The diamond nucleation can only occur after the saturation of the Ti surface with carbon and the carbide layer has certain thickness.[5, 26] Even though the TiC layer can cause the poor adhesion of the diamond layer, it is observed in most diamond/Ti films and its conducting property is important to ensure good electrical connection between the Ti substrate and the diamond coating.[12]
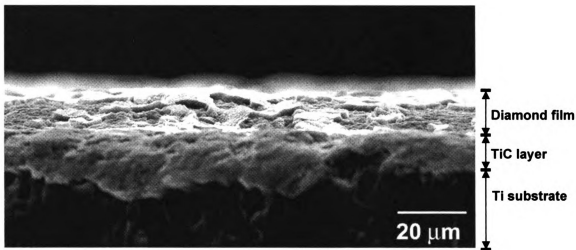
Figure 3.5 Cross sectional SEM image of a diamond/Ti electrode.

The microstructural quality and stability of the diamond/Ti film was

assessed by Raman spectroscopy. A typical Raman spectrum for the electrode prior to electrolysis is shown in Figure 3.6A.
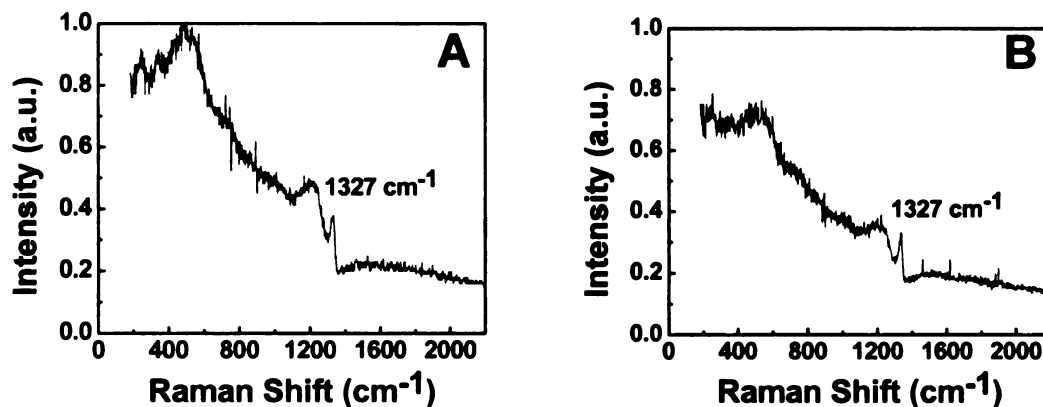
Figure 3.6 Raman spectra of diamond/Ti electrode (A) before and (B) after electrolysis in 0.1 M H_2SO_4 at 22 mA/cm^2 for 50 h.

The spectral features reflect a heavily boron-doped film and are quite different from those typical of a single crystal diamond reference sample. The apparent doping level in this film is $\geq 10^{20}$ cm^{-3} based on results from other groups who compared Raman spectra with actual doping levels.[3, 18, 27, 28] A weak first-order diamond phonon mode is seen at 1327 cm^{-1}. This peak is asymmetric and down-shifted from the expected position for a single crystal diamond at 1332 cm^{-1}. The weak intensity is attributed to the high optical density of the film due to the high doping level. The asymmetry is attributed to Fano-type interference, which is caused by a quantum interference between the phonon and a continuum of electronic transitions around the same energy involving the boron impurity band.[3] There is very weak scattering intensity between 1500 and 1600 cm^{-1},

which is associated with amorphous or nondiamond sp^2 carbon.[22] The sp^2 carbon (e.g., graphite) has a larger Raman scattering cross section than diamond so the weak intensity indicates that there is very little sp^2 carbon impurity in this film. A broad continuum exists toward lower wavenumbers with peaks at ca. 500 and 1200 cm^{-1}. These two maxima are often observed for heavily boron-doped films and their intensity tracks the boron-doping level.[3] The origin of the peak at 500 cm^{-1} was assigned to local vibrational modes of boron pairs by Bernard et al..[29-31] Disordered growth can result from a modification of the growth mechanism at the surface related to the high boron concentration.[3] The theoretical phonon density of state maximum for diamond occurs near 1200 cm^{-1},[3, 27] therefore, the peak is attributed to the disordered sp^3 bonding by the incorporation of the lighter boron.[3, 29-31] Gonon and coworkers proposed that these bands appear whenever a high concentration of impurities or defects is present.[27] This spectrum is characteristic of a heavily doped film, with the disorder in the diamond crystal structure resulting from the incorporation of boron.[32] Quite similar observations were reported by Gonon and coworkers[27] for boron-doped diamond on Si with a high doping level of 1.1×10^{21} B cm^{-3} and by Fryda and coworkers[32] for heavily doped diamond on metal substrates. Figure 3.6B shows a Raman spectrum of the diamond/Ti anode after a 50-h electrolysis (22 mA/cm^2) in 0.1 M H_2SO_4. No significant difference is observed in the spectral features suggesting that no microstructural changes occurred during the electrolysis.

The crystallinity of the diamond/Ti electrode before and after electrolysis

was examined by XRD. Figure 3.7A shows a typical diffraction pattern that reveals reflections for Ti, TiC and diamond. This is consistent with the three phases evidenced in the cross sectional SEM image shown in Figure 3.5. Peak assignments were made by comparing this diffraction pattern with patterns for Ti,[33] TiC[34] and cubic diamond standards[35] (shown in Figure 3.8, 3.9 and 3.10, respectively). The reference data for Ti, TiC and diamond are also summarized in Table 3.3, 3.4 and 3.5, respectively.

There are two primary diamond peaks present at 43.9 and 75.3 degrees (2θ) and are assigned to (111) and (220) reflections of cubic diamond. The relative intensity ratio of the (111) and (220) peaks in Figure 3.7A is 100/26 and is in good agreement with the expected ratio of 100/25 for cubic diamond.[35] This XRD pattern is in good agreement with that reported by Chen.[1] Figure 3.7B shows the XRD pattern for a diamond/Ti electrode after the 50-h electrolysis (22 mA/cm^2). Again, in terms of shape, no significant pattern changes are observed. The diamond, TiC and Ti peaks are still present, which indicates that the diamond film remained attached to the surface and that all these phases underwent no crystallographic changes during the electrolysis. The difference in signal intensity between the two XRD patterns is attributed to the fact that two different films were used. In summary, the characterization results indicate that the diamond/Ti electrodes are morphologically and microstructurally stable during these electrolysis conditions.
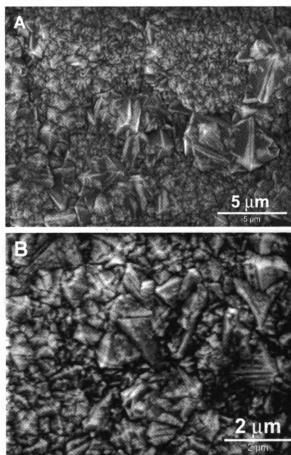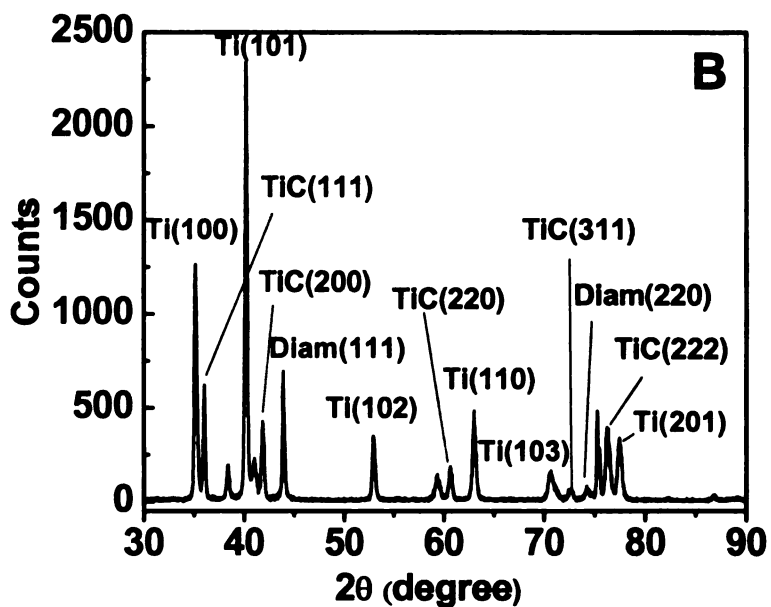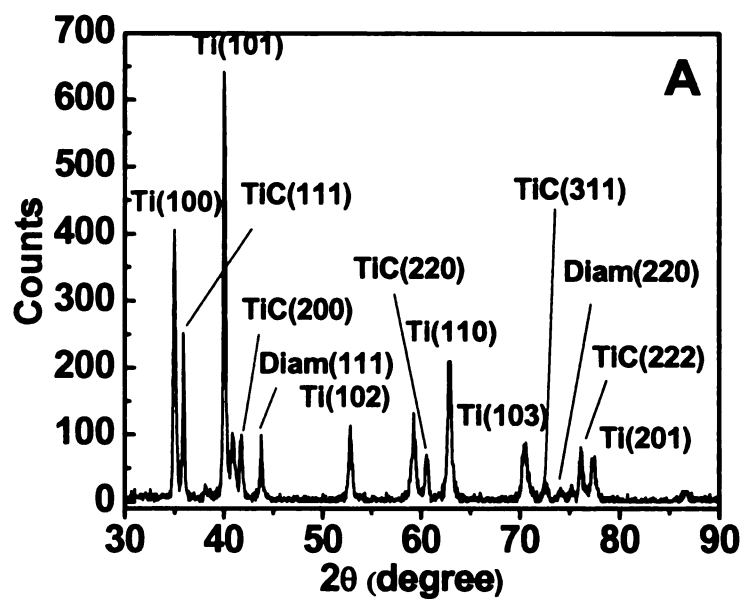
Figure 3.7 XRD pattern for a diamond/Ti electrode (A) before and (B) after electrolysis in 0.1 M H_2SO_4 at 22 mA/cm^2 for 50 h.
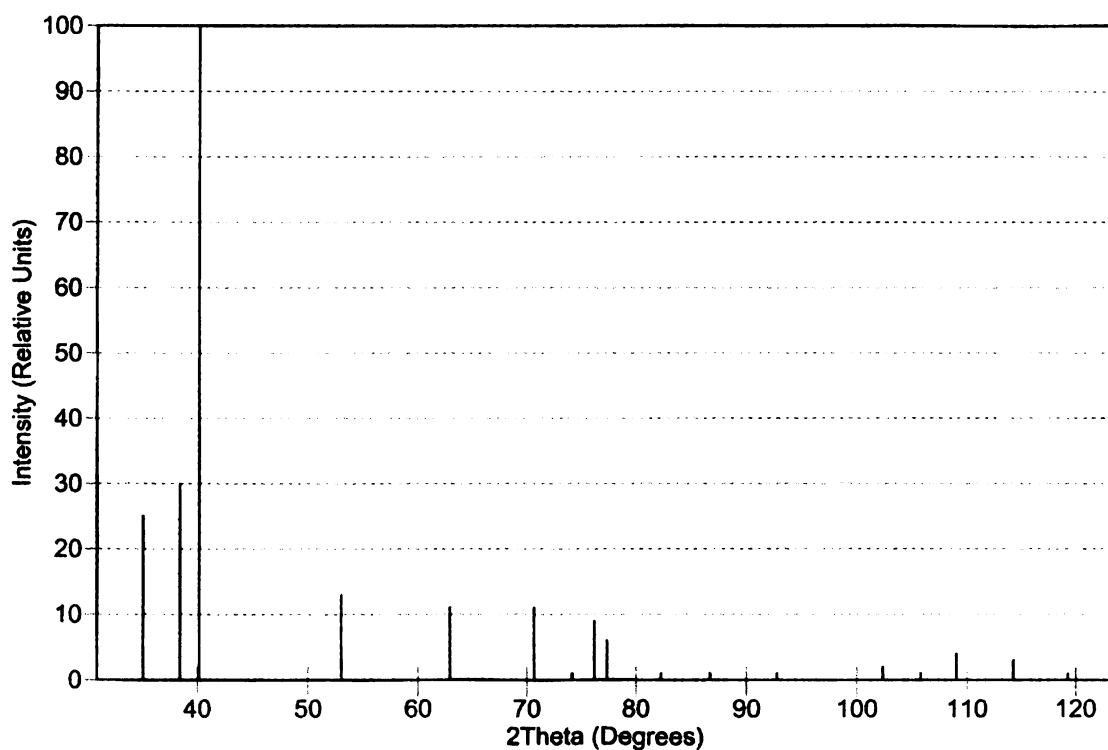
Figure 3.8   Standard XRD pattern for Ti.

Table 3.3   List of standard XRD pattern data for Ti.

2θ	d (Å)	Int-f	h	k	l	2θ	d (Å)	Int-f	h	k	l
35.093	2.5550	25	1	0	0	82.290	1.1707	1	0	0	4
38.421	2.3410	30	0	0	2	86.759	1.1215	1	2	0	2
40.170	2.2430	100	1	0	1	92.729	1.0643	1	1	0	4
53.004	1.7262	13	1	0	2	102.361	0.9887	2	2	0	3
62.949	1.4753	11	1	1	0	105.798	0.9658	1	2	1	0
70.660	1.3320	11	1	0	3	109.042	0.9459	4	2	1	1
74.157	1.2776	1	2	0	0	114.278	0.9170	3	1	1	4
76.218	1.2481	9	1	1	2	119.256	0.8928	1	2	1	2
77.368	1.2324	6	2	0	1						
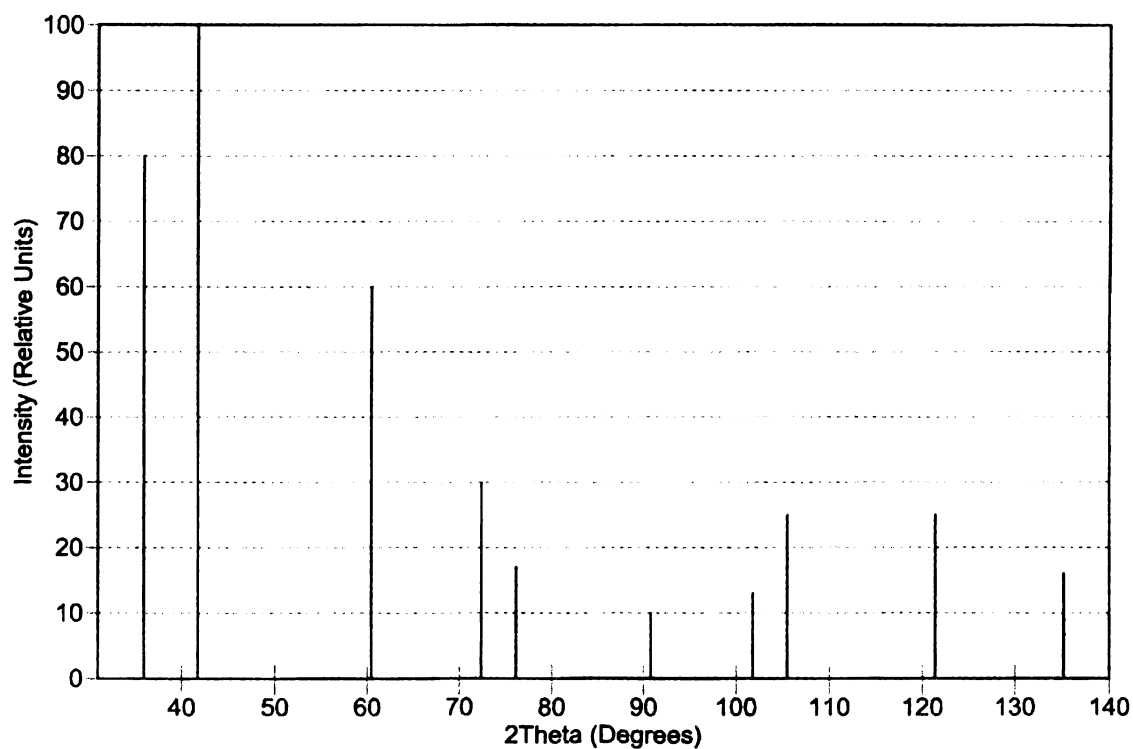
Figure 3.9   Standard XRD pattern for TiC.

Table 3.4   List of standard XRD pattern data for TiC.

2θ	d (Å)	Int-f	h	k	l
35.906	2.4990	80	1	1	1
41.710	2.1637	100	2	0	0
60.448	1.5302	60	2	2	0
72.369	1.3047	30	3	1	1
76.139	1.2492	17	2	2	2
90.802	1.0818	10	4	0	0
101.781	0.9927	13	3	3	1
105.498	0.9677	25	4	2	0
121.372	0.8834	25	4	2	2
135.348	0.8327	16	5	1	1
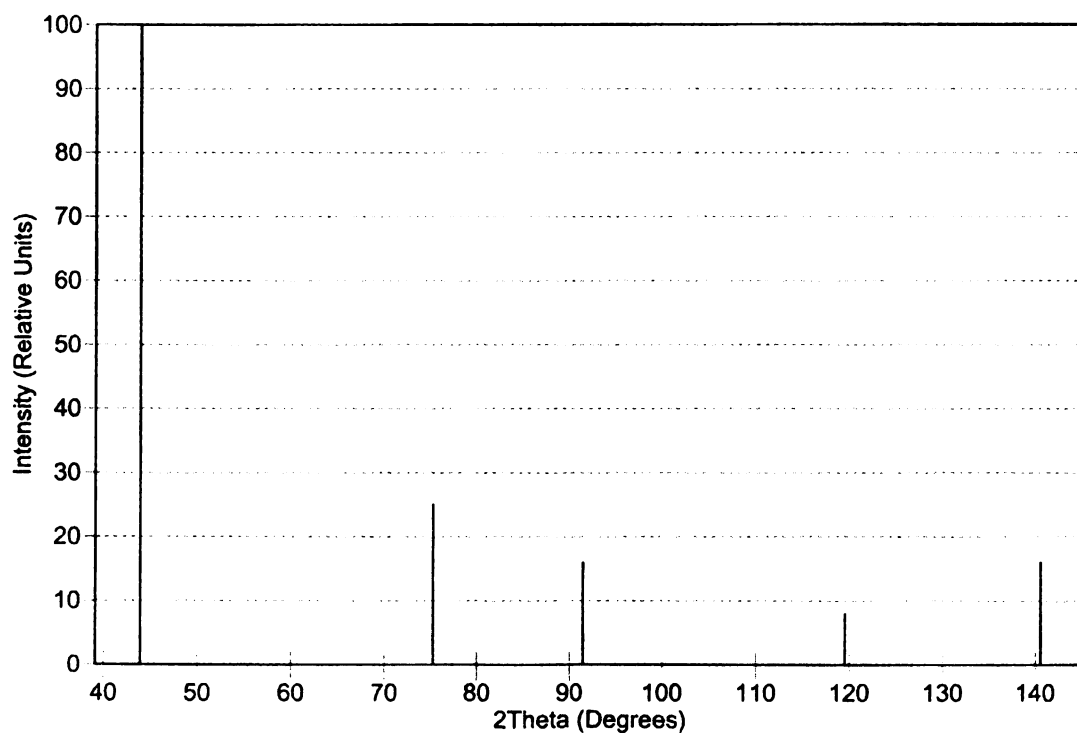
Figure 3.10 Standard XRD pattern for cubic diamond.

Table 3.5 List of standard XRD pattern data for cubic diamond.

2θ	d (Å)	Int-f	h	k	l
43.915	2.0600	100	1	1	1
75.302	1.2610	25	2	2	0
91.495	1.0754	16	3	1	1
119.521	0.8916	8	4	0	0
140.587	0.8182	16	3	3	1

3.3 Conclusions

The electrochemical and physical properties of the diamond/Ti electrode were investigated before and after 50 h of anodic polarization in 0.1 M H_2SO_4 at 22 mA/cm^2. Background cyclic voltammetric $i\text{-}E$ curves showed that the electrode was characterized by a featureless and low background current (e.g., 0.25 μA at 0.5 V vs. Ag/AgCl). This indicated the electrode surface was devoid of redox-active impurities, sp^2 carbon and carbon-oxygen functional groups. The diamond/Ti electrode also possessed a wide working potential window of 3.2 V, a property that is characteristic of good quality diamond. This value is comparable to that for diamond/Si electrodes and assures high current efficiency during pollutant oxidation. The electrode response for two redox probes, $Fe(CN)_6^{3-/4-}$ and $Ru(NH_3)_6^{3+/2+}$, for five electrodes was active and reproducible from film-to-film before and after electrolysis. ΔE_p for $Fe(CN)_6^{3-/4-}$ and $Ru(NH_3)_6^{3+/2+}$ were low with nominal value of 76 ± 5 mV and 76 ± 8 mV, respectively. These values are comparable with those reported for diamond/Si electrodes and lower than what have been reported for diamond/Ti. The results indicate that the diamond/Ti electrode is clean and hydrogen-terminated with density of high electronic states to support fast electron-transfer kinetics. No conventional pretreatment was required for activation. Apparent heterogeneous electron-transfer rate constants, k^o_{app}, for $Fe(CN)_6^{3-/4-}$ and $Ru(NH_3)_6^{3+/2+}$ before electrolysis were 0.010 and 0.019 cm/s, respectively. After electrolysis, k^o_{app} for $Fe(CN)_6^{3-/4-}$ decreased to 0.006 cm/s because of surface oxide incorporation on the electrode. k^o_{app} for $Ru(NH_3)_6^{3+/2+}$, though, was almost unchanged at 0.0144 cm/s after electrolysis.

While the electrolysis changed the electrode surface chemistry, it did not cause a major change in the density of electronic states. In other words, the electrodes remain highly conductive after the electrolysis. The SEM, Raman spectroscopy and XRD all confirmed that the diamond/Ti electrode was morphologically and microstructurally stable under the reported polarization conditions.

3.4 References

(1) Chen, X.; Chen, G.; Gao, F.; Yue, P. L. *Environmental Science and Technology* **2003**, *37*, 5021-5026.

(2) Fryda, M.; Herrmann, D.; Schafer, L.; Klages, C.-P.; Perret, A.; Haenni, W.; Comninellis, C.; Gandini, D. *New Diamond and Frontier Carbon Technology* **1999**, *9*, 229-240.

(3) AgerIII, J. W.; Walukiewicz, W.; McCluskey, M.; Plano, M. A.; Landstrass, M. I. *Applied Physics Letters* **1995**, *66*, 616-618.

(4) Baranauskas, V.; Ceragioli, H. J.; Peterlevitz, A. C.; Fontana, M. *Surface and Coatings Technology* **2005**, *200*, 2343-2347.

(5) Gerger, I.; Haubner, R.; Kronberger, H.; Fafilek, G. *Diamond and Related Materials* **2004**, *13*, 1062-1069.

(6) Chen, X.; Chen, G. *Journal of the Electrochemical Society* **2004**, *151*, B214-B219.

(7) Pleskov, Y. V.; Evstefeeva, Y. E.; Krotova, M. D.; Lim, P. Y.; Shih, H. C.; Varnin, V. P.; Teremetskaya, I. G.; Vlasov, I. I.; Ralchenko, V. G. *Journal of Applied Electrochemistry* **2005**, *35*, 857-864.

(8) Pleskov, Y. V.; Evstefeeva, Y. E.; Krotova, M. D.; Lim, P. Y.; Chu, S. S.; Ral'chenko, V. G.; Vlasov, I. I.; Kononenko, V. V.; Varnin, V. P.; Teremetskaya, I. G.; Shi, H. C. *Russian Journal of Electrochemistry* **2005**, *41*, 337-345.

(9) Beck, F.; Krohn, H.; Kaiser, W.; Fryda, M.; Klages, C. P.; Schafer, L. *Electrochimica Acta* **1998**, *44*, 525-532.

(10) Beck, F.; Kaiser, W.; Krohn, H. *Electrochimica Acta* **2000**, *45*, 4691-4695.

(11) Hian, L. C.; Grehan, K. J.; Compton, R. G.; Foord, J. S.; Marken, F. *Journal of The Electrochemical Society* **2003**, *150*, E59-E65.

(12) Fisher, V.; Gandini, D.; Laufer, S.; Blank, E.; Comninellis, C. *Electrochimica Acta* **1998**, *44*, 521-524.

(13) Fischer, A. E.; Show, Y.; Swain, G. M. *Analytical Chemistry* **2004**, *76*, 2553-2560.

(14) Terranova, M. L.; Piccirillo, S.; Sessa, V.; Compagnone, D.; Sbornicchia, P.; Rossi, M. *Diamond and Related Materials* **2001**, *10*, 627-630.

(15) Fagan, D. T.; Hu, I.-F.; Kuwana, T. *Analytical Chemistry* **1985**, *57*, 2759-2763.

(16) Granger, M. C.; Witek, M.; Xu, J.; Wang, J.; Hupert, M.; Hanks, A.; Koppang, M. D.; Butler, J. E.; Lucazeau, G.; Mermoux, M.; Strojek, J. W.; Swain, G. M. *Analytical Chemistry* **2000**, *72*, 3793-3804.

(17) Nicholson, R. S. *Analytical Chemistry* **1965**, *37*, 1351-1355.

(18) Show, Y.; Matsukawa, T.; Ito, H.; Iwase, M.; Izumi, T. *Diamond and Related Materials* **2000**, *9*, 337-340.

(19) Swain, G. M.; Rajeshuni, R. *Analytical Chemistry* **1993**, *65*, 345-351.

(20) Hupert, M.; Muck, A.; Wang, J.; Stotter, J.; Cvackova, Z.; Haymond, S.; Show, Y.; Swain, G. M. *Diamond and Related Materials* **2003**, *12*, 1940-1949.

(21) Swain, G. M. In *Electroanalytical Chemistry*; Rubinstein, I., Ed.; Marcel Dekker, Inc.: New York, 2003; Vol. 22, pp 181-277.

(22) Granger, M. C.; Xu, J.; Strojek, J. W.; Swain, G. M. *Analytica Chimica Acta* **1999**, *397*, 145-161.

(23) Swain, G. M. *Journal of the Electrochemical Society* **1994**, *141*, 3382-3393.

(24) Ramesham, R.; Rose, M. F. *Diamond and Related Materials* **1997**, *6*, 17-27.

(25) Stotter, J.; Zak, J.; Behler, Z.; Show, Y.; Swain, G. M. *Analytical Chemistry* **2002**, *74*, 5924-5930.

(26) Fu, Y.; Yan, B.; Loh, N. L. *Journal of Materials Science* **1999**, *24*, 2269-2283.

(27) Gonon, P.; Gheeraert, E.; Deneuville, A.; Fontaine, F.; Abello, L.; Lucazeau, G. *Journal of Applied Physics* **1995**, *78*, 7059-7062.

(28) Ushizawa, K.; Watanabe, K.; Ando, T.; Sakaguchi, I.; Nishitani-Gamo, M.; Sato, Y.; Kanda, H. *Diamond and Related Materials* **1998**, *7*, 1719-1722.

(29) Pruvost, F.; Bustarret, E.; Deneuville, A. *Diamond and Related Materials* **2000**, *9*, 295-299.

(30)   Bernard, M.; Baron, C.; Deneuville, A. *Diamond and Related Materials* **2004**, *13*, 896-899.

(31)   Bernard, M.; Deneuville, A.; Muret, P. *Diamond and Related Materials* **2004**, *13*, 282-286.

(32)   Fryda, M.; Dietz, A.; Herrmann, D.; Hampel, A.; Schafer, L.; Klages, C.-P.; Perret, A.; Haenni, W.; Comninellis, C.; Gandini, D. *Proceedings - Electrochemical Society* **2000**, *99-32 (Diamond Materials)*, 473-483.

(33)   Sailer, R.; McCarthy, G. *ICDD Grant-in-Aid*; North Dakota State University: Fargo, North Dakota, USA., 1993.

(34)   *National Bureau of Standards (U.S.), Monogr.* **1981**, *25*, 73.

(35)   *National Bureau of Standards (U.S.), Circ.* **1953**, *539*, 5.

CHAPTER 4

ELECTROCHEMICAL REMEDIATION OF ATRAZINE USING A DIAMOND/Ti ANODE

4.1 Introduction

In Chapter 3, the physical and electrochemical properties of the boron-doped diamond/Ti electrode were reported on. The electrode structure and electrochemical properties were stable during a 50-h electrolysis at 22 mA/cm^2 in 0.1 M H$_2$SO$_4$. These results indicate that diamond can function as a dimensionally stable electrode during anodic polarization; a requisite property for the remediation of organic contaminants. In this Chapter, the oxidative remediation of atrazine in aqueous media is reported on.

Various methods have been used to remediate atrazine (ATZ) in soil and water, such as ozonation[1-3], photochemical degradation[4-7] and bioaugmentation.[8, 9] These methods are able to degrade atrazine; however, by-products, such as hydroxyatrazine (HA), deethylatrazine (DEA) and deisopropylatrazine (DIA), are commonly formed. The effect of these by-products on the environment is still not fully understood, so they may be secondary contaminates. Therefore, a method that can fully oxidize ATZ to CO$_2$ would be desirable.

Besides the advantages of environmental compatibility and low energy consumption, electrochemical methods afford the possibility of completely oxidizing organic contaminants, either directly or indirectly, to CO$_2$. However, there are only two reports describing the electrochemical remediation of ATZ and

both used an indirect approach involving Fenton reaction.[10, 11]
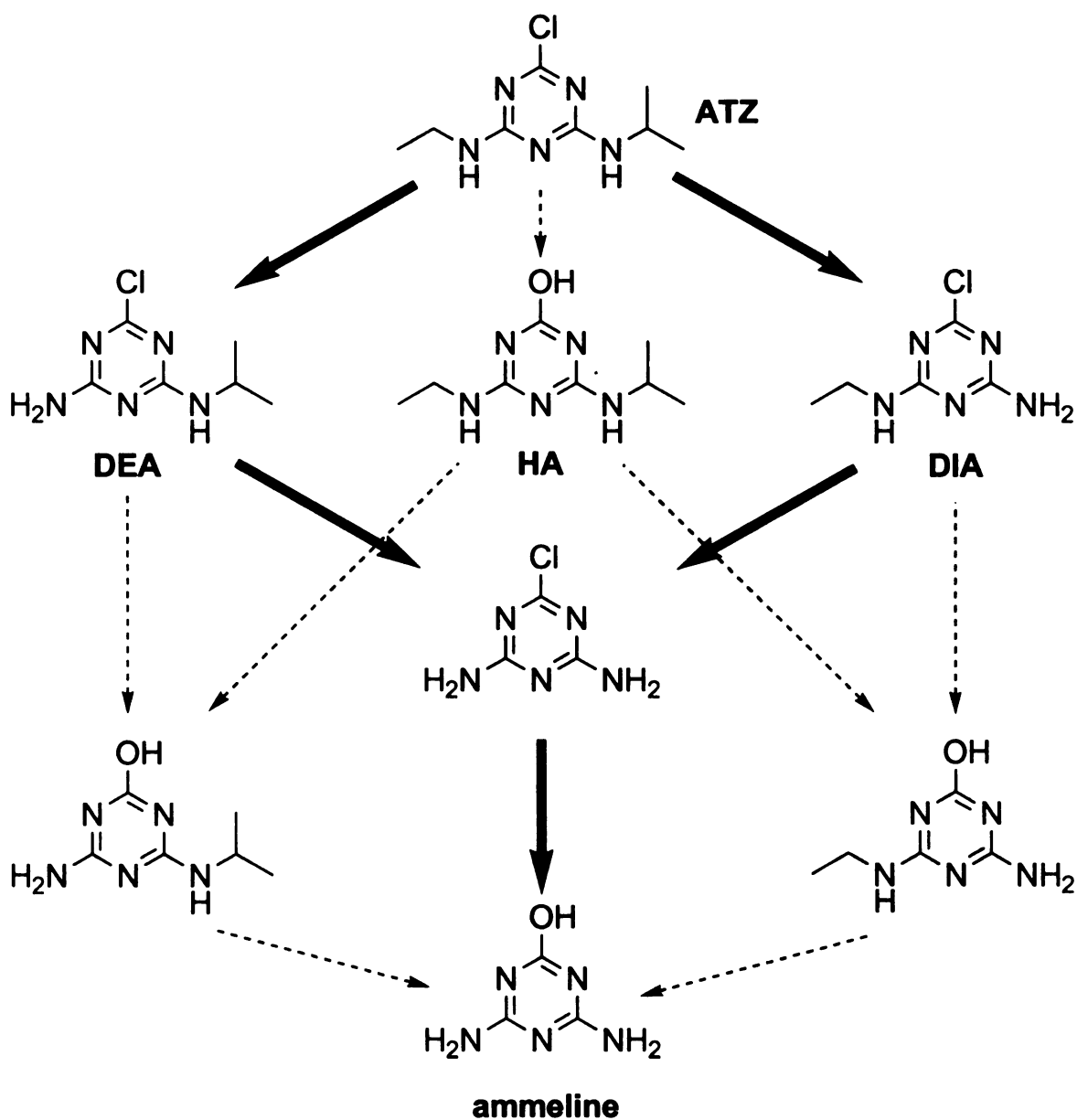
Figure 4.1 Proposed atrazine degradation pathway for electrochemical Fenton reaction with bold arrow shown the major pathway and dashed arrow shown the minor pathway. (Reproduced with permission from *Water Research* **2002**, *36*, 5113-5119. Copyright 2002 Elsevier Science Ltd.)

Degradation via the Fenton reaction is based on the chemical generation of OH•
as shown in the following reaction:[5]

$$Fe^{2+} + H_2O_2 \rightarrow Fe^{3+} + OH^- + HO^•$$

One of the Fenton reagents, Fe^{2+}, is generated electrochemically using a
sacrificial iron anode to deliver Fe^{2+} into solution and another iron electrode
serves as the inert cathode for the reduction of water. The other Fenton reagent,
H_2O_2, is added to the contaminated solution. Using this method, Saltmiras et al.
were able to degrade 70% of ATZ in 3 min with the formation of seven
degradation products, as shown in the proposed degradation pathway in Figure
4.1.[11, 12]

$$\text{Anode: } Fe \rightarrow Fe^{2+} + 2e^-$$

$$\text{Cathode: } 2\ H_2O + 2e^- \rightarrow H_2 + 2\ OH^-$$
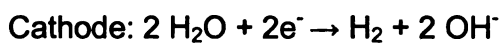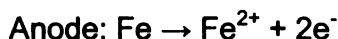
They proposed that dealkylation was the preferred pathway for atrazine
degradation, as shown by the bold arrows. Dechlorination was also observed but
was the minor pathway, as shown by the dashed arrows. Ammeline was the final
degradation product after 10 min. Interestingly, they did not observe any ring
cleavage.[11] Using a similar approach, Ventura et al. generated Fe^{2+} and H_2O_2
simultaneously in solution and reported that the reaction is more efficient at
generating OH• than the method Saltmiras et al. used.[10]

For both works, the major ATZ degradation product was not CO_2.
Saltmiras et al. detected only 12.5% CO_2 after ATZ oxidation using the Fenton
treatment. The factor limiting the complete mineralization may be the electrode
material. To effectively degrade organic contaminants to CO_2, the electrode

needs to have a wide working potential window, long service-life in harsh chemical environments, and good activity for OH• generation. Diamond/Ti electrodes possess these properties (as described in Chapter 3) and have been used electrochemically treat several types of chemical contaminants in water. For example, Chen et al. used a diamond/Ti anode for the oxidation of carboxylic acids, phenol, orange II and reactive red HE-3B.[13] Compared with a Ti/Sb_2O_5-SnO_2 electrode, diamond/Ti had 1.6-4.3 times higher current efficiency and was stable for over 300 h.[13] Fryda et al. deposited diamond films on different large area substrate materials, including Ti, and used them for the oxidation of alcohols, organic acids and halogenated aromatic molecules.[14] They found that the organic molecules could be oxidized to CO_2 without major amounts of other detectable by-products, even at very low concentrations (<3 ppm).[14]

The oxidation reaction mechanism for organic pollutants in acidic solution at boron-doped diamond electrodes has been studied. Marselli[15] and Michuaud[16] et al. proposed that the electrochemically generated hydroxyl radicals, OH•, are the important oxidant generated at diamond during the electrolysis. The generation of this oxidant is complex with a series of possible parallel reactions:[16]

(i) discharge of water on electrode surface with the formation of hydroxyl radicals,

$$H_2O \rightarrow OH\bullet + H^+ + e^-$$

(ii) oxidation of organic pollutants by the interfacial hydroxyl radicals,

$$Organic\ pollutants + OH\bullet \rightarrow CO_2 + H_2O$$
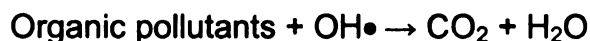
(iii) formation of H_2O_2 by two hydroxyl radicals,

$$2\ OH\bullet \rightarrow H_2O_2$$
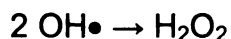
(iv) oxygen evolution or regeneration of $OH^\bullet$ by the dissociation of H_2O_2.

$$H_2O_2 \rightarrow O_2 + 2H^+ + 2e^-$$

$$H_2O_2 \rightarrow 2\ OH\bullet$$
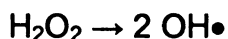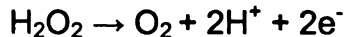
Diamond electrodes possess a highly stable microstructure and morphology during anodic polarization and a large overpotential for oxygen evolution. This gives the diamond anode high activity for organic pollutant oxidation to CO_2.[15]

In this Chapter, the electrochemical degradation of atrazine using a diamond/Ti anode was studied and the CO_2 conversion efficiency was determined. The atrazine concentration was monitored as a function of electrolysis time over 120 min. The effect of the current on the remediation was investigated by performing the electrolysis at 50 and 100 mA (11 mA/cm^2 and 22 mA/cm^2). The effect of convection on the conversion of atrazine was also studied. The main atrazine degradation intermediates were separated and identified by high performance liquid chromatography (HPLC) with UV/Vis detection. The atrazine degradation product, CO_2, was determined by the electrolysis of ^{14}C-labeled atrazine. The main goal of this work was to determine if ATZ could be completely mineralized to CO_2 at a diamond anode.

4.2   Results and Discussion

4.2.1 Separation and Detection of Atrazine and Metabolites

Atrazine (ATZ) and its three major intermediate degradation products, hydroxyatrazine (HA), deethylatrazine (DEA) and deisopropylatrazine (DIA), are shown in Figure 4.1. These compounds were detected by UV/Vis spectroscopy,

as they are all chromophoric. Figure 4.2 shows UV/Vis spectra for ATZ, HA, DEA and DIA (5 ppm each in 0.1 M H₂SO₄). A 0.1 M H₂SO₄ background spectrum was also recorded and is shown for comparison (i.e., blank).
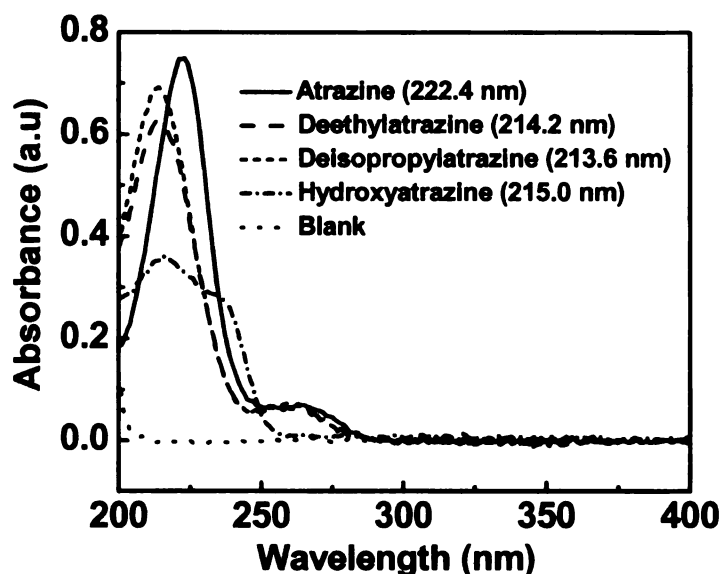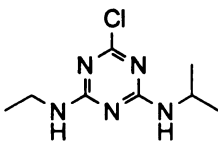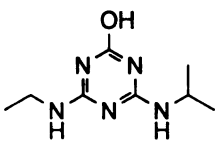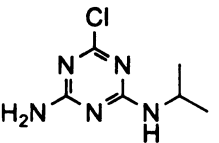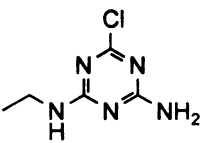
Figure 4.2 UV/Vis spectra for atrazine, hydroxyatrazine, deethylatrazine, deisopropylatrazine (5 ppm each) all dissolved in 0.1 M H₂SO₄. A background spectrum (blank), 0.1 M H₂SO₄, is also shown for comparison.

The blank spectrum is flat and has near zero absorbance over most of the wavelength range. All four compounds have high absorbance at wavelengths between 215 and 225 nm. It can be seen that the distinction coefficient, ε, is similar for ATZ, DEA and DIA within this wavelength range, but smaller for HA. The absorbance is attributed to the π to π* transition of electrons in the triazine ring. For ATZ, the maximum absorbance occurs at 222.4 nm and for HA, DEA and DIA, the maximum occurs at 215.0, 214.2 and 213.6 nm, respectively. Based

on these results, 216 nm was for use in the HPLC analysis.

Reversed-phase HPLC separation was used to determine if the electrolysis decreased the ATZ concentration and formed any of the intermediate degradation products (e.g., HA, DEA and DIA). The isocratic separation was optimal with a mixed mobile phase consisting of 0.05 M phosphate buffer (pH 3.5) and acetonitrile at a volumetric ratio of 60/40. The mobile phase flow rate was 1.0 mL/min. Table 4.1 lists the molecular structure and pK_a values for ATZ and three possible intermediates: HA, DEA and DIA.

Table 4.1   Molecular structure and pK_a value for ATZ, HA, DEA and DIA.

Name	ATZ	HA	DEA	DIA
Structure				
pK_a	1.71	5.15	4.57	4.65

A successful reversed-phase HPLC method requires the proper mobile phase to achieve optimum peak shape, low limit of detection and reproducible retention time. The concentrations of acid and conjugate base required to prepare the pH 3.5 buffer were calculated using the Henderson-Hasselback equation:

$$pH = pK_a + \log\left(\frac{[A^-]}{[HA]}\right)$$

(4.1)

80

At pH 3.5, about 90% of all four compounds exist in a single form because the solution pH is about one unit above or below the analytes' pK_a. A single form of each analyte assures good peak shape and resolution. The chromatogram for a solution of ATZ, HA, DEA and DIA is shown in Figure 4.3. The peaks were identified by peak retention time matching.
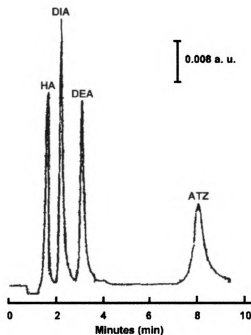
Figure 4.3 Isocratic separation of 1.25 ppm (each) ATZ, HA, DEA and DIA using a reversed-phase HPLC separation and UV/Vis detection at 216 nm. The mobile phase was 0.05 M phosphate buffer (pH 3.5) mixed with acetonitrile at a volumetric ratio of 60/40. The mobile phase flow rate was 1.0 mL/min and the sample injection volume was 20 μL.

Key parameters indicative of the efficiency of the separation are the retention time (t_R), retention factor or capacity factor (k') and plate number (N).

Retention time is the time during which the analyte moves from injection port to the detector. The longer the retention time, the more strongly the analyte is retained on the column.[17] Capacity factor is an important parameter that describes the migration rate of a solute. It can be calculated using the equation:

$$k' = \frac{t_R - t_M}{t_M}$$

(4.2)

where k' is the capacity factor, t_R is the retention time of analyte and t_M is the retention time of unretained species, also called the dead time. An unretained analyte will have a capacity factor close to unity while a strongly retained analyte will have a capacity factor >> 1. A capacity factor in the range of 2 to 10 is desired to avoid excessive zone broadening.[17] Plate number is used to quantitatively evaluate the efficiency of the separation. The efficiency of a separation increases with the plate number. The plate number can be calculated using the equation:

$$N = 16 \left(\frac{t_R}{W} \right)^2$$

(4.3)

where N is the plate number, t_R is the retention time and W is the peak width at the base.[17]

Table 4.2 summarizes the retention time, capacity factor and plate number of the four analytes: ATZ, HA, DEA and DIA. The elution order is consistent with the polarity of the compounds. For a reversed-phase separation, a more polar analyte will elute easier than a less polar one. HA with the hydroxyl group on the triazine ring is the most polar of the four solutes. DEA and DIA contain primary

82

amine groups and, at low pH, with the buffer protonates the acidic silanols on the silica surface, the amine retention times shorten and peak shape sharpens. The ATZ retention time is considerably longer than that for the degradation by-products. The retention time for ATZ under these conditions is 8.2 min, giving a k' of 11 and an N of 2165 plates. The retention times and capacity factors for the more polar degradation by-products are 1.7 min and 1.5 for HA, 2.4 min and 2.6 for DIA, and 3.1 min and 3.6 for DEA.

Table 4.2   Summary of the retention times, capacity factors and plate numbers for the four analytes: ATZ, HA, DEA and DIA.

Analyte	t_M (min)	t_R (min)	k'	W (min)	N (plates)
ATZ	0.67	8.2	11	0.71	2165
DEA	0.67	3.1	3.6	0.39	1037
DIA	0.67	2.4	2.6	0.32	894
HA	0.67	1.7	1.5	0.29	558

For each of the solutes, the peak height increased linearly with increasing injected concentration between 10 ppb and 10 ppm ($r^2 > 0.998$), as shown in Figure 4.4. The concentration of each compound in the electrolysis solution was then determined from the response curves generated from a set of standards.
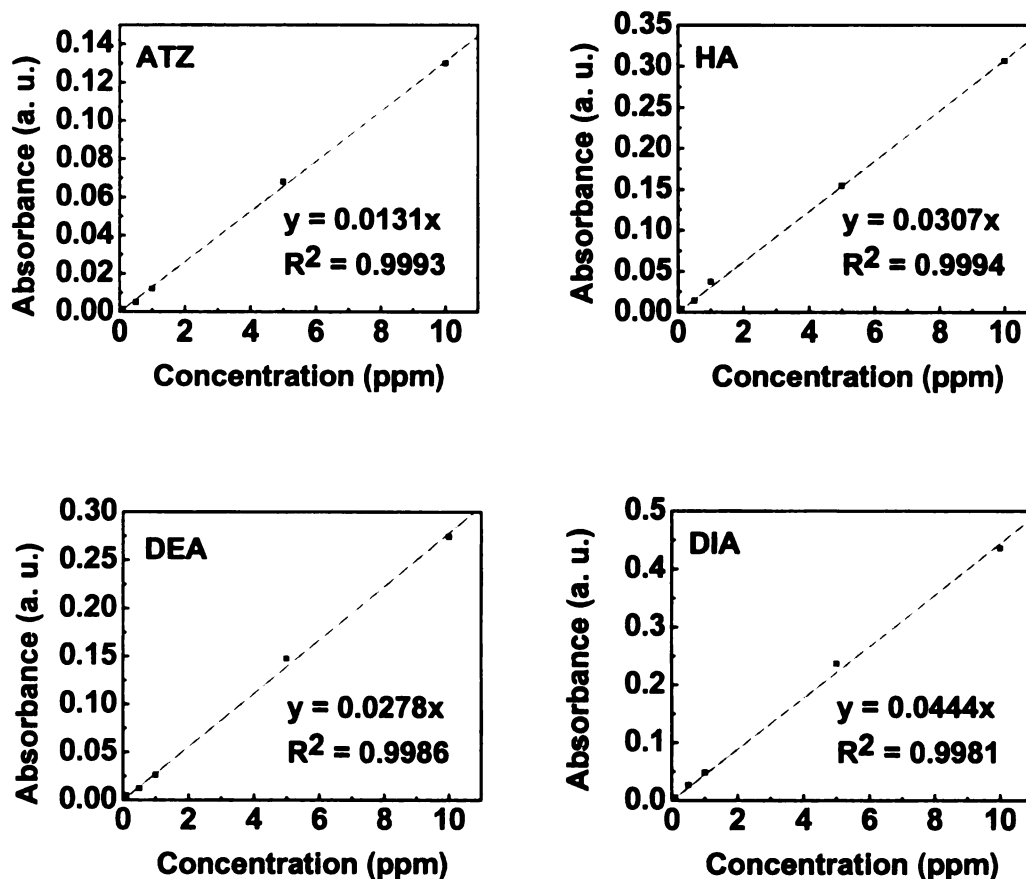
Figure 4.4 Response curves for standard solutions of ATZ, HA, DEA and DIA.

4.2.2 Electrochemical Degradation of Atrazine

The ATZ electrolysis tests were conducted in the H-cell shown in Figure 2.3. The electrolysis of 5 ppm ATZ in 0.1 M H_2SO_4 was investigated as a function of the electrolysis time and current density. The first task was to evaluate the anode response reproducibility and stability for ATZ oxidation. This was done using a constant current of 100 mA (22 mA/cm^2) for 20 min. A summary of the results are presented in Table 4.3.

Table 4.3   Atrazine concentration remaining in the anolyte compartment after 20 min of oxidative electrolysis of 5 ppm atrazine in 0.1 M H_2SO_4 at a diamond/Ti anode.

| | **Atrazine Concentration (ppm)** | | | | | | |
	1	2	3	4	5	Average	RSD (%)
Electrode 1	1.7	1.5	1.6	1.5	1.5	1.6	2.7
Electrode 2	2.4	2.3	2.2	2.1	1.9	2.2	4.1

Electrolysis was performed at a constant current of 100 mA (22 mA/cm^2). The data presented are the remaining ATZ concentrations in the anolyte compartment for five different runs, as determined by HPLC analysis. Results for five measurements using two different anodes are presented. The results indicate that the ATZ electrolysis is quite reproducible at the diamond/Ti anode. The relative standard deviation in the concentration remaining after electrolysis was 2.7% and 4.1%, respectively, for the two anodes. After electrolysis, the most intense peak in the chromatogram was for ATZ as its concentration decreased from 5 down to 1 or 2 ppm with three new peaks emerging. The peaks were for unknown solutes more polar than ATZ as their elution times were from 1 to 3 min. All three peaks were weak, as compared to the signal for ATZ, with the intensity being greatest at short electrolysis times. Their retention times did not match those for HA, DEA or DIA. No additional work was performed to identify these three apparent products.

In order to verify that the decreased ATZ concentration was not due to the

diffusion from the anolyte to the catholyte compartment, a test was performed to measure the ATZ concentration in the anolyte compartment every 20 min over a 120 min period without any electrolysis. 6 mL of 5 ppm ATZ in 0.1 M H_2SO_4 was placed into the anolyte compartment and 6 mL of 0.1 M H_2SO_4 solution was placed into the catholyte compartment. For the 120 min period and 6 measurements, the ATZ concentration in the anolyte compartment remained constant with a variance of only 5.5%. It was, therefore, concluded that the reduced ATZ concentration after electrolysis resulted from the electrochemical oxidation.

The effectiveness of the diamond/Ti anode for the oxidative degradation of ATZ, as a function of electrolysis time and current density, was then studied. The initial ATZ concentration was 5 ppm in 0.1 M H_2SO_4. Plots of the percentage of ATZ remaining in solution, as measured by HPLC, as a function of the electrolysis time at two different current densities, are shown in Figure 4.5.
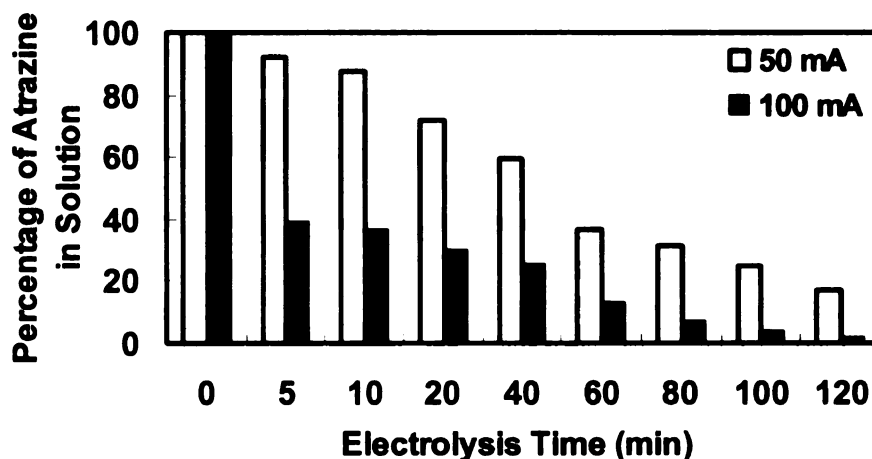
Figure 4.5 Percentage of atrazine remaining in solution as a function of the electrolysis time at two currents: 100 mA (22 mA/cm²) and 50 mA (11 mA/cm²).

At both currents, the ATZ concentration decreased over time, with the largest decrease seen during the first 60 min of electrolysis. After 120 min, greater than 97% of the ATZ was oxidatively removed at a current of 100 mA (22 mA/cm^2) and 83% of the ATZ at a current of 50 mA (11 mA/cm^2). As expected, ATZ degradation is more complete at the higher current density (i.e., more charge passed). At both current densities, the ATZ concentration decreased exponentially with time as semilogarithmic plots of the concentration and electrolysis time were linear ($r^2 > 0.99$), as shown in Figure 4.6.
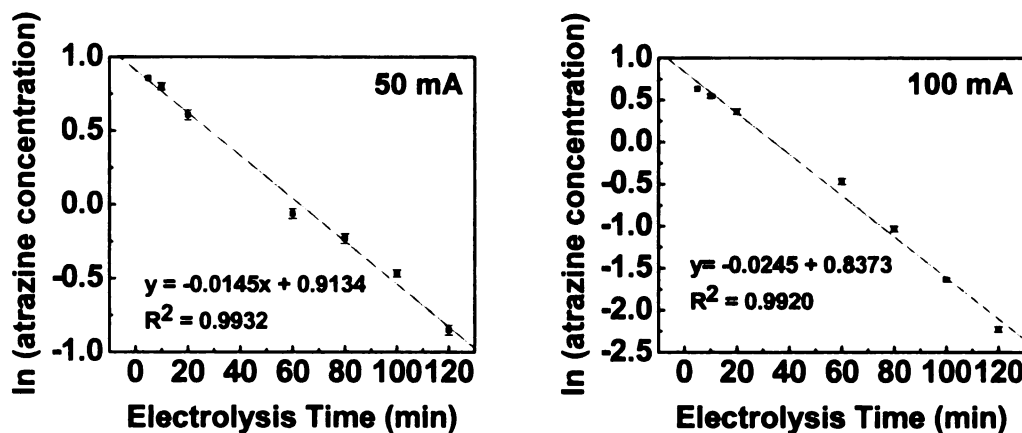
Figure 4.6   Semilogarithmic plots of atrazine concentration versus electrolysis time for a diamond/Ti anode at two constant currents: 100 mA (22 mA/cm^2) and 50 mA (11 mA/cm^2).

The linear relationship indicates that the reaction is first-order and reaction rates for each current density are the negative of the slopes.[18] So at the current of 100 mA (22 mA/cm^2), the reaction rate is 0.0145 min^{-1} and at the current of 50 mA

(11 mA/cm^2), the reaction rate is 0.0245 min^{-1}.

An effort to further increase the reaction rate was accomplished by introducing convection to the solution. A small stirring bar was placed in the anolyte compartment and rotated at 4 rps. The effect of convection was studied at the constant current of 50 mA (11 mA/cm^2). Plots of the percentage of ATZ remaining in solution, as assessed by HPLC, as a function of the electrolysis time with and without convection are shown in Figure 4.7.
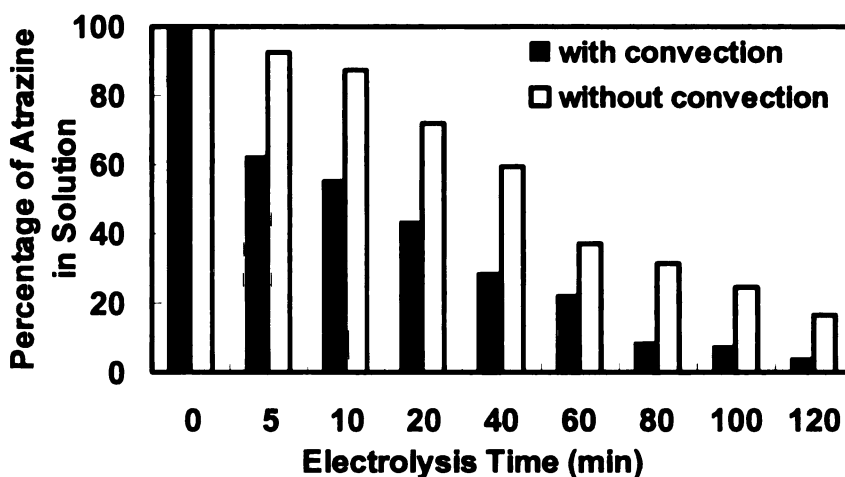
Figure 4.7 Percentage of atrazine remaining in solution as a function of the electrolysis time at a constant current of 50 mA (11 mA/cm^2) with and without convection.

With convection, the electrolysis rate of ATZ was increased due to an increased flux to the electrode. After 120 min, 96% of the ATZ was oxidized at the constant current of 50 mA (11 mA/cm^2) with convection while only 83% of the ATZ was oxidized without. The reaction rate was not first-order for ATZ degradation when convection was present. The logarithmic plots of the ATZ concentration and the

electrolysis time were not linear.

As mentioned earlier, none of the three major metabolites (HA, DEA or DIA) were detected in the HPLC analysis of the anolyte solutions, at least down to the 10 ppb level, although three low intensity peaks associated with the unidentified oxidation reaction products did develop. These observations are consistent with the conclusion that ATZ can be oxidized reproducibly and stably at a diamond/Ti anode and that the three major degradation products are not formed at appreciable levels under these conditions. One possible reaction product is CO_2, as shown in the reaction below:

$$C_8H_{14}N_5Cl + 31\ H_2O \rightarrow 8\ CO_2 + 5\ NO_3^- + 76\ H^+ + 70\ e^- + Cl^-$$
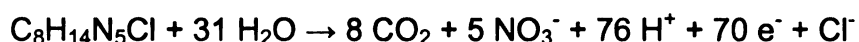
4.2.3 Determination of the CO_2 Conversion Efficiency

In order to test this supposition and to determine the conversion efficiency of ATZ oxidation to CO_2, if in fact oxidation does occur, the electrooxidation of ^{14}C-labeled atrazine was performed in a sealed assembly using a 0.1 M $KOH_{(aq)}$ trap for the generated CO_2 (see Figure 2.4). The reproducibility of the experiment was first tested by conducting the electrolysis three times using the same diamond/Ti anode under the exact conditions. A constant current of 100 mA (22 mA/cm^2) was applied to the cell, initially for 30 min, to oxidize 5 ppm of ^{14}C-labeled ATZ in 0.1 M H_2SO_4. Any ^{14}C-labeled ATZ oxidized to $^{14}CO_2$ was trapped in the KOH solution and analyzed by a liquid scintillation counter.

Table 4.4 Reproducibility test of the oxidation of ^{14}C-labeled atrazine in 0.1 M H_2SO_4 at a diamond/Ti anode using a constant current of 100 mA (22 mA/cm^2) for 30 min.

Time(min)	Total ^{14}C recovery	$^{14}CO_2$ percentage
30	93.6%	38.5%
30	87.5%	31.2%
30	86.2%	33.4%
Average	89.1 ± 3.9%	34.4 ± 3.7%
RSD	4.4%	10.8%

The results in Table 4.4 show that the percentage of total ^{14}C recovered as well as the percentage of $^{14}CO_2$ trapped in the $KOH_{(aq)}$ were reproducibly observed. The percentage of total ^{14}C recovered after electrolysis is equal to the total counts for ^{14}C measured from the anolyte and catholyte compartments of the cell and the KOH trap divided by the total counts recorded for the starting ATZ solution. The percentage of ^{14}C trapped in the 0.1 M $KOH_{(aq)}$ solution (trap level count divided by total count) reflects the amount of ATZ ring cleavage to CO_2. All of the counts recorded from the trap should be for $^{14}CO_2$. The nominal ^{14}C recovered after 30 min electrolysis was 89.1% and indicating that the H-cell assembly was largely free of air leaks. Nominally, 34.4% of the atrazine was converted to CO_2 via ring cleavage during the period. Good reproducibility in terms of the CO_2 produced was seen as the standard deviation of these tests was about 11%.

The electrolysis was then conducted for 60, 90 and 120 min periods in separate tests to examine how completely the ATZ can be mineralized to CO_2. The results are summarized in Table 4.5. The results for the electrolysis, with and without added convection, are presented in Figure 4.8.

Table 4.5   Total ^{14}C recovery and $^{14}CO_2$ production percentage after 30, 60, 90 and 120 min of electrolysis with convection.

Time(min)	Total ^{14}C recovery	$^{14}CO_2$ percentage
30	89.1%	34.4%
60	96.6%	58.2%
90	99.8%	75.8%
120	99.9%	81.2%
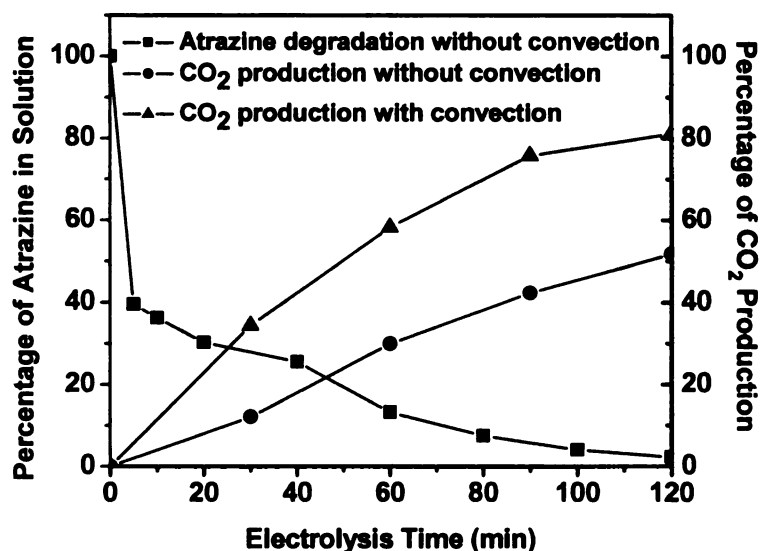
Figure 4.8   Comparison of percentage of atrazine oxidized to CO_2 over a 120 min electrolysis period at a constant current of 100 mA (22 mA/cm^2) with and without convection.

The data clearly show that CO_2 production increases with electrolysis time. From 30 to 120 min, the percentage of CO_2 produced increased from 34.4 to 81.2%. When convection was introduced at 120 min, for example, the CO_2 production increased from 51.8 to 81.2%. The data unequivocally demonstrate that the diamond/Ti anode is effective at oxidatively degrading ATZ to CO_2. The CO_2 conversion percentage at 120 min (81.2%), is greater than the total ATZ converted to CO_2 (12.5%) as reported by Saltmiras et al. using anodic Fenton treatment, even with a longer electrolysis period.[11]

4.3   Conclusions

The electrolysis of 5 ppm ATZ in 0.1 M H_2SO_4 using a diamond/Ti anode was investigated at two currents: 50 mA (11 mA/cm^2) and 100 mA (22 mA/cm^2). The diamond/Ti anode was shown to function reproducibly and stably for the mineralization of ATZ. At the current of 100 mA (22 mA/cm^2), 97% of the ATZ was oxidized during a 120 min electrolysis period and the ^{14}C-labeled experiments showed that 81.2% of the contaminant was converted to CO_2. Convection had a significant effect on the degradation rate suggesting that the oxidation was occurring at a mass transfer limited rate. At a constant current of 50 mA (11 mA/cm^2), without convection in the solution, only 83% of ATZ was degraded in 120 min while with convection, 96% of the ATZ was oxidized. None of the three common degradation products, HA, DEA and DIA, for ATZ were detected by HPLC-UV/Vis during the electrolysis. However, three unknown

peaks associated with compounds more polar than ATZ appeared at shorter degradation times. They might be degradation products containing multiple hydroxyl groups. These results prove that the major oxidative degradation product of ATZ during electrolysis on diamond/Ti was CO_2. The reaction was first-order as the logarithm of the ATZ concentration changed linearly with the electrolysis time. These results showed that a diamond/Ti anode is effective for the oxidative degradation of organic pollutants to CO_2. They portend the possibility of using the electrode as an industrial anode for efficient wastewater decontamination.

4.4 References

(1) Benitez, F. J.; Beltran-Heredia, J.; Gonzalez, T.; Acero, J. L. *Ozone: Science & Engineering* **1995**, *17*, 237-258.

(2) Beltran, F. J.; Garcia-Araya, J. F.; Alvarez, P. M.; Rivas, J. *Journal of Chemical Technology & Biotechnology* **1998**, *71*, 345-355.

(3) Nelieu, S.; Stobiecki, M.; Einhorn, J. *Journal of Chromatography A* **2000**, *866*, 195-201.

(4) Bourgine, F. P.; Chapman, J. I.; Kerai, H.; Duval, J. L.; Green, J. G.; Hamilton, D. *Journal of the Chartered Institution of Water and Environmental Management* **1995**, *9*, 417-423.

(5) Hequet, V.; Gonzalez, C.; Le Cloirec, P. *Water Research* **2001**, *35*, 4253-4260.

(6) Arantegui, J.; Prado, J.; Chamarro, E.; Santiago; Esplugas *Journal of Photochemistry and Photobiology, A: Chemistry* **1995**, *88*, 65-74.

(7) Schmitt, P.; Freitag, D.; Sanlaville, Y.; Lintelmann, J.; Kettrup, A. *Journal of Chromatography, A* **1995**, *709*, 215-225.

(8) Runes, H. B.; Jenkins, J. J.; Bottomley, P. J. *Applied Microbiology and Biotechnology* **2001**, *57*, 427-432.

(9) Silva, E.; Fialho, A. M.; Sa-Correia, I.; Burns, R. G.; Shaw, L. J. *Environmental Science and Technology* **2004**, *38*, 632-637.

(10) Ventura, A.; Jacquet, G.; Bermond, A.; Camel, V. *Water Research* **2002**, *36*, 3517-3522.

(11) Saltmiras, D. A.; Lemley, A. T. *Water Research* **2002**, *36*, 5113-5119.

(12) Walling, C. *Accounts of Chemical Research* **1975**, *8*, 125-131.

(13) Chen, X.; Chen, G.; Gao, F.; Yue, P. L. *Environmental Science and Technology* **2003**, *37*, 5021-5026.

(14) Fryda, M.; Herrmann, D.; Schafer, L.; Klages, C.-P.; Perret, A.; Haenni, W.; Comninellis, C.; Gandini, D. *New Diamond and Frontier Carbon Technology* **1999**, *9*, 229-240.

(15) Marselli, B.; Garcia-Gomez, J.; Michaud, P.-A.; Rodrigo, M. A.; Comninellis, C. *Journal of the Electrochemical Society* **2003**, *150*, D79-D83.

(16) Michaud, P.-A.; Panizza, M.; Ouattara, L.; Diaco, T.; Foti, G.; Comninellis, C. *Journal of Applied Electrochemistry* **2003**, *33*, 151-154.

(17) Skoog, D. A.; Holler, F. J.; Nieman, T. A. *Principles of Instrumental Analysis Fifth Edition*; Saunders College Pub. : Harcourt Brace College Publishers: Philadelphia, 1998.

(18) Atkins, P. *The Elements of Physical Chemistry Second Edition*; W. H. Freeman and Company: New York, 1996.

CHAPTER 5

A SENSITIVE METHOD FOR INORGANIC As DETECTION USING ANODIC STRIPPING VOLTAMMETRY AND A Au-COATED DIAMOND THIN-FILM ELECTRODE

5.1 Introduction

Inorganic arsenic contamination in drinking water is a serious worldwide threat to human health. As(III) and (V) are inorganic forms found in ground water and are much more toxic than the organic forms with As(III) being the most toxic of them all.[1, 2] The EPA required arsenic maximum contaminant level (MCL) in drinking water is as low as 10 ppb.[3] Therefore, a sensitive, reproducible and inexpensive method is desired to accurately monitor inorganic arsenic in water. The methods that are used for arsenic monitoring have been discussed in Chapter 1. Anodic stripping voltammetry (ASV) is the method of choice because it provides high sensitivity, good resolution, portability and relatively low cost. Electrode material is one of the most important factors that affect the detection of inorganic arsenic using ASV. Several electrode materials were used for arsenic detection such as Hg,[1, 3-7] Pt,[8-10] Au[2, 11-15] and Au-coated carbon electrodes (graphite[2, 13, 16, 17] and glassy carbon[18-20]) and their limitations were discussed in Chapter 1. Au-coated diamond turns out to be the electrode of choice because the interaction of As with Au facilitating its deposition and stripping[21, 22] and the stability of diamond makes it an ideal support material for reproducible and stable detection of arsenic.[23-36]

96

The As stripping peak current and potential for Au-As intermetallic compounds are sensitive to both the solution pH and the electrolyte composition. For example, it has been reported that the As oxidation half-wave potential ($E_{1/2}$) is strongly influenced by the activity of not only H^+ but also Cl^-.[37, 38] The stripping peak potential is sensitive to pH as can be seen in the redox reaction:

$$HAsO_2 + 3\ H^+ + 3\ e^- \leftrightarrow As + 2\ H_2O$$

$$E = E^0 + \frac{0.059}{3} \log[H^+]^3 [HAsO_2]$$

With increasing pH, the standard reduction potential for this reaction shifts negatively. In addition, the As stripping peak current and potential are affected by the Cl^- activity as Arnold and Johnson reported the anion can facilitate As formation by acting as a salt bridge between the working electrode and the arsenic ions.[37, 38]

$$As(OH)_2^+ + Cl^- + e^- \rightarrow As\ (OH)Cl + OH^-\ (fast)$$

$$2\ As(OH)Cl + Cl^- + e^- \rightarrow 2\ AsCl + 2\ OH^-\ (slow)$$

$$AsCl + e^- \rightarrow As^0 + Cl^-\ (fast)$$
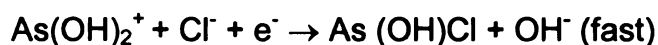
In terms of the supporting electrolyte, HCl at concentrations greater than 0.5 M has been reported by many researchers to be the best for As(III) detection based on the sharpness and reproducible nature of the stripping peak.

Due to the stability of As(V), an extremely negative potential is required to reduce it electrochemically.[15, 19] However, at such potentials, hydrogen evolution becomes problematic and greatly inhibits As formation. As(V) is usually determined by first chemically reducing it to As(III) and then detecting the As(III) species by ASV. Several reducing agents have been investigated, such as

$N_2H_4/HCl/HBr$,[39] $NaBr/N_2H_4/H_2SO_4$,[40] Cu_2Cl_2,[13, 41] Na_2SO_3,[12, 14, 42] $NaHSO_3$,[43] gaseous SO_2,[5] H_2S,[44] $Na_2S_2O_3$,[3] L-cysteine,[7] mannitol,[45] ascorbic acid and KI.[6, 46-48] Some of these agents are not suitable for ASV and are commonly used for cathodic stripping voltammetry with a Hg electrode, such as $N_2H_4/HCl/HBr$, $NaBr/N_2H_4/H_2SO_4$, ascorbic acid and KI, $Na_2S_2O_3$, and mannitol. Some of these agents can also chemically react with gold, such as L-cysteine. The use of Cu_2Cl_2 requires a complex setup and would not facilitate on-site application. Na_2SO_3 and $NaHSO_3$ provide efficient conversion of As(V) to As(III) and both have a minimal effect on Au. They are also more easily used and controlled than gaseous reagents (e.g., SO_2 and H_2S).

In this Chapter, we report on a sensitive, reproducible and stable method for total inorganic arsenic analysis in water samples using DPASV and a Au-coated diamond electrode. The electrode and method were tested using both laboratory-prepared and local river water samples. We sought (i) to better understand Au metal phase formation on diamond surfaces, (ii) to optimize the DPASV experimental parameters for arsenic determination and (iii) to improve the sensitivity, reproducibility and stability of the method for total inorganic arsenic analysis as compared to the figures of merit commonly achieved with Au and Au-coated glassy carbon electrodes. The electrode and method were tested using both laboratory-prepared and local river water samples.

5.2 Results and Discussion

5.2.1 Particle Analysis of As and Au Deposition on a Boron-Doped Diamond Electrode

As discussed in the Introduction, Au is the electrode of choice for As(III) detection by ASV with the best supporting electrolyte being HCl.[2] The first task was, therefore, to learn about Au deposition on diamond thin-film surfaces. SEM was used to investigate the morphology and distribution of the Au and Au + As deposits on diamond after electrodeposition at a constant potential. (shown in Figure 5.1). A summary of the particle analysis data is presented in Table 5.1.

Figure 5.1(a) shows a bare diamond surface without any metal deposition. The polycrystalline morphology is evident with a crystallite size ranging from a few micrometers down to several hundred nanometers. The surface is largely free of secondary growths (i.e., smaller crystallites formed on the primary ones). There is some surface charging (bright spots) on some of the crystalline facets indicative of unequal electrical conductivity.[49-53] For comparison, Figure 5.1(b) shows a diamond surface after 90 s of deposition at -0.45 V in 10 ppm Au(III) + 1 M HCl. The Au particles are evenly distributed over the diamond surface and are located in both the grain boundaries and on the facet surfaces. The particle shapes are generally round or elliptical. The particle size is relatively uniform with a nominal diameter of 23 ± 5 nm, a particle area of 3.6 (± 1.6) × 10^{-12} cm^2 and a particle density of 6.4 (± 1.2) × 10^9 cm^{-2}. The narrow particle size distribution is consistent with that expected for an instantaneous nucleation mechanism and a relatively constant rate of particle growth.[54, 55] This nominal particle density is

comparable to the value Dai et al. reported (~7.5 × 10^9 cm^{-2} for a 15 s deposition) for Au deposited on glassy carbon. However, the Au particle diameter is larger in the present case because of the longer deposition time (90 s).[18]

Figure 5.1(c) shows a diamond surface after 90 s of deposition in 10 ppm As(III) + 1 M HCl at -0.45 V. No As particles were detected, even at a magnification of 50,000×. This indicates that little or no As deposits on the bare diamond surface. At best, only a monolayer of As would be expected because of the semiconducting electronic properties of the metal.[2, 11, 18] This is why bare diamond can not be used for arsenic analysis. Figure 5.1(d) shows a diamond surface after 90 s of deposition at -0.45 V in 10 ppm As(III) and 10 ppm Au(III) + 1 M HCl. Au provides a medium onto which As can deposit and form a stable intermetallic compound. The nominal particle diameter is 22 ± 3 nm, the particle area is 2.4 (± 0.7) × 10^{-12} cm^2 and the particle density is 3.8 (± 0.5) × 10^{10} cm^{-2}. The nominal particle size is about the same but the particle density is higher than that for the Au-only coated surface (Figure 5.1(b)). In both cases, the particles are dispersed over the entire diamond surface. Presumably because of its electronic properties, As reduces the Au particle size when co-deposited.[56] It has been reported that As deposits on the surface of the Au rather than within the bulk metal.[56] Therefore, we suppose the reason for the larger particle density when Au and As are co-deposited is because once As covers a Au particle surface, further growth of the Au particle is inhibited. Therefore, additional Au deposition can only occur at new sites on the surface.[56]
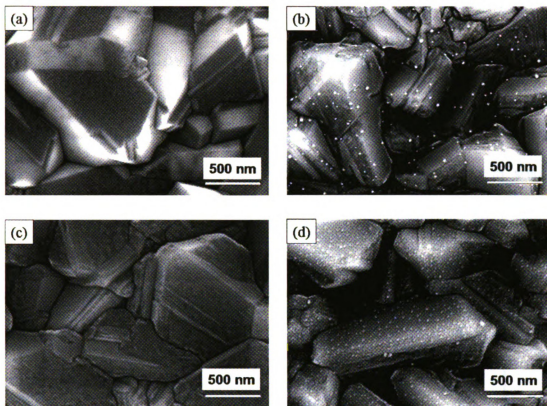
Figure 5.1 SEM images of (a) a bare diamond electrode surface without any metal deposition, (b) a diamond surface after 90 s of deposition at -0.45 V in 10 ppm Au(III) + 1 M HCl solution, (c) a diamond surface after 90 s of deposition at -0.45 V in 10 ppm As(III) + 1 M HCl solution and (d) a diamond surface after 90 s of deposition at -0.45 V in 10 ppm As(III) and 10 ppm Au(III) + 1 M HCl.

Table 5.1 Particle analysis results for Au and As/Au metal phase formation on diamond.

	10 ppm Au(III)	10 ppm Au(III) + 10 ppm As(III)
Mean particle diameter (nm)	23 ± 5	22 ± 3
Mean particle area (cm^2)	$3.6\ (\pm 1.6) \times 10^{-12}$	$2.4\ (\pm 0.7) \times 10^{-12}$
Particle density (cm^{-2})	$6.4\ (\pm 1.2) \times 10^{9}$	$3.8\ (\pm 0.5) \times 10^{10}$

5.2.2 Effect of Au Coverage on the As Stripping Peak Current

The effect of the Au coverage on the As stripping peak current was investigated. Figure 5.2 shows DPASV i-E curves for 100 ppb As(III) + 1 M HCl at a diamond electrode as a function of the Au(III) concentration in solution added by standard addition from 0 to 750 ppb.
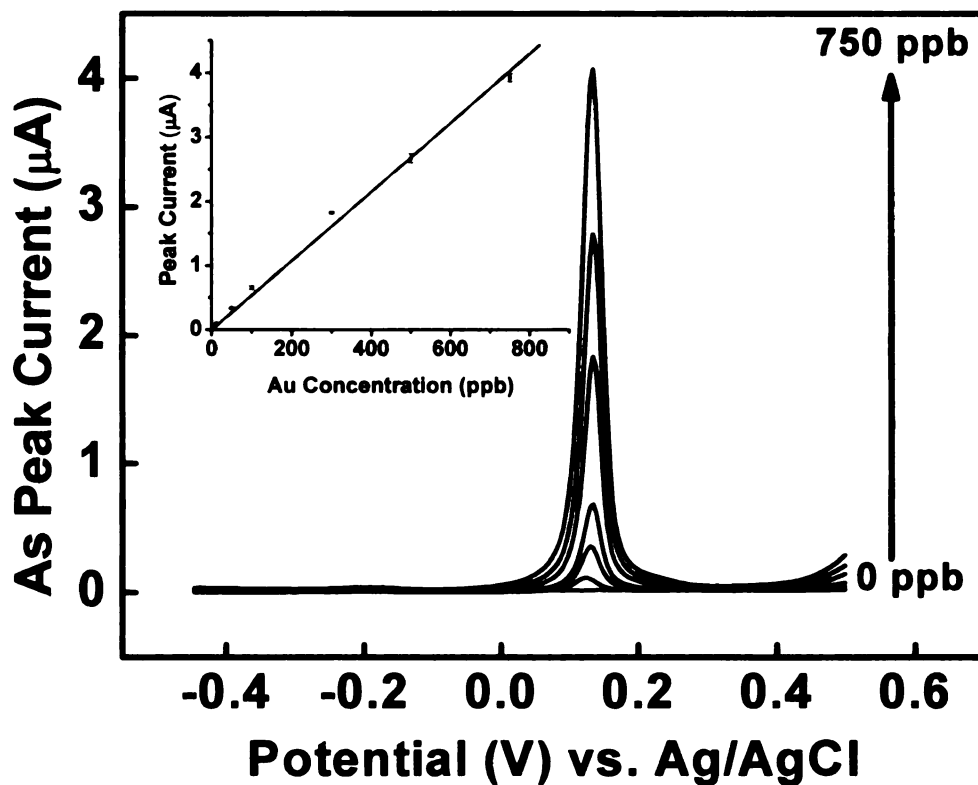
Figure 5.2 DPASV i-E curves for 100 ppb As(III) + 1 M HCl at a diamond electrode as a function of the Au(III) concentration in solution. A plot of the As stripping peak current versus the Au(III) solution concentration is provided as an inset. DPASV parameters: E_{dep} = -0.45 V, t_{dep} = 120 s, pulse width = 50 ms, pulse

amplitude = 50 mV, step height = 4 mV, cycle period 200 ms, and sampling time = 8.33 ms.

In these measurements, Au was co-deposited along with As. A plot of the As stripping peak current versus the Au(III) concentration in solution is provided as an inset. Note that no As stripping peak current was recorded for the bare diamond. The As stripping peak, centered at 0.13 V and observed only with co-deposited Au, is narrow and sharp for all the Au(III) concentrations. The peak widths ($\Delta w_{1/2}$) range from 30 to 35 mV, depending on the Au surface coverage. The As stripping current scaled proportionally with the Au(III) solution concentration (i.e., Au coverage), as the response curve has a slope of 5.19 μA/ppm and a linear regression correlation coefficient of 0.997. The fact that the stripping peak current increased proportionally with the Au(III) concentration indicates the As is depositing on and interacting with the Au rather than the diamond. Based on these results, an Au(III) concentration of 100 ppb was selected for use in the method.

5.2.3 Electrochemical Measurements

Figure 5.3 shows cyclic voltammetric *i-E* curves for a diamond electrode in contact with a 100 ppb Au(III) + 1 M HCl solution as a function of the As(III) solution concentration. Curves were recorded for standard additions of As(III) from 500 to 1000 ppb. The potential was scanned between -0.40 and 0.40 V at a scan rate of 100 mV/s. Therefore, the cathodic potential limit was sufficient for

the co-deposition of both Au and As. The peak current at 0.16 V is due to the oxidation of As to As(III). The oxidation peak current increased linearly with the As(III) concentration in solution and linearly with the square root of the potential sweep rate. The latter trend indicates that the oxidation reaction rate is limited by semi-infinite linear diffusion of As(III) away from the surface. The mass transfer limitation was further confirmed by noting that the As stripping peak current increased 4 to 5 times when convection was introduced by simple N_2 gas bubbling. The cathodic peak observed at about -0.38 V increased proportionally with the As(III) concentration and is attributed to the three-electron reduction of As(III) to As (i.e., formation of Au-As intermetallic).[18]
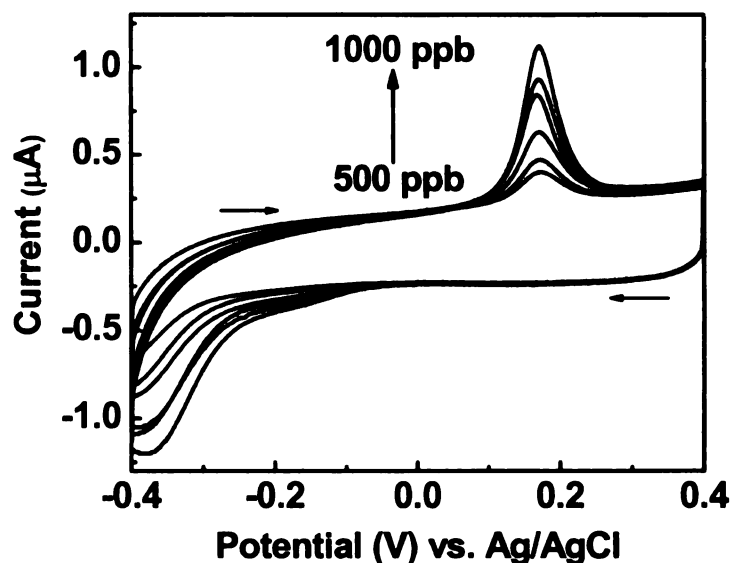
Figure 5.3 Cyclic voltammetric *i-E* curves for a diamond electrode in contact with a 100 ppb Au(III) + 1 M HCl solution as a function of the As(III) solution concentration, which ranged from 500 to 1000 ppb. Scan rate = 100 mV/s.

A series of measurements was made to investigate the effect of the deposition potential and time on the As stripping peak. Figure 5.4 shows how the As stripping peak current density changed as a function of the deposition potential at a Au-coated diamond. The current density was calculated by dividing the peak current by the electrode's geometric area (0.2 cm^2).
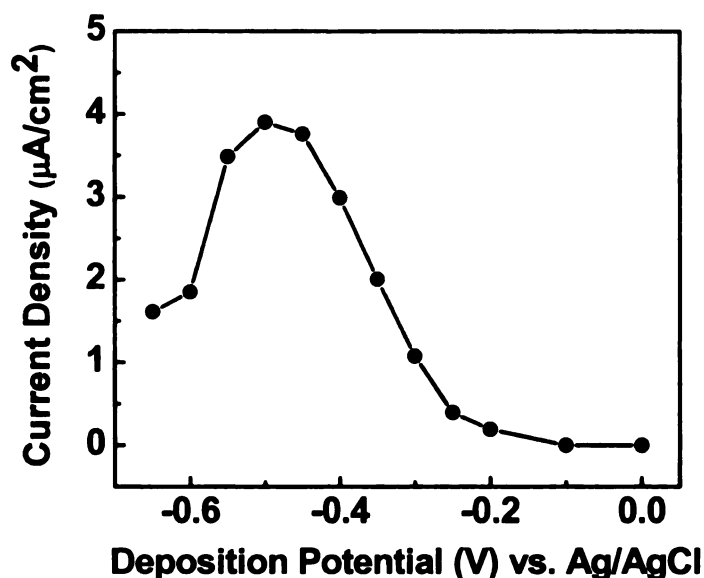
Figure 5.4 A comparison of the effect of the deposition potential on the As stripping current density at a Au-coated diamond and Au foil electrode in a solution of 200 ppb As(III) and 50 ppb Au(III) + 1 M HCl. DPASV parameters: t_{dep} = 110 s, pulse width = 50 ms, pulse amplitude = 50 mV, step height = 4 mV, cycle period 200 ms and sampling time = 8.33 ms.

For the Au-coated diamond electrode, deposition of As commenced at -0.2 V vs. Ag/AgCl. The stripping peak current increased as the deposition potential was made more negative up to -0.5 V. For deposition at potentials negative of this value, a decrease in the stripping peak current was observed.

This suggests that less elemental As was formed due to the competitive generation of H_2 or AsH_3.[2] This result is in agreement with the observation of Feeney and Kounaves for a Au ultramicroelectrode array.[2] Based on these results, an optimum deposition potential of -0.45 V was selected for the Au-coated diamond electrode.
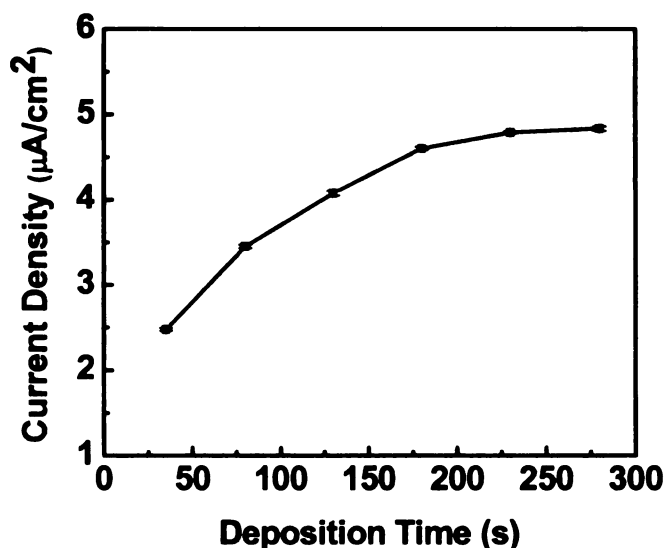
Figure 5.5 Effect of deposition time on the As stripping peak current density at a Au-coated diamond electrode in a solution of 200 ppb As(III) and 50 ppb Au(III) + 1 M HCl. DPASV parameters: E_{dep} = -0.45 V, pulse width = 50 ms, pulse amplitude = 50 mV, step height = 4 mV, cycle period 200 ms and sampling time = 8.33 ms.

Figure 5.5 shows the relationship between the As stripping peak current density and the deposition time at -0.45 V for a Au-coated diamond electrode. The peak current increased proportionally with time between 35 and 160 s. However, for deposition times greater than 160 s, the stripping peak current

leveled off. This is consistent with a saturation of the available Au surface sites for As deposition. It is supposed that once As covers the entire Au particle surface, no more As can be deposited.[2] Based on these results, a deposition time of 120 s was selected for use in the method; a balance between maximum signal and excessive deposition time.
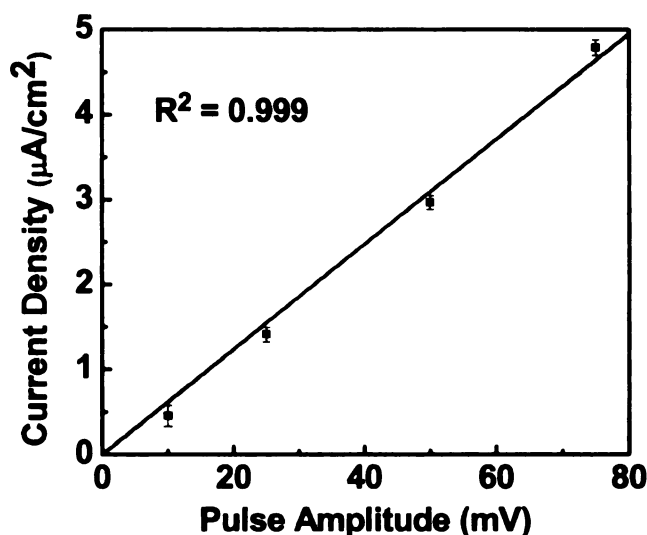
Figure 5.6   Effect of the pulse amplitude on the As stripping peak current density at a Au-coated diamond electrode in a solution of 200 ppb As(III) and 50 ppb Au(III) + 1 M HCl. DPASV parameters: E_{dep} = -0.45 V, t_{dep} = 120 s, pulse width = 50 ms, step height = 4 mV, cycle period 200 ms and sampling time = 8.33 ms.

Figure 5.6 shows how the As stripping peak current density changed with the pulse voltage amplitude at a Au-coated diamond electrode. According to the equation derived by Lund and Onshus for the differential pulse voltammetric response of a hanging mercury drop electrode (HMDE), the peak current should

scale proportionally with the pulse amplitude.[57]

$$\Delta i_p = kn^2r\Delta Eu^{1/2}t_dC_b$$

In this equation, k is the electron transfer rate constant, n is the number of the electrons transferred, r is the radius of the mercury drop, ΔE is the pulse amplitude, u is the rotation speed of the stirrer, t_d is the deposition period and C_b is the concentration of metal ion in the sample solution. The linearity between the As stripping peak current and the pulse amplitude (10 to 75 mV) is shown in Figure 5.6. Increasing the pulse amplitude caused an increase in the sensitivity of the measurement but a decrease in the peak resolution.[58] A pulse amplitude of 50 mV was selected for use in the method.

5.2.4 Au-Coated Diamond vs. Au Foil for As(III) Detection

Figure 5.7A shows DPASV *i-E* stripping curves for As co-deposited with Au from standard additions of As(III) in 100 ppb Au(III) + 1 M HCl for Au-coated diamond electrode. A response curve in the inset shows the proportionality between the As stripping peak current and the As(III) solution concentration between 0.01 and 40 ppb. Figure 5.7B shows comparison curves for Au foil. Each point is an average of 3 measurements with the bars representing the standard deviation. The As stripping peak current increased at both electrodes proportionally with the As(III) solution concentration as both curves had linear regression coefficients of > 0.990.
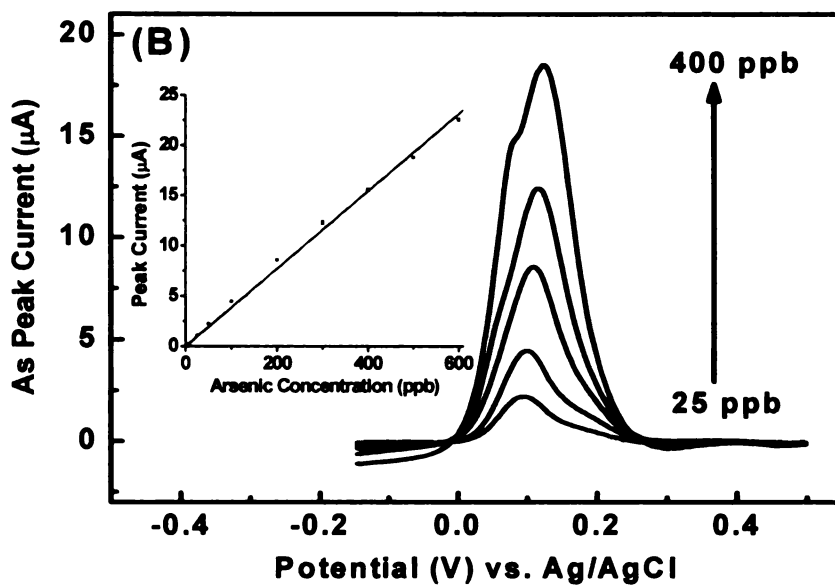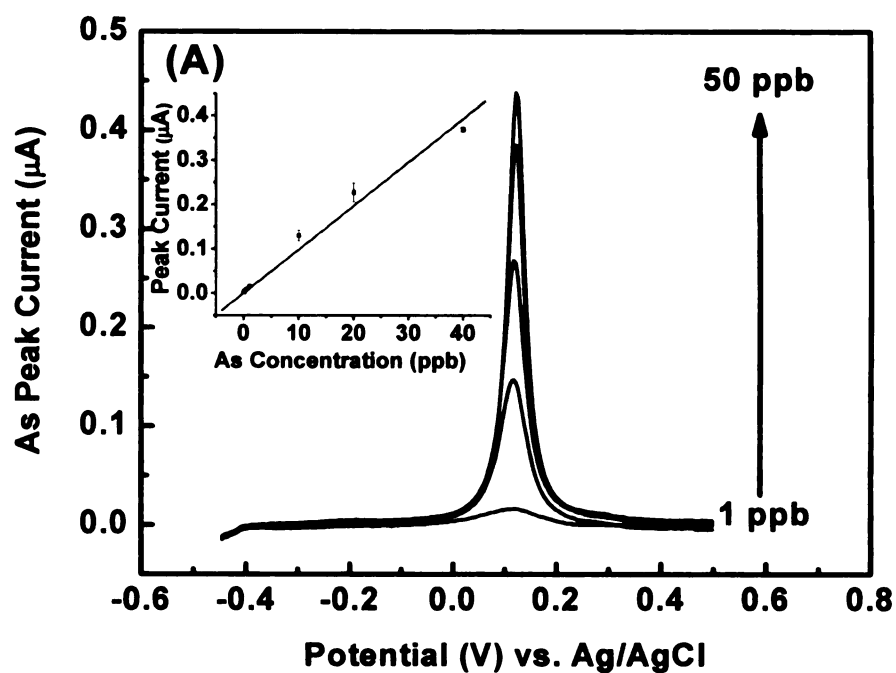
Figure 5.7 DPASV *i-E* stripping curves for As using standard additions of As(III)

at (A) a Au-coated diamond electrode in a solution of 100 ppb Au(III) + 1 M HCl

and (B) a Au foil electrode in a solution of 1 M HCl. The As(III) concentration ranged from 1 to 50 ppb. A response curve in the inset shows the proportionality between the As stripping peak current and the As(III) solution concentration. DPASV parameters: E_{dep} = -0.45 V, t_{dep} = 120 s, pulse width = 50 ms, pulse amplitude = 50 mV, step height = 4 mV, cycle period 200 ms and sampling time = 8.33 ms.

Table 5.2   Comparison of the ASV detection figures of merit for As at Au-coated diamond and Au foil electrodes.

	Au-Coated Diamond	Au Foil
LOD (S/N = 3)	0.005 ppb	0.25 ppb
LOD (R^2 = 0.99)	0.01 – 40 ppb	0.25 – 1200 ppb
Sensitivity	9.7 ± 2.5 µA/ppm	48.2 ± 10.2 µA/ppm
Response Precision (RSD)	4.4%	4.7%
FWHM at 50 ppb	38 mV	85 mV

Table 5.2 presents a summary of the As(III) detection figures of merit for the two electrodes. The LOD for diamond was estimated to be 0.005 ppb (S/N = 3) with a linear dynamic range (LDR) from 0.01 to 40 ppb and a slope or a sensitivity of 9.7 ± 2.5 µA/ppm. The lowest concentration actually measured was 0.01 ppb. The response reproducibility for both electrodes was excellent with values less than 5% for 10 consecutive measurements. The As stripping peaks for the Au-coated diamond were a factor of two or more narrow than the peaks

for the Au foil. This is attributed to As oxidizing from Au sites on diamond that are more morphologically and electronically homogeneous than the sites on Au foil. The larger sensitivity for the Au foil can be attributed to a higher Au surface area available for As deposition.

The LOD and response sensitivity for the Au-coated diamond electrode are as good or superior to other methods reported in the literature.[13, 16-20, 42, 59] A summary of data reported for Au-coated carbon electrodes is presented in Table 5.3. The data from the present work are included. The Au-coated diamond electrode has an LOD (0.005 ppb) lower than any of the other Au-coated carbon electrodes (0.0096 ppb for Au-coated glassy carbon[18] and 0.4 ppb for Au-coated graphite[19]) with a smaller amount of Au (0.1 ppm) in solution and a similar deposition time (120 s). The linear dynamic range from 0.01 to 40 ppb is wider than other reports for both Au-coated glassy carbon (5 to 50 ppb)[20] and Au-coated graphite (0 to 20 ppb)[19]. The sensitivity for the Au-coated diamond electrode (9.7 ± 2.5 µA/ppm) is smaller than that reported for the Au-coated glassy carbon (240 µA/ppm)[18] and Au-coated graphite (22.5 ± 0.9 × 10^6 µA/ppm)[19], but this can be attributed to a reduced Au surface area available for deposition. The precision and accuracy of Au-coated diamond electrode are comparable to the other Au-coated carbon electrodes. In summary, the Au-coated diamond electrode provides as good or superior detection figures of merit for As(III) as compared to other electrodes and can be used without any time consuming pretreatment. There are additional advantages of this electrode that are described in Chapter 6.

Table 5.3   Comparison of the ASV Detection Figures of Merit for As at Au-Coated Carbon Electrodes.

Electrode	C_{Au} (ppm)	Au t_{dep} (s)	Method	E_{dep} (V vs. Ag/AgCl)	t_{dep} (s)	LOD (ppb)	LDR	Sensitivity (µA/ppm)	Precision	Accuracy[a]
Boron-doped diamond	0.1	Co-deposit	ASV	-0.45	120	0.005	0.01 - 40 ppb	9.7 ± 2.5	4.44%	11% (ICP-MS)
Glassy carbon[18]	7.5	15	LSV	-0.26	180	0.0098	—	240	—	—
Glassy carbon[20]	160	Co-deposit	PS	-0.1	60	0.55	5 - 50 ppb	—	6 - 9%	0.8-1.4%
Glassy carbon[59]	236	240 - 480	PS	-0.01	120	0.32	75 - 3746 ppb	—	8% - 10%	—
Pyrolytic graphite[13]	10	—	ASV	-0.15	120	—	0 - 0.5 mg	—	2% - 28%	1.4% - 45%
Graphite[19]	500	800	ASV	-0.3	100	0.4	0 - 20 ppb	$(22.5 \pm 0.9) \times 10^6$	15%	8.15% - 15.01%
Graphite[16]	100	800	ASV	-0.5	120	17.2	15 - 524 ppb	2.32 ± 0.17	—	—

[a] If not stated, the value was the difference% compared with a certified value or a group average
ASV: anodic stripping voltammetry; PS: potentiometric stripping; LSV: linear sweep voltammetry
C_{Au}: Au concentration; Au t_{dep}: predeposition time of Au; LOD: limit of detection; LDR: linear dynamic range

112

5.2.5 As(V) Detection

Due to kinetic limitations, As(V) is difficult to detect directly by ASV. Therefore, its analysis is often performed by an initial chemical reduction to As(III) followed by ASV detection. Na_2SO_3 was used as the reducing agent because of its high efficiency.[12, 14, 42] Several factors can affect the As(V) to As(III) conversion efficiency when using this reducing agent: heating temperature, heating time, Na_2SO_3 concentration and solution pH because they determine the amount of SO_3^{2-} reactant available. 50 °C was used for heating because at this temperature the SO_3^{2-} production rate is high without great loss due to the formation of SO_2. A 30 min heating period was found to provide a high conversion efficiency (92.6 ± 10.9%, n=5). A Na_2SO_3 concentration of 20 mM was determined to be sufficient to reduce 50 ppb As(V) to As(III) under such heating conditions.
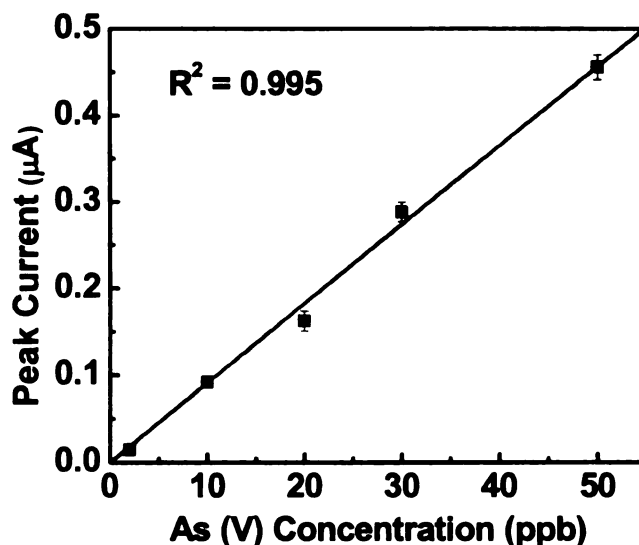
Figure 5.8 A response curve showing the proportionality between the As stripping peak current and the As(V) solution concentration at a Au-coated diamond electrode. The As(V) concentration ranged from 1 to 50 ppb. DPASV parameters: E_{dep} = -0.45 V, t_{dep} = 120 s, pulse width = 50 ms, pulse amplitude = 50 mV, step height = 4 mV, cycle period 200 ms and sampling time = 8.33 ms.

Figure 5.8 shows that the stripping peak current for As (As → As(III)) increased linearly with the As(V) solution concentration. This indicates the As(V) reduced to As(III) with high efficiency. The LOD was determined to be 0.08 ppb, the linear dynamic range was from 0.08 to 50 ppb and the sensitivity was 9.1 μA/ppm. The sensitivity is very close to that for As(III) detection, as expected. A small error bar was obtained for every concentration of As(V) tested (from 2 to 50 ppb), which means the method is reproducible.

5.2.6 Real Sample Analysis

The Au-coated diamond electrode and the DPASV method were used to determine the concentration of As(III) in the local Red Cedar River water. Using the standard addition method, the river water was found to contain 0.6 ± 0.1 ppb As(III). This value was arrived at by making standard additions of As(III) to the river water and generating a response curve. Figure 5.9 shows DPASV stripping voltammetric *i-E* curves and the corresponding response curve for standard additions of As(III) from 2.5 to 40 ppb to acidified river water containing 100 ppb Au(III). An electrode response sensitivity of 5 μA/ppm was obtained from the

curve. Higher baseline noise and lower sensitivity were observed for the electrode in river water, as compared to the standard solutions.
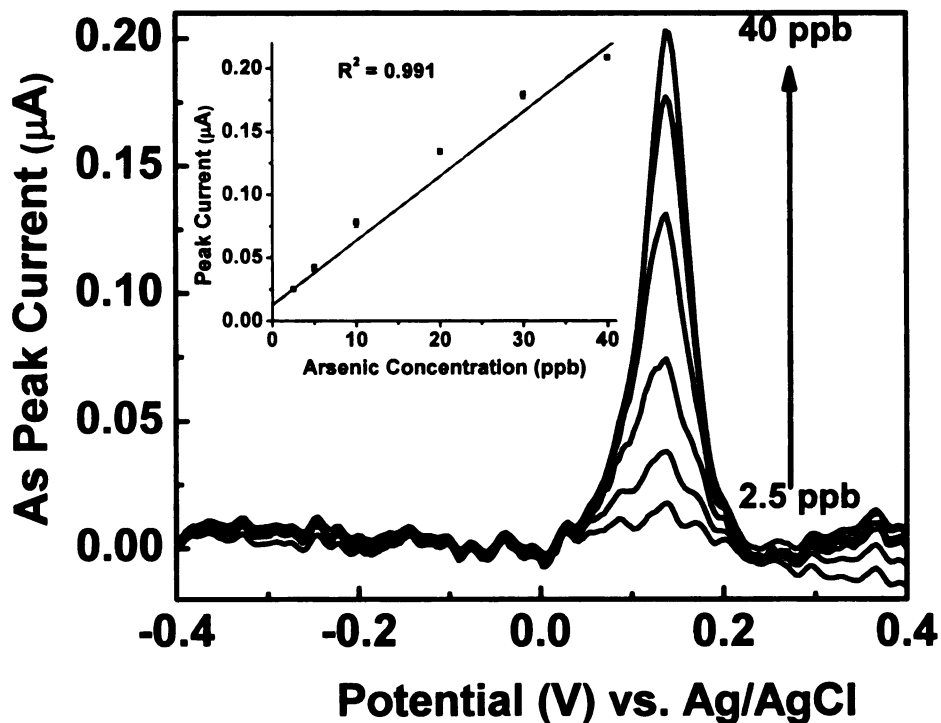
Figure 5.9   DPASV *i-E* curves and the corresponding response curve for the addition of 2.5 - 40 ppb As(III) to Red Cedar River water acidified with 100 ppb Au(III) + 1 M HCl on a Au-coated diamond electrode. DPASV parameters: E_{dep} = -0.45 V, t_{dep} = 120 s, pulse width = 50 ms, pulse amplitude = 50 mV, step height = 4 mV, cycle period 200 ms and sampling time = 8.33 ms.

The As deposition charge was measured for both the standards and river water samples containing 100 ppb As(III) by holding the potential at -0.45 V for 120 s and integrating the current-time profile. It was found that the deposition

charge for the same concentration of As(III) in the river water was about half of that for the standard sample. This is the reason for the lower sensitivity and can be attributed to the deleterious influence of other metal ion or organic matter interferences present in the river water. For example, it has been reported that Cu(II), Hg(II) and Pb(II) can all cause a decrease in the As stripping peak current.[2] Pb(II) poses a significant interference for As deposition, particularly when its concentration is 5 times higher than that of arsenic. Hg(II) also interferes with As deposition when present at equal or greater concentrations. Cu forms a complex with As in the solid phase, thereby reducing the As(III) activity in solution and decreasing the amount available for codeposition with Au.[2] According to the ICP-MS analysis, the river water contained about 0.1 ppb Cu(II) and 5 ppb Pb(II). Therefore, both contaminants are a cause for the lower sensitivity. Organic matter in the water could also have been another reason since these molecules can adsorb on the electrode, block reaction sites and prevent As deposition. However, results described in Chapter 6 show that the presence of up to 5 ppm of humic acid did not cause a significant decrease in the Au-coated diamond electrode response magnitude and reproducibility. Therefore, it is concluded that the main reason for the decreased electrode sensitivity for inorganic arsenic in river water was the presence of interfering Cu(II) and Pb(II). Results described in Chapter 6 show that the effect of metal ion interferences can be mitigated by the use of solid phase extraction (cation exchange) in the sample preparation.

The reproducibility and long-term response stability of the Au-coated

diamond was assessed using acidified Red Cedar River water (1 M HCl) spiked with 20 ppb As(III). Au-coated diamond and glassy carbon electrodes were compared under the same conditions. A run-to-run reproducibility test was performed over 10 consecutive measurements. Longer term stability studies were carried out by leaving the electrode exposed continuously to the As(III) solution for 10 h and periodically measuring the As stripping peak current (each hour). For the 10 consecutive measurements, the Au-coated diamond showed RSD < 2% for both peak current and charge, while the Au-coated glassy carbon yielded a 4.4% RSD in the peak current and a 7.5% RSD in the peak charge. For the 10-h stability test, the Au-coated diamond showed superior stability with response loss of only 9.1% in the peak current and 6.9% in the peak charge as compared to the Au-coated glassy carbon, which showed a response loss of >15% in both the peak current and charge. The reproducibility and stability results are summarized in Table 5.4.

Table 5.4   Comparison of As Stripping Peak Reproducibility and Stability at Au-Coated Diamond and Glassy Carbon Electrodes in River Water.

RSD (n = 10)	Peak Current		Peak Charge	
	Au-coated Diamond	Au-coated Glassy Carbon	Au-coated Diamond	Au-coated Glassy Carbon
Run-to-run test	1.5%	4.4%	1.9%	7.5%
10 h test	9.1%	15.5%	6.9%	15.7%

The   accuracy   of   the   method   was   assessed   by   comparing   the

electrochemical results with those obtained by ICP-MS. A standard solution containing 15 ppb As(III) was analyzed using both methods. Response curves were generated by measuring the signals of different concentrations of As(III) standard solutions. A value of 14.5 ± 0.2 ppb was obtained by ICP-MS and a value of 16.1 ± 0.4 ppb was found electrochemically. This represents a difference of 11%.

5.3 Conclusions

The Au-coated diamond electrode provided a sensitive, reproducible and stable response for inorganic arsenic in both standard and real samples. The Au-coated diamond electrode offers advantages over commonly used electrode materials, such as Au and Au-coated carbon electrodes, in terms of the peak shape and detection figures of merit. Au deposited on diamond from an Au(III) solution in the form of relatively small particles with a small variance (22 ± 3 nm) and high particle density (10^{10} cm^{-2}). Sub-ppb LODs were obtained for As(III) and As(V) in both standard and local river water samples. The responses of Au-coated diamond and a Au foil electrode for As(III) detection were compared using the same experimental conditions. Au-coated diamond was found to yield narrower stripping peaks and a lower LOD than Au foil. This method was shown to be practical for real sample analysis as 0.6 ppb of As(III) was detected in local river water with the electrode response variance less than 2% (RSD) for 10 consecutive measurements and a response stability over a 10-h period of better than 94%.

5.4 References

(1)   Li, H.; Smart, R. B. *Analytica Chimica Acta* **1996**, *325*, 25-32.

(2)   Feeney, R.; Kounaves, S. P. *Analytical Chemistry* **2000**, *72*, 2222-2228.

(3)   Ferreira, M. A.; Barros, A. A. *Analytica Chimica Acta* **2002**, *459*, 151-159.

(4)   Sadana, R. S. *Analytical Chemistry* **1983**, *55*, 304-307.

(5)   Holak, W. *Analytical Chemistry* **1980**, *52*, 2189-2192.

(6)   Barra, C. M.; Correia dos Santos, M. M. *Electroanalysis* **2001**, *13*, 1098-1104.

(7)   Adeloju, S. B.; Young, T. M.; Jagner, D.; Batley, G. E. *Analytica Chimica Acta* **1999**, *381*, 207-213.

(8)   Williams, D. G.; Johnson, D. C. *Analytical Chemistry* **1992**, *64*, 1785-1789.

(9)   Hignett, G.; Wadhawan, J. D.; Lawrence, N. S.; Hung, D. Q.; Prado, C.; Marken, F.; Compton, R. G. *Electroanalysis* **2004**, *16*, 897-903.

(10)   Wei, Z.; Somasundaran, P. *Journal of Applied Electrochemistry* **2004**, *34*, 241-244.

(11)   Simm, A. O.; Banks, C. E.; Compton, R. G. *Analytical Chemistry* **2004**, *76*, 5051-5055.

(12)   Forsberg, G.; O'Laughlin, J. M.; Megargle, R. G. *Analytical Chemistry* **1975**, *47*, 1586-1592.

(13)   Davis, P. H.; Dulude, G. R.; Griffin, R. M.; Matson, W. R.; Zink, E. W. *Analytical Chemistry* **1978**, *50*, 137-143.

(14)   Feeney, R.; Kounaves, S. P. *Talanta* **2002**, *58*, 23-31.

(15)   Prakash, R.; Srivastava, R. C.; Seth, P. K. *Electroanalysis* **2003**, *15*, 1410-1414.

(16)   Kamenev, A. I.; Orlov, S. E.; Lyakhov, A. B. *Jouranal of Applied Electrochemistry* **2001**, *56*, 850-854.

(17) Simm, A. O.; Banks, G. E.; Wilkins, S. J.; Karousos, N. G.; Davis, J.; Compton, R. G. *Analytical and Bioanalytical Chemistry* **2005**, *381*, 979-985.

(18) Dai, X.; Nekrassova, O.; Hyde, M. E.; Compton, R. G. *Analytical Chemistry* **2004**, *76*, 5924-5929.

(19) Viltchinskaia, E. A.; Zeigman, L. L.; Garcia, D. M.; Santos, P. F. *Electroanalysis* **1997**, *9*, 633-640.

(20) Munoz, E.; Palmero, S. *Electroanalysis* **2004**, *16*, 1528-1535.

(21) Akhmedzhanova, G. M.; Tikhomirova, V. I. *Experiment in Geosciences* **1995**, *4*, 26-28.

(22) Tikhomirova, V. I.; Akhmedzhanova, G. M.; Nekrasov, I. Y. *Experiment in Geosciences* **1994**, *3*, 1-9.

(23) Swain, G. M. *Journal of The Electrochemical Society* **1994**, *141*, 3382-3393.

(24) Swain, G. M.; Ramesham, R. *Analytical Chemistry* **1993**, *65*, 345-351.

(25) Muna, G. W.; Tasheva, N.; Swain, G. M. *Environmental Science and Technology* **2004**, *38*, 3674-3682.

(26) Haymond, S.; Babcock, G. T.; Swain, G. M. *Electroanalysis* **2003**, *15*, 249-253.

(27) Granger, M. C.; Xu, J.; Strojek, J. W.; Swain, G. M. *Analytica Chimica Acta* **1999**, *397*, 145-161.

(28) Granger, M. C.; Witek, M.; Xu, J.; Wang, J.; Hupert, M.; Hanks, A.; Koppang, M. D.; Butler, J. E.; Lucazeau, G.; Mermoux, M.; Strojek, J. W.; Swain, G. M. *Analytical Chemistry* **2000**, *72*, 3793-3804.

(29) Hupert, M.; Muck, A.; Wang, J.; Stotter, J.; Cvackova, Z.; Haymond, S.; Show, Y.; Swain, G. M. *Diamond and Related Materials* **2003**, *12*, 1940-1949.

(30) Show, Y.; Matsukawa, T.; Ito, H.; Iwase, M.; Izumi, T. *Diamond and Related Materials* **2000**, *9*, 337-340.

(31) Iniesta, J.; Michaud, P. A.; Panizza, M.; Cerisola, G.; Aldaz, A.; Comninellis, C. *Electrochimica Acta* **2001**, *46*, 3573-3578.

(32)   Rodrigo, M. A.; Michaud, P. A.; Duo, I.; Panizza, M.; Cerisola, G.; Comninellis, C. *Journal of the Electrochemical Society* **2001**, *148*, D60-D64.

(33)   Iniesta, J.; Exposito, E.; Gonzalez-Garcia, J.; Montiel, V.; Aldaz, A. *Journal of the Electrochemical Society* **2002**, *149*, D57-D62.

(34)   Terashima, C.; Rao, T. N.; Sarada, B. V.; Tryk, D. A.; Fujishima, A. *Analytical Chemistry* **2002**, *74*, 895-902.

(35)   Sonthalia, P.; McGaw, E.; Show, Y.; Swain, G. M. *Analytica Chimica Acta* **2004**, *522*, 35-44.

(36)   McGaw, E. A.; Swain, G. M. *Analytica Chimica Acta* **2006**, *575*, 180-189.

(37)   Cavicchioli, A.; La-Scalea, M. A.; Gutz, I. G. R. *Electroanalysis* **2004**, *16*, 697-711.

(38)   Arnold, J. P.; Johnson, R. M. *Talanta* **1969**, *16*, 1191-1207.

(39)   Kotoucek, M.; Vasicova, J.; Ruzicka, J. *Mikrochimica Acta* **1993**, *111*, 55-62.

(40)   Sancho, D.; Vega, M.; Deban, L.; Pardo, R.; Gonzalez, G. *Analyst* **1998**, *123*, 743-747.

(41)   Lee, S. W.; Meranger, J. C. *Analytical Chemistry* **1981**, *53*, 130-131.

(42)   Hamilton, T. W.; Ellis, J.; Florence, T. M. *Analytica Chimica Acta* **1980**, *119*, 225-233.

(43)   Henry, F. T.; Kirch, T. O.; Thorpe, T. M. *Analytical Chemistry* **1979**, *51*, 215-217.

(44)   Rochette, E. A.; Bostick, B. C.; Li, G.; Fendorf, S. *Environmental Science and Technology* **2000**, *34*, 4714-4720.

(45)   Greulach, U.; Henze, G. *Analytica Chimica Acta* **1995**, *306*, 217-223.

(46)   Kowalska, J.; Stryjewska, E.; Szymanski, P.; Golimowski, J. *Electroanalysis* **1999**, *11*, 1301-1304.

(47)   Kowalska, J.; Golimowski, J. *Electroanalysis* **1998**, *10*, 857-859.

(48)   Kowalska, J.; Golimowski, J.; Kazimierska, E. *Electroanalysis* **2001**, *13*, 872-875.

(49) Holt, K. B.; Bard, A. J.; Show, Y.; Swain, G. M. *Journal of Physical Chemistry B* **2004**, *108*, 15117-15127.

(50) Enea, O.; Riedo, B.; Dietler, G. *Nano Letters* **2002**, *2*, 241-244.

(51) Bennett, J. A.; Show, Y.; Wang, S.; Swain, G. M. *Journal of The Electrochemical Society* **2005**, *152*, E184-192.

(52) Honda, K.; Noda, T.; Yoshimura, M.; Nakagawa, K.; Fujishima, A. *Journal of Physical Chemistry B* **2004**, *108*, 16117-16127.

(53) Wilson, N. R.; Clewes, S. L.; Newton, M. E.; Unwin, P. R.; Macpherson, J. V. *Journal of Physical Chemistry B* **2006**, *110*, 5639-5646.

(54) Scharifker, B.; Hills, G. *Electrochimica Acta* **1983**, *28*, 879-889.

(55) Vinokur, N.; Miller, B.; Avyigal, Y.; Kalish, R. *Journal of The Electrochemical Society* **1999**, *146*, 125-130.

(56) Dinan, T. E.; Jou, W.-F.; Cheh, H. Y. *Journal of The Electrochemical Society* **1989**, *136*, 3284-3287.

(57) Lund, W.; Onshus, D. *Analytica Chimica Acta* **1976**, *86*, 109-122.

(58) Wang, J. *Stripping Analysis*; VCH publishers, Inc.: Deerfield Beach, 1985.

(59) Jagner, D.; Josefson, M.; Westerlund, S. *Analytical Chemistry* **1981**, *53*, 2144-2146.

CHAPTER 6

TOTAL INORGANIC As DETECTION IN REAL WATER SAMPLES USING DPASV AND A Au-COATED DIAMOND THIN-FILM ELECTRODE

6.1 Introduction

In Chapter 5, a sensitive and reproducible method was developed for total inorganic arsenic determination in real water samples using differential pulse anodic stripping voltammetry (DPASV) and a Au-coated boron-doped diamond thin-film electrode. In the analysis, the As(III) present in the samples was first detected by DPASV. The As(V) present was then reduced to As(III) by reaction with Na_2SO_3 and this was followed by a second detection of As(III) by DPASV. In general, Au-coated diamond showed lower LOD and higher stability compared with Au and Au-coated carbon electrodes.[1, 2] However, when applying Au electrodes and ASV for real sample analysis, many researchers have reported decreased sensitivity for As due to metal ion interferences commonly present in ground water (e.g., Cu(II), Pb(II) and Hg(II)).[3-12] For example, Feeney and Kounaves reported that at a 1:1 concentration ratio Pb(II) caused a 10% decrease, Cu(II) caused a 65% decrease and Hg(II) caused a 30% decrease in the As stripping current on a Au ultramicroelectrode array.[5] Many other metal ions, such as Fe(II),[9] Zn(II),[9] Tl(I) and (III)[7, 13] and Sn(II) and (IV),[7, 13] can also interfere with As detection and cause decreased sensitivity. There are two mechanisms by which these metal ions interfere: (i) competition with As during

the deposition step or (ii) formation of an intermetallic complex with As.[3] In order to accurately determine trace levels of inorganic arsenic in real water samples, metal ion interferences must be removed.

Several approaches have been used to reduce metal ion interferences. For example, Tanaka and Sato eliminated Fe(III) effects by reducing Fe(III) to Fe(II) with KI.[14] Hamilton separated Cu(II) and Sb(III) from As(III) and (V) by solid phase extraction (SPE) using a Chelex 100 column.[6] The Chelex 100 cation exchange resin not only has high affinity for Cu(II), but also for Fe(II) and other heavy metal ions, as well as good selectivity for divalent over monovalent ions (approximately 5,000 to 1).[15] Chelex 100 resin is a styrene divinylbenzene copolymer containing paired iminodiacetate ions. The iminodiacetate ions are the chelating groups binding polyvalent metal ions. At pH < 4, the resin acts as an anion exchanger, while at pH > 4, the resin acts as a cation exchanger.[15] In this application, to separate inorganic arsenic from the interfering metal ions at pH = 4-7, use of the cation exchange resin is ideal. This is because inorganic arsenic exists as a neutral or an anion in solution in this pH range. As(III) exists as AsO_3^{3-} (pH = 14), $HAsO_3^{2-}$ (pH = 13), $H_2AsO_3^-$ (10 < pH < 12) and H_3AsO_3 (0 < pH < 9). As(V) exists as $[AsO_4(H_2O)_{12}]^{3-}$ (pH > 13), $[HAsO_4(H_2O)_6]^{2-}$ (7 < pH < 11), $[H_2AsO_4(H_2O)_2]^-$ (3.5 < pH < 6) and H_3AsO_4 (pH < 3.5).[16] At pH 4 to 7, most of the interfering metal ions will exist as cations and during passage through the resin, they will be electrostatically attracted to the ion exchange sites while arsenic will pass through unretained.

When using ASV for water analysis, another interference that can cause

decreased sensitivity is organic matter in the sample matrix. Humic material is a form of organic matter often found in soil and ground water. Humic material is produced by the decomposition or transformation of organic matter and consists of free and bound phenolic OH groups, quinone functionalities, N and O bridge units and acidic COOH functionalities located on aromatic rings.[17] Humic substances can be divided into three types: fulvic acid, humic acid and humin. Each type is different in terms of color, molecular weight, functional group density and extent of polymerization. From fulvic acid to humin, the molecular weight increases from a few hundred to several hundred thousand, and the functional group density and extent of polymerization also increase. Deprotonation of the acid groups imparts negative charge to humic substances. Cationic metal ions can bind at these negatively charged sites, thus reducing their activity in solution. These high molecular weight substances have a tendency to adsorb on electrode surfaces, driven by chemical and/or electrostatic forces. Adsorbed humic material fouls the electrode and reduces the response stability and reproducibility for a target analyte.[18, 19]

Boron-doped diamond possesses beneficial properties for water quality monitoring. These properties distinguish it from the conventionally used metal and sp^2 carbon electrodes and include: (i) low and stable background current, (ii) wide background window, (iii) an active response for many redox analytes without extensive surface pretreatment, (iv) stable surface microstructure and morphology in harsh electrochemical environment and (v) weak adsorption of polar molecules due to the nonpolar, hydrogen surface termination. The last

property is particular important when applying the material for water quality analysis.[19-30]

In this Chapter, we report on a sensitive, reproducible and accurate method for total inorganic arsenic analysis in real samples by DPASV using a Au-coated boron-doped diamond thin-film electrode. In the method, As(III) present in the sample was first determined by DPASV. The As(V) present was then chemically reduced to As(III) by Na_2SO_3 and this was followed by a second As(III) determination. The difference between the two stripping currents is related to the As(V) concentration in solution. Interfering metal ions (e.g., Cu(II), Hg(II) and Pb(II)) were removed by passing the water sample through a cartridge containing Chelex 100 cation exchange resin (pH 4-7). The interfering metal ions (e.g., Cu(II)) were retained while the neutral arsenious acid (H_3AsO_3) and anionic arsenate ($[H_2AsO_4(H_2O)_2]^-$) passed through unretained. The effect of humic acid was also studied by measuring the ASV response for As(III) as a function of its concentration from 1-5 ppm. Finally, the practical applicability of the method was shown for the total inorganic arsenic in two real water samples.

6.2 Results and Discussion

6.2.1 Effect of Metal Ions on As Detection

The effect of Cu(II) on the As stripping peak current was studied using the Au-coated diamond electrode and the results are presented in Figure 6.1A and B.

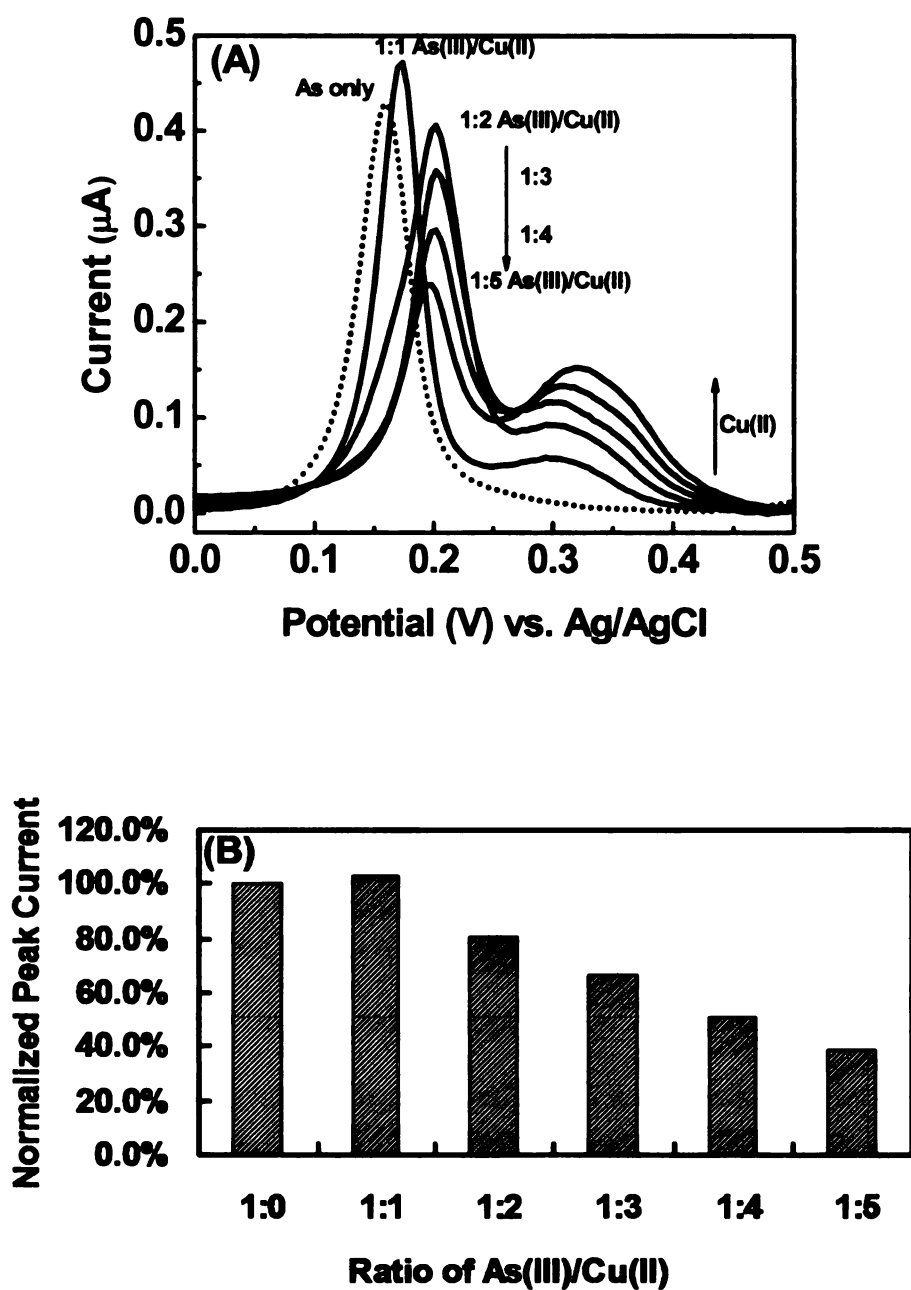**Figure 6.1** Effect of Cu(II) on the As stripping peak current at a Au-coated diamond electrode in a solution of 50 ppb As(III) and 100 ppb Au(III) + 1 M HCl. (A) DPASV stripping voltammetric *i-E* curves. (B) Plot of the normalized As stripping peak current as a function of the concentration ratio of As(III) and Cu(II) in solution. DPASV parameters: E_{dep} = -0.45 V, t_{dep} = 120 s, pulse width = 50 ms,

pulse amplitude = 50 mV, step height = 4 mV, cycle period 200 ms and sampling time at the end of the pulse = 8 ms.

Figure 6.1A shows the DPASV i-E stripping curves for As as a function of the amount of Cu(II) present in solution. The dotted line shows the i-E curve for the original solution containing only 50 ppb of As(III) and 100 ppb Au(III) in 1 M HCl. A peak for As oxidation to As(III) is observed at 0.17 V. With the addition of Cu(II) into the solution at a As(III)/Cu(II) concentration ratio of 1:1, the As stripping peak current slightly increased and the peak potential shifted positive by 8 mV. The increased peak current was caused by Cu(II) as it has been reported that the metal ion can facilitate As deposition on Hg and carbon electrodes by serving as a deposition initiator via the formation of a Cu_3As intermetallic species.[8] The Cu-As intermetallic species must be slightly more stable than the Au-As intermetallic compound because a more positive potential is needed to oxidize the As. As the concentration of Cu(II) increased though, the As stripping peak current decreased and the peak shifted slightly positive. A new peak also emerged at ca. 0.3 V that grew in magnitude with the Cu(II) concentration. This new peak is attributed to the oxidation of Cu metal (deposited on the Au particles and diamond surface during the preconcentration step).[31] The progressive attenuation of the As stripping peak current with increasing Cu(II) was caused by the formation of a different stoichiometric Cu-As intermetallic compound. The formation of this stable compound reduces the amount of As available for stripping. The bar graph in Figure 6.1B shows how the As stripping peak current

128

was affected by the As(III)/Cu(II) solution concentration ratio. Except at a ratio of 1:1, the As peak current decreased with increasing As(III)/Cu(II) ratio. For example, at As(III)/Cu(II) ratio of 1:3, the As peak current decreased by about 30%.

Without question, to accurately determine the inorganic arsenic concentration in a water sample, Cu(II) or other metal ion contaminants must be removed. Chelex 100 is a cation exchange resin that is effective at removing these interferences. Figure 6.2A shows a comparison of the DPASV i-E stripping curves for As in a solution devoid of Cu(II) and one that contained 1:3 As(III)/Cu(II) concentration ratio but was passed through the cation exchange resin prior to analysis. It is clear that solution passage through this resin eliminates the interfering Cu(II). The Cu(II) ions are removed by electrostatic binding with the negatively charged iminodiacetate sites on the resin. The inorganic arsenic, which exists as neutral arsenious acid (H_3AsO_3) and anionic arsenate ($[H_2AsO_4(H_2O)_2]^-$) at pH 4-7, passed through the resin unretained. It can be seen that there was no significant change in the stripping peak current and peak potential with the Cu(II) interference (compare with Figure 6.1). Recall that a response attenuation of about 30% was seen when Cu(II) was present at this ratio. Figure 6.2B shows a comparison of DPASV i-E stripping curves for As in the presence and absence of other interfering metal ions. Passing these solutions through the cation exchange resin prior to analysis is effective at removing these interferences when present originally at a 1:1:1:1 As(III)/Cu(II)/Hg(II)/Pb(II) concentration ratio. As was co-deposited with 100 ppb

of Au in all of these measurements. Important when using any solid phase for sample preparation is the analyte recovery, which for As(III) was determined to be 94.8 ± 2.4% (n = 5).
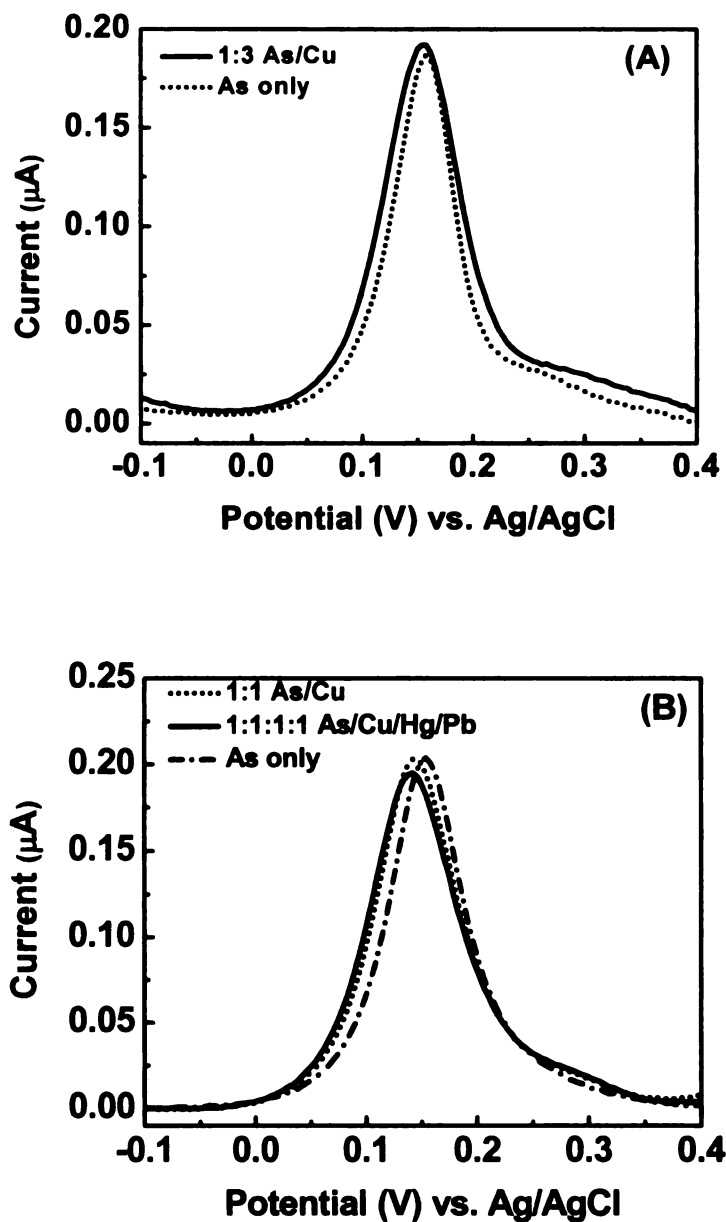

Figure 6.2 Comparison of the As stripping voltammetric *i-E* curves in solutions with and without interfering metal ions after passage through the cation exchange

resin. (A) Curves for 25 ppb As(III) + 75 ppb Cu(II) and (B) Curves for 25 ppb As(III) + 25 ppb Cu(II) and 25 ppb As(III) + 25 ppb Cu(II), Hg(II), Pb(II) each. DPASV parameters: E_{dep} = -0.45 V, t_{dep} = 120 s, pulse width = 50 ms, pulse amplitude = 50 mV, step height = 4 mV, cycle period 200 ms and sampling time at the end of the pulse = 8 ms.

6.2.2 Effect of Humic Substances on As Detection

The presence of organic matter can pose a serious threat to any electroanalytical measurement due to molecular adsorption and electrode fouling. A comparison of the effect of humic substance on the As stripping peak charge at Au-coated diamond and Au foil electrodes is presented in Figure 6.3. A bar graph of the normalized As stripping peak charge as a function of the humic acid concentration from 0 to 5 ppm is presented.
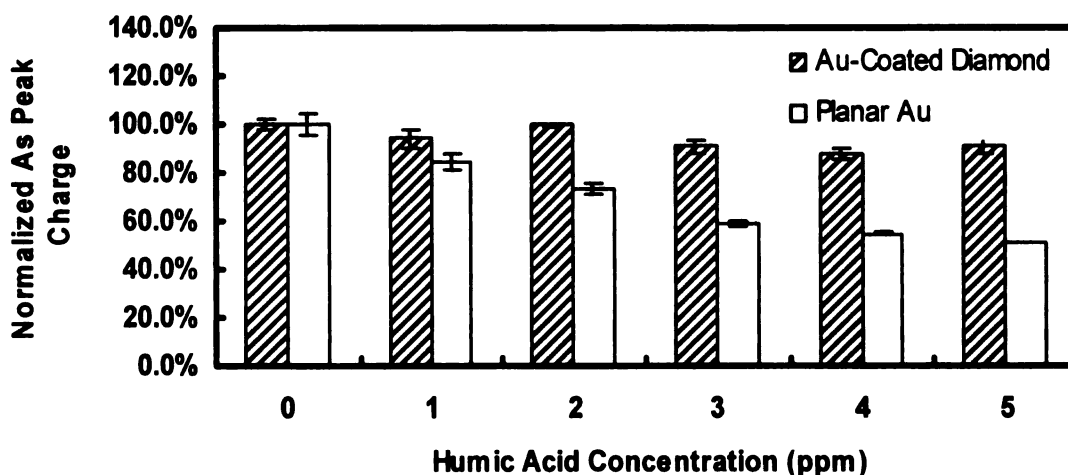

Figure 6.3   Comparison of the effect of added humic substances (0 to 5 ppm) on the As stripping peak charge in a solution of 50 ppb As(III) and 100 ppb Au(III)

+ 1 M HCl at a Au-coated diamond and a Au foil electrode. DPASV parameters: E_{dep} = -0.45 V, t_{dep} = 120 s, pulse width = 50 ms, pulse amplitude = 50 mV, step height = 4 mV, cycle period 200 ms and sampling time at the end of the pulse = 8 ms.

Humic acid clearly had a greater fouling effect on Au foil than on Au-coated diamond. At a concentration of 5 ppm, humic acid caused a 50% decrease in the As stripping peak charge for Au foil but only about a 9% decrease for Au-coated diamond. This observation indicates that the non-polar, hydrogen-terminated diamond near the metal particles plays a role in terms of influencing molecular adsorption on the metal by virtue of the hydrophobic chemical environment. As discussed in the Introduction, the humic substances cause decreased electrode sensitivity by binding with positively charged multivalent metal ions (the analytes) and reducing their activity and/or by strong and irreversible adsorption on the electrode surface (i.e., blocking effect). In these measurements, the solution contained no added interfering metal ions so the reason for the response attenuation is fouling by the humic acid. It is presumed that adsorbed humic acid blocks the Au surface preventing the deposition of As. Based on these results, the Au-coated diamond electrode provides a clear advantage compared with Au foil in terms of fouling resistance and response reproducibility and stability.

6.2.3 Analysis of Inorganic As in Real Water Samples

Two contaminated water samples were analyzed for their total inorganic

arsenic content using the DPASV method and a Au-coated diamond electrode. Four measurements were made with each sample using the sample preparation and DPASV conditions described above. The results are summarized in Table 6.1 and compared with the concentrations determined by the U.S. Bureau of Reclamation. For the UV plant influent water, 23.2 ± 2.9 ppb of total inorganic arsenic was found compared with the 24.2 ppb specified value; a difference of 4%. Well 119 water was found to contain 16.4 ± 0.9 ppb of inorganic arsenic, compared with the 16.8 ppb specified value; a difference of 2.4%. Clearly, for both samples, the results provided by DPASV with the Au-coated diamond were reproducible and accurate.

Table 6.1   Total Inorganic As Concentration in Real Water Samples.

	UV Water (ppb)	Tap 119 Water (ppb)
1	23.7	16.5
2	27.1	17.4
3	21.3	15.2
4	20.6	16.4
Average	23.2 ± 2.9	16.4 ± 0.9
Quoted Value	24.2	16.8
Difference%	4.0%	2.4%

6.3 Conclusions

The work reported on herein demonstrates that the Au-coated diamond electrode, combined with DPASV, provides a sensitive, reproducible and

accurate method for determining total inorganic arsenic levels in real samples. The properties of the diamond are key for obtaining high quality detection figures of merit and impart a greater degree of response stability, as evidenced by the humic acid studies. For example, a 5 ppm humic acid concentration caused a 50% decrease in the As stripping peak charge for Au foil and only a 9% decrease for Au-coated diamond. Solid phase extraction (cation exchange) was employed to remove interfering metal ions (e.g., Cu(II)) prior to analysis. The As(III) recovery after passage through the resin was high at 94.8 ± 2.4%. For two real water samples, the total inorganic arsenic concentration determined with the Au-coated diamond differed from the specified value by 4%, or less. It is our contention that this new electrode and method are practical for use in on-site analysis of total inorganic arsenic, offering advantages over commonly used Au and Au-coated glassy carbon electrodes.

6.4 References

(1) Song, Y.; Swain, G. M. *Submitted.*

(2) Hignett, G.; Wadhawan, J. D.; Lawrence, N. S.; Hung, D. Q.; Prado, C.; Marken, F.; Compton, R. G. *Electroanalysis* **2004**, *16*, 897-903.

(3) Dai, X.; Compton, R. G. *Electroanalysis* **2005**, *17*, 1325-1330.

(4) Simm, A. O.; Banks, C. E.; Compton, R. G. *Analytical Chemistry* **2004**, *76*, 5051-5055.

(5) Feeney, R.; Kounaves, S. P. *Analytical Chemistry* **2000**, *72*, 2222-2228.

(6) Hamilton, T. W.; Ellis, J.; Florence, T. M. *Analytica Chimica Acta* **1980**, *119*, 225-233.

(7) Henry, F. T.; Kirch, T. O.; Thorpe, T. M. *Analytical Chemistry* **1979**, *51*, 215-217.

(8) Cavicchioli, A.; La-Scalea, M. A.; Gutz, I. G. R. *Electroanalysis* **2004**, *16*, 697-711.

(9) Feeney, R.; Kounaves, S. P. *Talanta* **2002**, *58*, 23-31.

(10) Simm, A. O.; Banks, C. E.; Compton, R. G. *Electroanalysis* **2005**, *17*, 1727-1733.

(11) Sadana, R. S. *Analytical Chemistry* **1983**, *55*, 304-307.

(12) Pretty, J. R.; Blubaugh, E. A.; Caruso, J. A. *Analytical Chemistry* **1993**, *65*, 3396-3403.

(13) Jackson, K. W.; West, T. S.; Balchin, L. *Analytical Chemistry* **1973**, *45*, 267-271.

(14) Tanaka, T.; Sato, T. *Journal of Trace and Microprobe Techniques* **2001**, *19*, 521-531.

(15) Bio-Rad Laboratories, Chelex 100 and Chelex 20 Chelating Ion Exchange Resin Instruction Manual, pp 1-24.

(16) Tomilov, A. P.; Smetanin, A. V.; Chernykh, I. N.; Smirnov, M. K. *Russian Journal of Electrochemistry* **2001**, *37*, 997-1011.

(17) Stevenson, F. J. *Humus Chemistry: Genesis, Composition, Reactions*; Wiley: New York, 1982.

(18) Gattrel, M.; Kirk, D. W. *Journal of The Electrochemical Society* **1992**, *139*, 2736-2744.

(19) Terashima, C.; Rao, T. N.; Sarada, B. V.; Tryk, D. A.; Fujishima, A. *Analytical Chemistry* **2002**, *74*, 895-902.

(20) Swain, G. M. *Journal of The Electrochemical Society* **1994**, *141*, 3382-3393.

(21) Swain, G. M.; Ramesham, R. *Analytical Chemistry* **1993**, *65*, 345-351.

(22) Muna, G. W.; Tasheva, N.; Swain, G. M. *Environmental Science and Technology* **2004**, *38*, 3674-3682.

(23) Haymond, S.; Babcock, G. T.; Swain, G. M. *Electroanalysis* **2003**, *15*, 249-253.

(24) Granger, M. C.; Xu, J.; Strojek, J. W.; Swain, G. M. *Analytica Chimica Acta* **1999**, *397*, 145-161.

(25) Granger, M. C.; Witek, M.; Xu, J.; Wang, J.; Hupert, M.; Hanks, A.; Koppang, M. D.; Butler, J. E.; Lucazeau, G.; Mermoux, M.; Strojek, J. W.; Swain, G. M. *Analytical Chemistry* **2000**, *72*, 3793-3804.

(26) Hupert, M.; Muck, A.; Wang, J.; Stotter, J.; Cvackova, Z.; Haymond, S.; Show, Y.; Swain, G. M. *Diamond and Related Materials* **2003**, *12*, 1940-1949.

(27) Show, Y.; Matsukawa, T.; Ito, H.; Iwase, M.; Izumi, T. *Diamond and Related Materials* **2000**, *9*, 337-340.

(28) Iniesta, J.; Michaud, P. A.; Panizza, M.; Cerisola, G.; Aldaz, A.; Comninellis, C. *Electrochimica Acta* **2001**, *46*, 3573-3578.

(29) Rodrigo, M. A.; Michaud, P. A.; Duo, I.; Panizza, M.; Cerisola, G.; Comninellis, C. *Journal of the Electrochemical Society* **2001**, *148*, D60-D64.

(30) Iniesta, J.; Exposito, E.; Gonzalez-Garcia, J.; Montiel, V.; Aldaz, A. *Journal of the Electrochemical Society* **2002**, *149*, D57-D62.

(31) Bonfil, Y.; Brand, M.; Kirowa-Eisner, E. *Analytica Chimica Acta* **1999**, *387*, 85-95.

CHAPTER 7

KEY FINDINGS AND FUTURE WORK

7.1 Water Treatment

Boron-doped diamond thin-film coated on Ti (diamond/Ti) was used for the anodic degradation of atrazine. As stated, the electrode material has many favorable attributes for this application, which include a large working potential window, a chemically inert surface and good electrical conductivity. The key findings from this dissertation on water treatment/decontamination are:

- The diamond/Ti anodes are morphologically and microstructurally stable under the reported polarization conditions as confirmed by SEM, Raman spectroscopy and XRD. Residual stress, a common problem with diamond film on Ti substrates, did not cause any pinholes or microcracks in the diamond film under the deposition conditions used.

- The diamond/Ti electrode exhibited good, reproducible and stable electrochemical activity for the electrochemical redox systems, $Fe(CN)_6^{3-/4-}$ and $Ru(NH_3)_6^{3+/2+}$.

- The degradation of ATZ on diamond/Ti was a first-order reaction as the logarithm of the ATZ concentration changed linearly with the electrolysis time. The reaction rate calculated from the slope of the curve was proportional to the applied current.

- The degradation of ATZ at diamond/Ti anodes was reproducible from film-to-film and stable long-term for a given electrode. From radio-labeling

137

studies, the major degradation product was found to be CO_2 at a high yield of 81.2% for a 120 min electrolysis period.

Compared with the other tests reported in the literature, the yield of CO_2 was substantially higher due to the dimensional stability of diamond and the large overpotential for oxygen evolution. The results showed that diamond/Ti anode is effective for the oxidation of organic pollutants to CO_2.

Importantly, though, was the fact that the calculated coulometric efficiency $(Q_{ox}^{atrazine}/Q_{ox}^{total})$ was low. (0.1~0.2%) Since the conversion efficiency was improved with added convection, we suppose that the efficiency could be further improved by:

- Conducting the electrolysis in a flow-through electrolysis cell so as to improve the mass transport of ATZ to the electrode.

- Making the electrode surface area larger (e.g., mesh electrode) so as to increase the active surface sites and the electrode area available for reaction.

7.2 Water Quality Monitoring

Au-coated boron-doped diamond thin-film electrode, combined with differential pulse anodic stripping voltammetry (DPASV), was used for total inorganic arsenic detection in water samples. The key findings in this dissertation on water quality monitoring project are:

- The Au-coated diamond electrode provided a sensitive, reproducible and stable response for inorganic arsenic in both standard and real samples.

- As was codeposited (preconcentrated) with Au on the diamond surface. When codeposited with As, Au was in the form of relatively small round particles of small nominal size and variance (22 ± 3 nm) and high particle density (10^{10} cm^{-2}).

- Compared with commonly used electrode materials, such as Au and other Au-coated carbon electrodes, the Au-coated diamond electrode offers advantages in terms of the peak shape and detection figures of merit. Sub-ppb LODs were obtained for As(III) and As(V) using both standard and local river water samples.

- This method was shown to be practical for real sample analysis as 0.6 ppb of As(III) was detected in local river water with a response variance less than 2% (RSD) for 10 consecutive measurements and a response stability of better than 94% over a 10-h period.

- The properties of the diamond are key for obtaining high quality detection figures of merit. They render the electrode resistant to fouling as the response attenuation caused by humic acid (up to 5 ppm) for Au-coated diamond was smaller than that for a Au foil electrode. The method was improved by employing solid phase extraction (SPE) for sample preparation. Specifically, SPE (cation exchange) was used to remove interfering metal ions (e.g., Cu(II)). The As(III) recovery after passage through the resin was high at 94.8 ± 2.4%.

- The method is accurate for inorganic arsenic detection in contaminated water samples supplied by the U.S. Bureau of Reclamation. For two real

water samples, the total inorganic arsenic concentration determined with the Au-coated diamond differed from the specified value by 4%, or less.

It is our contention that this new electrode and method are practical for use in on-site analysis of total inorganic arsenic, offering advantages over commonly used Au and Au-coated glassy carbon electrodes. Further research could be conducted to design a field employable instrumental set-up for the on-site As analysis. A portable potentiostat and sample preparation set-up would be necessary. The Au-coated diamond deserves further study because it can have many other applications (e.g., detection of peptide) due to the high sensitivity provided by the nanometer size of Au particles and the high stability provided by the inert diamond support.